Testing Robustness of WMAP Temperature Calibration to Timing Offsets

Petr Malik*

Department of Physics

Durham University

2012

*petr.malik@hotmail.com

Abstract

Results derived from data obtained by Wilkinson Microwave Anisotropy Probe (WMAP) are extensively used in many areas of physics. It has been claimed recently that the published WMAP calibrated data and maps might be in question because of an undocumented timing offset in the official processing pipeline [1]. This timing error was shown to induce a quadrupole pattern in the final maps that is very similar to the officially published quadrupole mode. It is clear that a timing offset at the map-making stage will strongly affect the quadrupole scale, since the map-making in [1] was based on the official WMAP calibrated TOD. But there is also a possibility that the calibration process itself could be affected as well and we test this here. In this work we approximately reproduce the original dipole-based iterative calibration procedure to produce a calibrated data set starting from raw uncalibrated data. Using the calibrated data we generate a set of sky maps that we compare to the officially released maps and note some differences between our and official results. We also investigate the effects of various timing offsets introduced in the calibration stage on the final products. We find that a timing offset in the calibration process has little effect on the calibrated data and induced quadrupole.

1 Historical Detour

The Cosmic Microwave Background (CMB), a remnant from the time when the Universe was young and hot, has been indirectly detected since 1940s (W. S. Adams [2], A. McKellar [3]) and theoretically predicted by G. Gamow, R. Alpher and R. Herman in 1948 [4]. R. H. Dicke, P. J. E. Peebles, P. G. Roll, D. T. Wilkinson [5] and F. Hoyle, R. Taylor also predicted existence of the CMB in 1960s independently of the group mentioned above. The CMB was directly observed in 1965 by A. Penzias and R. Wilson in Bell Labs [6]. The two radio astronomers received the Nobel Prize for their discovery thirteen years later.

Huge effort has been directed towards the study of the Cosmic Microwave Background, namely its anisotropies, in the last two decades. Apart from all balloon-based experiments that provided high resolution pictures of only small portions of the sky such as MAXIMA (1995 - 1999) and BOOMERanG (1997 - 2003), two missions stand apart. Cosmic Background Explorer (COBE) satellite launched on 18/11/1989 first detected anisotropies in the CMB. Its successor, the Microwave Anisotropy Probe (MAP), later renamed to Wilkinson Microwave Anisotropy Probe (WMAP) in honour of David Todd Wilkinson (1935 - 2002), significantly expanded on the COBE's observations. Finer resolution and increased sensitivity of WMAP allowed scientists to use the CMB power spectra to infer some of the most important properties of our universe such as its energy contents, age and the rate of expansion. The results published in 2003 meant a breakthrough in our knowledge of the evolution and composition of our universe.

CMB anisotropies and polarization can be predicted based on cosmological models. Once observed the CMB power spectrum can be used to determine viability of the underlying model and the best fit cosmological param-

eters such as the energy content of the universe. Together with luminosity-distance tests based on observations of light curves of distant supernovae, CMB is the most important tool for determining composition and evolution of our universe available to us today.

The European Space Agency launched Planck, the next generation satellite designed for CMB observations, on 14/05/2009. Planck should continue work of COBE and WMAP with even higher resolution and sensitivity, promising potential refinement of our models of the Universe. The mission is expected to deliver first CMB results by January 2013.

2 Theory

2.1 Origin of the CMB

According to the widely accepted Big Bang theory by G. Gamow, R. Alpher and R. Herman [4] the universe originated from an extremely hot and dense state with its evolution governed by the Friedmann Equation ever since.

$$\left[\left(\frac{1}{R}\frac{dR}{dt}\right)^2 - \frac{8}{3}\pi G\rho - \frac{1}{3}\Lambda c^2\right] R^2 = -kc^2, \tag{1}$$

where R is a dimensionless scale factor and k a constant measure of curvature of the universe. ρ and Λ are total matter (energy) density and cosmological constant contained in the universe. The equation says that the universe must evolve with time. It either expands or collapses. Based on observations of the Hubble flow we believe that the universe currently expands with an accelerated rate of expansion. As it expands the matter and energy density decrease and the universe cools down. When we trace its evolution back in time we inevitably arrive at a point when the universe was much smaller and therefore denser and hotter than it is today. The physics of processes ongoing

in such a universe is not yet well understood but we can at least attempt to build a simple mental picture of our universe when it was only a fraction of second old.

As the universe cools down with expansion the energy density of black-body radiation (ρ_{rel}) decreases as the fourth power of the scale factor [R(t)].

$$\rho_{rel}(R) = \frac{\rho_{rel,0}}{R^4}, \tag{2}$$

where $\rho_{rel,0}$ is the value today. The R^3 in (2) is due to the increase in volume of the universe while the additional R^1 factor comes from the cosmological redshift of photon wavelengths. Given the proportionality between energy density and temperature $\rho_{rel} \propto T^4$, the temperature scales as

$$T(R) = \frac{T_0}{R}, \tag{3}$$

where T_0 is the temperature of the universe today.

At early times when the temperature was above $10^{13}K$, the universe was filled by a soup of free electron-positron and quark-antiquark pairs in thermodynamic equilibrium with photons. When temperature dropped below this value quarks and anti-quarks recombined to free nucleons with relative amounts (N) of protons and neutrons according to their rest masses (m).

$$\frac{N_n}{N_p} = e^{-\frac{(m_n - m_p)c^2}{kT}}, \tag{4}$$

where T is the temperature at the time of recombination.

In the meantime electrons and positrons were being created from high-energetic photons. When the temperature dropped below 1MeV photons no longer had enough energy to produce elementary particles and the spontaneous creation ceased.

Thanks to violation of fundamental symmetries of nature there was roughly one particle excess over its anti-partners in 10^9. The rest mutually annihi-

lated and that small excess fraction is all the matter filling our universe today.

Free neutrons are not stable and decay into protons with half-life of approximately fifteen minutes. However, by the time the universe was three minutes old its temperature dropped sufficiently enough for stable nuclei to form. Neutrons stopped decaying leaving mainly H, He and traces of deuterium and Li behind.

After the phase of matter-antimatter annihilation and nucleosynthesis the universe swarmed with photons, free electrons and light nuclei. The latter two are insignificant in numbers to the photons as there are approximately 10^9 photons per every baryonic particle.

With the most interesting time over the universe was still quite an unfamiliar place. The temperature was high enough for the photons to have enough energy to kick electrons from their orbitals around atomic nuclei preventing formation of stable atoms. The universe was opaque due to Compton scattering of photons on free electrons. Although the scattering rate was slowly decreasing with expansion it took hundreds of thousands of years for another major change to occur.

The ratio of ionized to neutral hydrogen can be estimated from the Saha Equation given the number density of electrons (n_e), electron rest mass (m_e), temperature (T), hydrogen ionization energy (χ_I) and the partition functions (Z).

$$\frac{N_{II}}{N_I} = \frac{2}{n_e}\frac{Z_{II}}{Z_I}\left(\frac{2\pi m_e kT}{h^2}\right)e^{-\frac{\chi_I}{kT}} \tag{5}$$

Using equation (3) we can rewrite the Saha Equation in terms of the scale factor (temperature of the universe in the equilibrium era still obeys (3), although the temperature of non-relativistic particles scales as R^{-2} rather than R^{-1} as there are many more photons than non-relativistic particles)

and the current baryonic density and temperature.

$$\frac{N_{II}}{N_I} = \frac{f}{1-f} = \frac{m_H R^3}{f\rho_{bar,0}} \left(\frac{2\pi m_e k T_0}{h^2 R}\right)^{\frac{3}{2}} e^{-\frac{\chi_I R}{k T_0}}, \tag{6}$$

where f is the fraction of ionized hydrogen atoms and m_H is the hydrogen mass.

Using the equation above one can estimate the temperature and age of the universe at the time of recombination when nuclei started capturing free electrons and forming stable hydrogen atoms. We believe this happened when the universe was about 380,000 years old and had temperature around 3000K. With the process of recombination largely finished the universe became transparent to electromagnetic radiation.

When we look deep into space back to the time of recombination we see the surface of last scattering as a spherical shell at redshift $z_{CMB} \cong 1100$ centered at our view point. The universe is believed to be homogeneous and isotropic and so should be the microwave background seen as the surface of last scattering. It is, at least on the large scales. When one looks closer it exhibits a random pattern of fluctuations in temperature on scales below 1°. These are cosmic microwave background fluctuations.

2.2 Primordial CMB Fluctuations

The cosmic microwave background fluctuations are imprints of primordial density fluctuations enlarged by inflation that occurred shortly after the Big Bang. When the universe was only about $10^{-34}s$ old the energy density was dominated by a false vacuum state with negative pressure [7, p.1241]. When a portion of the universe went from this "supercooled" state to the lower-energy true vacuum the greater pressure in the region caused an exponential expansion.

The inflationary phase probably lasted for $10^{-32}s$ or more, during which the size of the universe increased by a factor of approximately e^{100} [7, p.1243]. When the strong force decoupled from the other three fundamental forces the elevated "latent" energy of the false vacuum was released and reheated the universe to nearly $10^{27}K$ [7, p.1243] causing an outbreak of particle-antiparticle creation. Any matter (magnetic monopoles?) formed prior to inflation was diluted to insignificance.

According to the uncertainty principle the energy (temperature) of any given system is not precisely determined, but can rather fluctuate over time.

$$\Delta E \Delta t \geq \frac{\hbar}{2}, \tag{7}$$

where ΔE is the energy fluctuation and Δt the time over which the energy fluctuates.

The field filling the universe prior to inflation fluctuated in the same manner. These primordial quantum fluctuations were on the Planck scale. It was the inflation what expanded them to cosmological dimensions. The CMB fluctuations are therefore primordial quantum fluctuations in temperature magnified by the inflation.

Temperature closely relates to energy and pressure. A fluctuation with higher temperature also has a deeper gravitational potential well and therefore attracts more matter and becomes denser and hotter. At some point the pressure arising from higher temperature stops the gravitational collapse of the fluctuation and forces it to re-expand. As the temperature drops and the fluctuation becomes less dense decreasing pressure is sooner or later overcame by gravitational attraction and the fluctuation starts collapsing once again. This process together with inertia associated with massive particles leads to acoustic oscillations about the equilibrium point between gravitational attraction and pressure. The process ceased at the time of recombination

when photons stopped interacting with matter. The resulting field of density fluctuations provided seeds for subsequent structure formation.

The fluctuation field visible in the cosmic microwave background can be decomposed into a set of mutually orthogonal basis functions on a sphere called spherical harmonics.

$$\frac{\Delta T(\vec{n})}{T} = \sum a_{lm} Y_{lm}(\vec{n}), \tag{8}$$

where a_{lm} coefficients are the components along the basis vectors Y_{lm}. In a homogeneous and isotropic universe, such as our universe, it holds that $\langle a_{lm} a^*_{l'm'} \rangle = C_l \delta_{ll'} \delta_{mm'}$, where C_l defines the power spectrum. The first non-vanishing quantity is the correlation between the temperature anisotropies along two directions $\vec{n}$ which with a little bit of algebra evaluates to

$$\langle \Delta T(\vec{n}_1) \Delta T(\vec{n}_2) \rangle = T^2 \sum \frac{2l+1}{4\pi} C_l P_l(\cos(\theta)), \tag{9}$$

where $P_l(\cos(\theta))$ are the Legendre polynomials, another set of orthogonal functions, and θ is the angular separation between $\vec{n}_1$ and $\vec{n}_2$ unit vectors.

The properties of the CMB are closely related to the properties of our universe such as the amount of baryonic matter, dark energy content and curvature. The CMB power spectrum can be therefore used to test our cosmological models and tell us much about evolution and composition of the Universe.

2.3 The Sunyaev-Zel'dovich (SZ) Effect

When low-energy photons of CMB pass through hot ionized gas in rich galactic clusters the photons are scattered to higher energies by the high-energy electrons through inverse Compton scattering. This increases frequency of the scattered photons by an average amount $\Delta\nu$ [7, p.1169].

$$\frac{\overline{\Delta\nu}}{\nu} = 4 \frac{kT_e}{m_e c^2}, \tag{10}$$

where T_e is the temperature of the electron gas. The SZ effect is independent of the cluster's redshift showing that the CMB spectrum is the same for all observers moving with the Hubble flow, depending only on the observer's peculiar velocity. The effect can be used to investigate properties of galactic clusters throughout the history of the Universe.

3 WMAP Observatory

WMAP, as its predecessor COBE, is a differential instrument. It measures temperature differences between two points on the sky (this design is necessary to overcome inherent instabilities in the detectors [8]). To do this it is equipped with two telescopes (A-side and B-side optics) approximately 141° apart. The large sweep circle is important for calibration since WMAP sees a significant portion of the dipole anisotropy every spin period (see section on data calibration). The probe has ten detector assemblies operating at different wavelengths [10, p.4]. Table (1) gives frequency characteristics for all five WMAP radiometers.

	K	Ka	Q	V	W
$\nu[GHz]$	19.5 - 25	28 - 37	35 - 46	53 - 69	82 - 106

Table 1: Frequency characteristics of WMAP radiometers.

Each assembly has two two-channel radiometers sensitive to orthogonal polarization modes. There are altogether forty independent channels in the instrument. Each radiometer records raw counts of photons of a given wavelength and polarization.

In order for WMAP or any other experiment to be successful it has to be able to detect weak fluctuations in temperature with magnitudes on the order

of $10^{-5}K$ on angular scales smaller than 1°. This can be done after careful data reduction. The success of this step depends largely on the adopted scanning strategy as it not only affects the area of the sky covered, but also things like thermal stability (the satellite's temperature changes as it changes its attitude with respect to the Sun), contamination by radiation received from various solar system bodies, data redundancy (important for instrument calibration and data reduction) and time available for radio communication with ground based facilities.

The primary requirement of the WMAP mission is to observe the full sky. One reason for full sky coverage is the statistical nature of CMB anisotropies. The larger observation sample allows us to determine statistical properties of the CMB with higher certainty. Full sky coverage is also needed for accurate determination of low-order multipoles, such as the dipole moment, so crucial for data reduction (process of converting raw photon counts to temperatures in K). It also serves as a good test of COBE results on large multipole moments.

WMAP attempts to rapidly scan a large portion of the sky without unnecessary attitude corrections while maintaining good redundancy (observe each sky pixel many times from different angles). Data redundancy is especially important for data reduction and polarization measurements.

WMAP is located at the L2 point tilted by 22.5° from the line joining the Sun to the Earth. The satellite spins about its axis of symmetry with a two-minute period while slowly precessing about the Sun-Earth line with a period of one hour. This way WMAP observes about 30% of the entire sky every day, covering the whole celestial sphere every six months, allowing for consistency checks and improving data statistics.

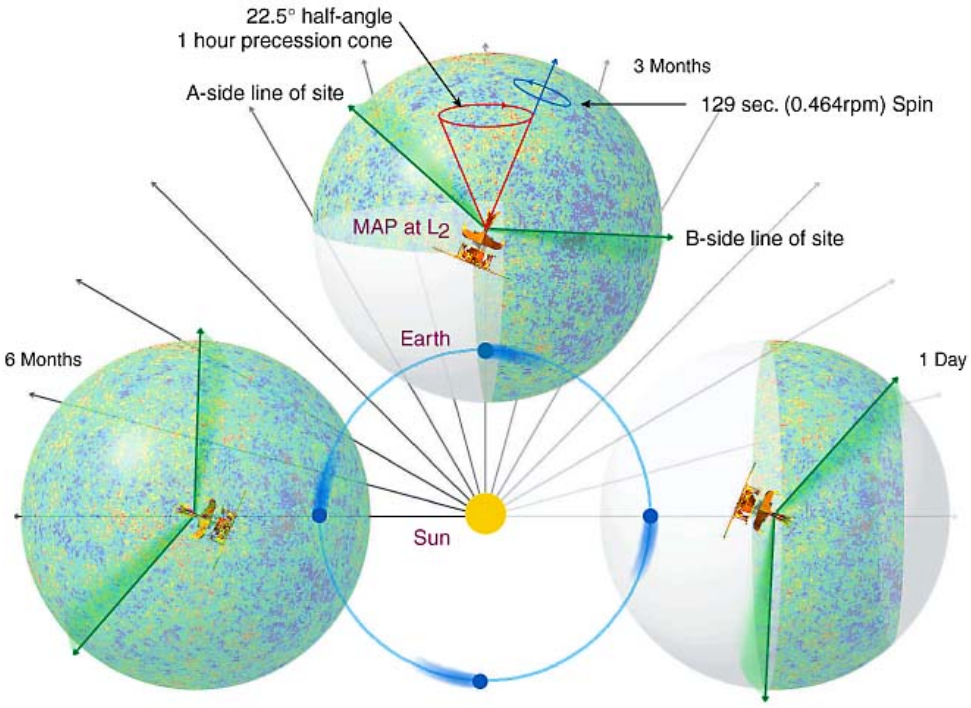

Figure 1: WMAP scan strategy (http://map.gsfc.nasa.gov/mission/observatory_scan.html).

4 Data

4.1 Time Ordered Data (TOD)

Scientific and telemetry data from the satellite is stored in so called TOD (Time-Ordered Data) archives [10, p.120]. Archives are implemented as Flexible Image Transport Standard (FITS) files with several tables. Each file contains one day of scientific and telemetry data.

The Scientific Table contains temperature measurements for all forty channels and associated quality flags. The measurements are recorded in 46.08-second blocks. A single block contains thirty 1.536-second sub-blocks also called major science frames. Each frame contains a certain number of

observation records depending on the integration time necessary for the associated band. The following table (2) summarizes frame sizes of WMAP detectors.

	K	Ka	Q	V	W
# of records	12	12	15	20	30

Table 2: Major science frame sizes.

Each detector assembly has a timestamp associated with every TOD record. There is only one timestamp per scientific observation. Both polarizations and channels are recorded at the same time for a given assembly.

Quality flags are included to mark corrupted and suspicious science frames. Some target whole assemblies, others individual detectors. Data can be marked invalid if, for instance, a technical issue occurs somewhere along the processing pipeline or one of the telescopes points at a known solar system body.

The Meta Data Table consists of 46.08-second blocks. It contains position and velocity data recorded every 120.0 second and interpolated to the beginning of each block. Both position and velocity are expressed as Cartesian vectors in the Celestial coordinate system. The attitude data received every second is converted to four quaternions for every major science frame. Quaternions play an important role in pointing determination. They can be used to interpolate the exact pointing of the satellite for every observation in any given science frame.

The Analog Instrument Housekeeping (AIHK) Data Table and The Digital Instrument Housekeeping (DIHK) Data Table contain instrument specific data and are not important for the subsequent analysis.

The Line-Of-Sight (LOS) Table provides lines-of-sights for each detector

assembly in the spacecraft coordinates. These are necessary for accurate pointing interpolation mentioned earlier.

4.2 Maps

Maps are stored in FITS format. The Archive Map Table holds sky temperatures in mK and the number of observations for each pixel. Maps use the Healpix [1] pixelization. The most common Healpix resolution $N_{side} = 512$ gives 3,145,728 pixels corresponding to an angular resolution of 7 arcmin. We also present smoothed maps in resolution $N_{side} = 8$ corresponding to 768 pixels. Given the resolution parameter of a map one can transform between pixel numbers and actual pointing vectors using the Healpix application programming interface (API) documented at the Healpix website [2].

Masks used to remove known emission sources from the processing pipeline follow the same format. Pixels with number of observations equal to zero are rejected. Diffuse emission in temperature is masked using a combination of K band and Q band cuts, as described in [11]. Point sources are masked based on external catalogues and WMAP-detected sources. There are several masks (point sources, polarization, temperature analysis) provided on the WMAP website. The mask used in TOD calibration is the standard resolution ($N_{side} = 512$) WMAP3 processing mask which masks 5.7% of the sky [9].

[1] http://healpix.jpl.nasa.gov/index.shtml

[2] http://healpix.jpl.nasa.gov/healpixSoftwareDocumentation.shtml

5 Data Calibration

The WMAP team proposes a simple relationship in which one models the raw differential temperature counts (c) as a function of physical temperature differences (ΔT) and a set of parameters.

$$c(g, b) = g\Delta T + b, \tag{11}$$

where g stands for the instrument's gain (conversion factor between physical temperatures in degrees and raw photon counts) and b for the baseline parameter (the zero-level noise of the instrument expressed in photon counts). Aside from the linearity of the model with respect to its parameters it is also assumed that the parameters themselves vary only slowly over time. As far as the thermal environment of the satellite is sufficiently stable this is a reasonable assumption. The WMAP team chose a one-hour calibration period.

In order to transform the raw photon counts measured by the probe into more useful physical temperatures in degrees one can make use of the model's linearity and perform a simple linear regression fit on the raw data.

It would be unfeasible to precisely model CMB temperatures including fluctuations. Such an attempt would also establish a link between data calibration and the fluctuation background. A strongly undesirable connection given that the primary goal of the satellite is to study fluctuation patterns themselves. The approach taken by people behind WMAP data processing is to ignore the CMB fluctuations altogether and focus on significantly more prominent dipole mode induced into the cosmic background by the motion of the satellite relative to the Hubble flow.

This dipole anisotropy can be relatively easily derived [12, p.129] by con-

sidering the number density of photons in a momentum phase-space.

$$N_\gamma(\vec{p}) = \frac{1}{h^3}\frac{1}{e^{\frac{|\vec{p}|c}{kT}} - 1} \tag{12}$$

One can Lorentz-transform the four-momentum from a stationary coordinate system to one moving with respect to the CMB.

$$|\vec{p}| = \gamma(1 + \beta\cos(\theta))|\vec{p}'|, \tag{13}$$

where β is the ratio of velocity to the speed of light in vacuum and γ is the relativistic Lorentz factor. Since the photon density and the phase-space volume are Lorentz invariant.

$$N'_\gamma(\vec{p'}) = \frac{1}{h^3}\frac{1}{e^{\frac{|\vec{p}'|c}{kT'}} - 1} \tag{14}$$

Leading to the following relationship between the temperatures (T and T') observed in the two inertial frames.

$$T' = \frac{T}{\gamma(1 + \beta\cos(\theta))}, \tag{15}$$

where θ is the angle between the incoming photons and the observer's velocity vector. The above equation (15) is sometimes Taylor-expanded and simplified to its non-relativistic form.

$$T' = T(1 + \beta\cos(\theta)) \tag{16}$$

As the dipole is many times stronger (on the order of $500\times$) than the assumed CMB fluctuations it can be used as a simple first-approach calibration model for the CMB sky.

WMAP data-processing pipeline uses independent measurements of the CMB monopole temperature and known pointing of the satellite and velocity to evaluate the dipole temperature at any given time. The monopole temperature and motion of the Galaxy are known from previous experiments

(namely COBE). The satellite's pointing and velocity can be extracted from the telemetry data recorded by the instrument. For the sake of future discussion it is important to note that the pointing data is not available for every single temperature measurement, but instead must be extrapolated from evenly distributed telemetry records.

Given a simplified (dipole) model of the sky and raw data from the probe one can obtain the calibration parameters $(g,\ b)$ by one of the well-known fitting techniques such as χ^2 minimization. Where χ^2 is as follows:

$$\chi^2 = \sum \frac{[c - (g\Delta T + b)]^2}{\sigma_0^2} \tag{17}$$

σ_0 is the measurement error. Since we lack the information necessary to estimate the error term we set $\sigma_0 = 1.0$. This choice limits our ability to use the value of χ^2 as an independent measure of the model's performance. This is done for every detector, channel and polarization treating each single hour as an independent data set leading to a set of hourly calibration parameters.

As noted above the sky model used in this approach is only a simplified dipole model. However, we believe the sky is more than just the dipole. There is plenty of contamination coming from our own galaxy in addition to well-known point and extended radio sources such as planets and Magellanic Clouds. These can be masked-out prior to data processing. Equally important are the systematic effects induced by CMB fluctuations neglected by our simple dipole model. Unfortunately, it is not possible to remove the fluctuations the same way we handle other contamination sources. WMAP processing pipeline assumes a simple iterative approach. The idea behind is summarized in figure (2).

We begin by obtaining a calibration solution by fitting the dipole model on

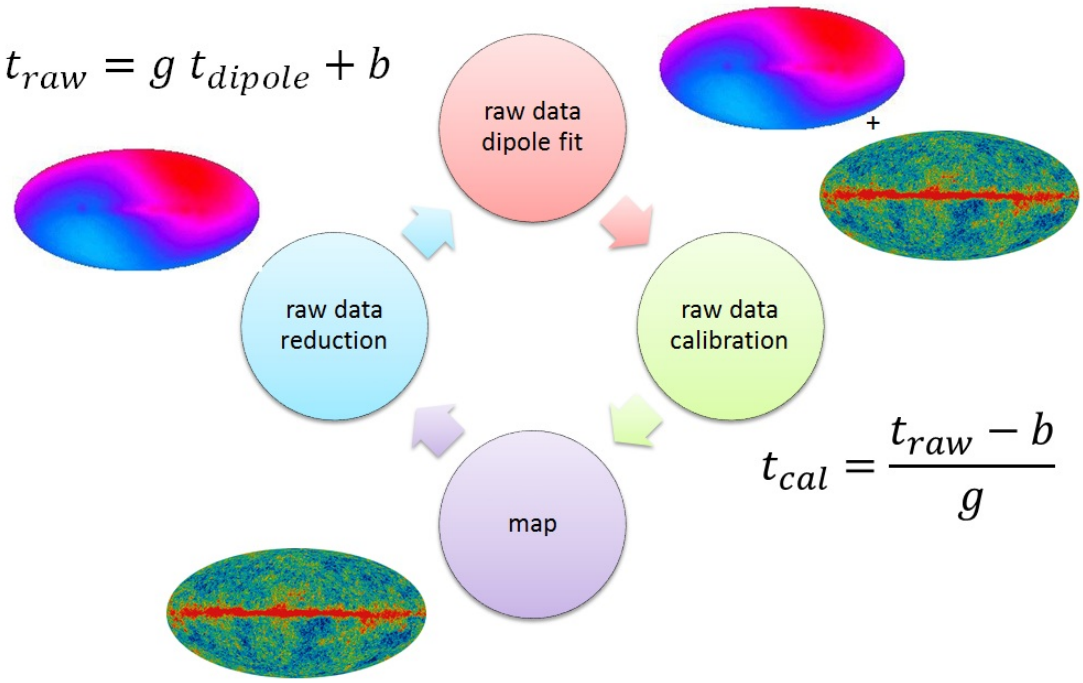

Figure 2: Iterative TOD calibration.

the raw data ignoring the CMB fluctuations. This leads to a set of calibration solutions that can be used to calibrate the raw data and produce a fluctuation map. This map can be subsequently subtracted from the raw data effectively subtracting the estimate of the CMB fluctuations leaving only the dipole mode. The new "reduced" raw data from the previous step can be used to generate a new set of calibration solutions using this improved dipole. The whole procedure can be iterated as many times as desirable. Each run should contain less fluctuation noise leading to better estimates of calibration parameters. The best-fit calibration parameters can be then used to calibrate raw TOD and construct high-quality sky maps.

Our calibration procedure is based on the official procedure described in [19] with several rather minor modifications. We omit the baseline filtering

explained in section 2.4.2 of the cited article. The official WMAP team also adopts an analytic gain model presented in [21] for the final calibration step which we do not use. However, we use an improved differential dipole model from equation (3) in [20] which accounts for different transmission of sky signals from the telescopes (A-side and B-side optics) into the radiometers (see “WMAP Observatory"). The transmission imbalance coefficients (x_{im}) are available in Table (2) in [22]. The galactic velocity components used for dipole evaluation are WMAP7 values available in Table (6) of [23]. We apply the processing mask from WMAP3 release. Finally, we use the relativistic dipole model (15) everywhere including map-making.

6 Processing Pipeline

The calibration software is based on three independent components. There is a set of IDL routines and helper C++ libraries used to extract necessary data such as telemetry, attitude and scientific records from TOD FITS archives.

The main program written in C++ serves several purposes including fitting of a given model on data, calibration of raw data given a set of calibration parameters and raw data reduction (fluctuation removal).

Finally, the IDL map-making routines released by Hao Liu and Ti-Pei Li [13] are responsible for generation of maps from calibrated TOD. The routines were left unchanged except for a few minor updates necessary to make them compatible with the rest of the pipeline. These are documented in the source code. The original non-relativistic dipole model was also replaced by its relativistic version in order to improve the calibration convergence.

Here we note that although the map-making software was thoroughly tested by its authors and shown to reproduce the official WMAP maps in

[14] and [13], we were not able to reproduce the official maps available on the WMAP website [1] with the same degree of confidence. The maps produced from the official calibrated TOD by the original map-making software exhibit a dipole-like difference (± 0.1 mK in amplitude) from the official maps. This difference could be potentially explained by some post-processing applied to the official maps. In our subsequent discussion we therefore work only with maps consistently generated by the map-making software and we shall only make differential comparisons between these.

In order to avoid repetitive pointing interpolations the application uses cache files to store its input data. The input data is extracted from uncalibrated TOD FITS archives using publicly available WMAP IDL routines [2] and stored in cache files implemented as SQLite [3] databases.

SQLite is a relational database working over the underlying file system. It was chosen for its good performance characteristics. Database allows to organize, read and store large amounts of data quickly and easily using a rich set of database queries. Another advantage is that the data is stored and read in binary. Removing any need for slow and dangerous string conversions. The same format is used for output too.

The extraction routines read input TOD FITS archives, pre-compute pointings for given detector assemblies and store them together with time data in pointing tables (there is one such table for each assembly). Telemetry (error codes and quality flags) for all detectors is stored in a telemetry table and attitude data (satellite's velocity vectors) in an attitude table. There is one telemetry and attitude table in each archive. Finally, scientific records (temperatures) are stored in tables one for each detector bearing its

[1] http://lambda.gsfc.nasa.gov/product/map/current/

[2] http://lambda.gsfc.nasa.gov/product/map/current/m_sw.cfm

[3] http://www.sqlite.org/

name.

The processing pipeline follows. Files are processed one day/database at a time (there is one database archive for each day). Pointing data and attitude for selected detectors are read from input databases after filtering flagged and suspicious points out based on the telemetry table. The pointing data is subsequently masked using a supplied mask file. Each pointing (galactic coordinates) is converted to a Healpix pixel number and this number is checked against the mask and possibly removed from the set. The filtered pointing data is stored in a temporary in-memory table in order to avoid unnecessary repetitions in case more detectors from the same assembly are processed. Corresponding scientific data is then loaded.

Once the data is in memory we pre-compute dipole temperatures at given pointings and pass them together with raw temperatures to a fitting routine. Linear model discussed above (11) is fitted on the data using a linear regression algorithm available from Numerical Recipes 3rd Edition [18].

Fit results including best-fit parameters and error estimates for each calibration period are stored in output database files on a table per detector basis. If there is no data in any given period (this can happen due to aggressive flagging and masking) it is not processed and there are therefore no calibration parameters available for that particular period.

WMAP uses a set of bit-coded flags to express quality and validity of science frames. Not all of the flag values are documented though [10, p.124]. Namely, general-flag value 192. Exclusion of non-documented flags can significantly reduce the number of points available for calibration. We perform the calibration and map-making in what the Chinese map-making group refers to as "m-mode" accepting the undocumented flags and therefore improving the calibration convergence.

The next step in the iterative calibration procedure is raw data calibration. The calibrated data serves as the input to the map-making software. Raw data is loaded always accompanied by calibration solutions for that particular day. The raw data is calibrated by inversion of equation (11) and the results are written to provided WMAP FITS archives. In case there is no data in a calibration period it is filled with zeros. This should not cause any problems as the map-making software uses the same mask and quality flags and the data therefore does not enter the pipeline whatsoever.

Following calibration is map-making. This is simply accomplished by calling the map-making routine with calibrated FITS archives as the input directory.

Every point in the raw data is then reduced by subtracting the corresponding map pixel from it. The pixel must be first de-calibrated through equation (11) though.

The resultant reduced raw data enters the next iterative run and again undergoes the procedure just described. The pipeline from fitting through calibration, map-making to data reduction repeats as many times as appropriate. The original WMAP calibration iterated ten to twenty times [19]. We opt for ten iterations based on our own trials (see the section on “Iterative Calibration") and time constraints (one iteration commonly takes several hours to complete).

7 Questions

Since the official WMAP calibration and map-making code has never been released to public a group of Chinese scientists attempted to reproduce the map-making pipeline [13] and successfully generated their own maps from the

official WMAP calibrated TOD. They tested their procedure by comparing their maps with the maps officially released by the WMAP team and are confident about the correctness of their results. Nevertheless they discovered a striking systematic difference between their results and WMAP results for certain pointing offset settings.

As already mentioned in the section on TOD, the satellite does not record pointing for every single observation. It rather records roughly one quaternion for every 1.536s long science frame containing 12 - 30 observations depending on the assembly in question. The quaternion is recorded at the beginning of the frame and all other pointings must be interpolated relative to this point.

The official WMAP pipeline interpolates pointings to the center of each observation. In other words, having 15 observations in a science frame, the first pointing is interpolated at 0.033, the second at 0.099 and so on up to the last observation at 0.967 fractional offset relative to the beginning of the frame. However, the Chinese group also tried to run their map-making code with a different offset setting evaluating pointing at the beginning rather than center of each observation. The fractional offsets in that case would be 0.0 in case of the first record, 0.066 for the second all the way up to 0.933 in the last observation. What they found was an induced quadrupole in the difference between their and official WMAP maps [1] shown in figure (3).

Even more surprising is the fact that this quadrupole moment is very well consistent with the released WMAP quadrupole component [1] shown below.

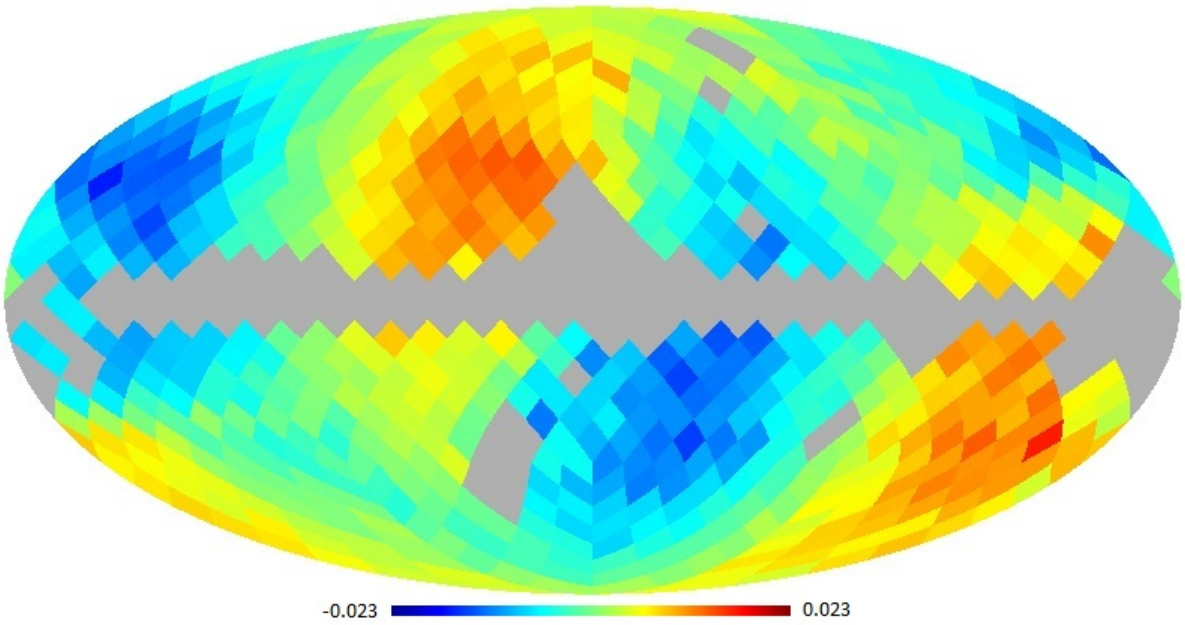

Figure 3: The difference between the released WMAP3 year-1 map and the Chinese map produced from the same WMAP Q1-band data, in Galactic coordinates and in units of mK ($N_{side} = 8$). [1]

This finding suggests that the released WMAP quadrupole (Figure 4) is almost completely artificial and the real CMB quadrupole is near zero.

A closer look at the time ordered data reveals an undocumented 25.6ms offset [1] between the meta-data (quaternions) and scientific data (temperatures) timestamps. To correct this offset one has to evaluate the pointing at zero rather than center offset. This is exactly what the Chinese group did leading to conclusion that the official quadrupole is indeed artificial and the pipeline should be re-examined.

They also devised an independent method for diagnosing the timing offset using the official TOD [14] by minimizing the following function.

$$V(\Delta t) = \sum [d(t) - D(t + \Delta t)]^2, \tag{18}$$

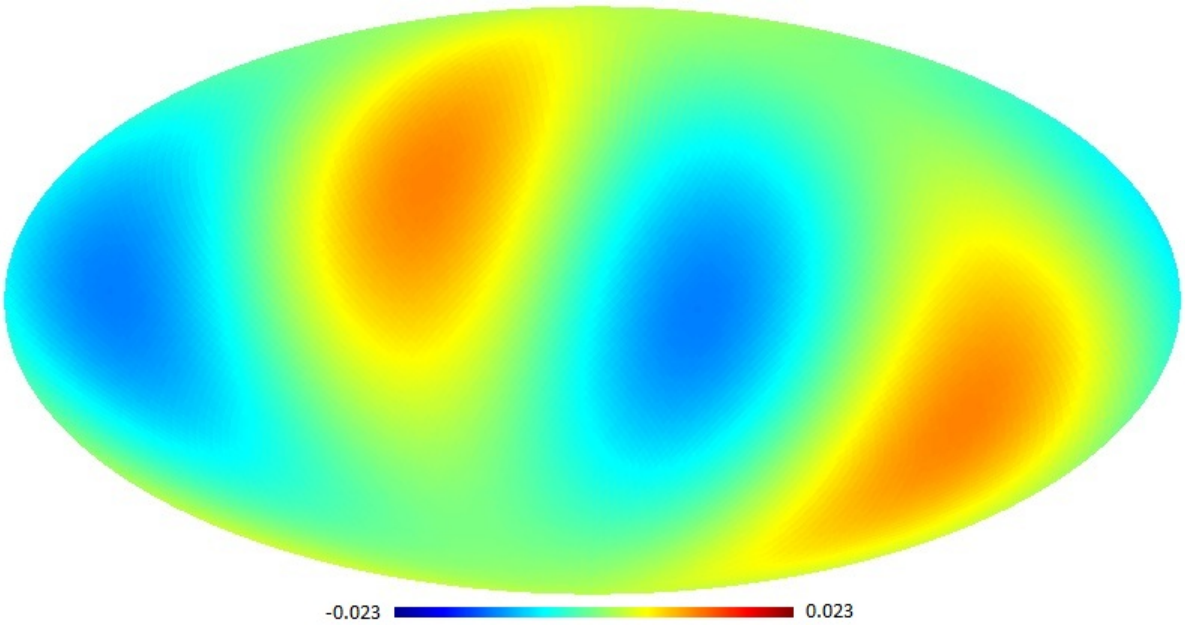

Figure 4: The released WMAP CMB quadrupole component derived from WMAP5 V and W data in Galactic coordinates and in units of mK. [1]

where d is the calibrated TOD and D is the real physical dipole contained in the data. If there is no offset present the function is on average minimized at $\Delta t = 0$. However, if there exists an offset the merit function is minimized at a non-zero value Δt. Using this method they discovered consistently non-zero offset in all wavebands of the official WMAP TOD [14, Table 1] of $25ms \pm 1ms$.

A. Moss et al [17] also presented a model that confirmed a timing offset would induce an artificial quadrupole consistent with the WMAP released cosmological quadrupole, although the Moss's result indicates somewhat weaker signal.

B. F. Roukema analyzed [15] images of point sources recorded by WMAP and concluded that the map-making procedure applied by the WMAP collaboration was correct, nevertheless he did not exclude the possibility of an

erroneous timing offset entering the calibration stage. He extended his original analysis in [16] by investigating the variance in map pixels. He once again concludes that the official TOD was likely wrongly calibrated.

A possible WMAP beam profile dependence on the flux has also been discussed by U. Sawangwit and T. Shanks in [24] and [25]. It appears that the radio point sources detected by WMAP in Q, V and W bands generally have a broader profile than Jupiter which is used by the WMAP team to debeam the CMB power spectra. As the CMB rms fluctuation flux is much closer to the point radio sources than to Jupiter and because the CMB power spectrum is strongly dependent on the beam profile this flux-profile relationship may lead to wrong conclusions about our cosmological models. There is a possibility that the observed flux-profile relationship may be explained by the timing offset discussed above [17].

8 Results

8.1 Iterative Calibration

The WMAP team published first-year calibration results including gain and baseline plots for detectors DK113 and DV113 in [19, p.72] presented in figure (5). Our calibration results for detector DV113 after 10 calibration iterations are shown in figures (6) and (7). The x-axis shows the work-unit-id (WUID) which is the index of a given calibration period within the whole data set. We used one-hour calibration period to process the first year from WMAP3 data set. In order to demonstrate calibration convergence we also show the change in solutions between subsequent calibration runs in figures (8 - 21). Table (3) then summarizes statistics (mean over the whole parameter set) of the solutions from individual iterative runs. Based on visual comparison of

the official and our plots DV113 gain and baseline appear to be consistent with the official calibration results. The progressive improvement of the solutions tends to zero with every subsequent iteration suggesting that the solutions converge. The change is most pronounced between the first and the second iterative run. This is expected as most of the fluctuation background should be removed in the first iteration. Although, the yearly means of calibration parameters appear to be constant, figures (8 - 21) clearly show that the solutions converge with every iteration. However, as can also be seen from the figures the average change over a period of one year is near zero, leading to constant yearly means. This effect is most marked on the baseline parameter. For the same reason as above, one should also be careful when drawing conclusions about effects on the final maps based on yearly averages of calibration parameters.

iteration #	gain	baseline
1	0.449490 ± 0.000254	$19048.472935 \pm 0.037725$
2	0.449492 ± 0.000350	$19048.472816 \pm 0.037725$
3	0.449460 ± 0.000349	$19048.472816 \pm 0.037725$
4	0.449444 ± 0.000348	$19048.472816 \pm 0.037725$
5	0.449434 ± 0.000348	$19048.472815 \pm 0.037725$
6	0.449425 ± 0.000348	$19048.472815 \pm 0.037725$
7	0.449417 ± 0.000348	$19048.472815 \pm 0.037725$
8	0.449408 ± 0.000348	$19048.472815 \pm 0.037725$
9	0.449400 ± 0.000348	$19048.472814 \pm 0.037725$
10	0.449391 ± 0.000348	$19048.472814 \pm 0.037725$

Table 3: DV113 iterative calibration gain and baseline yearly means and standard errors-of-the-mean.

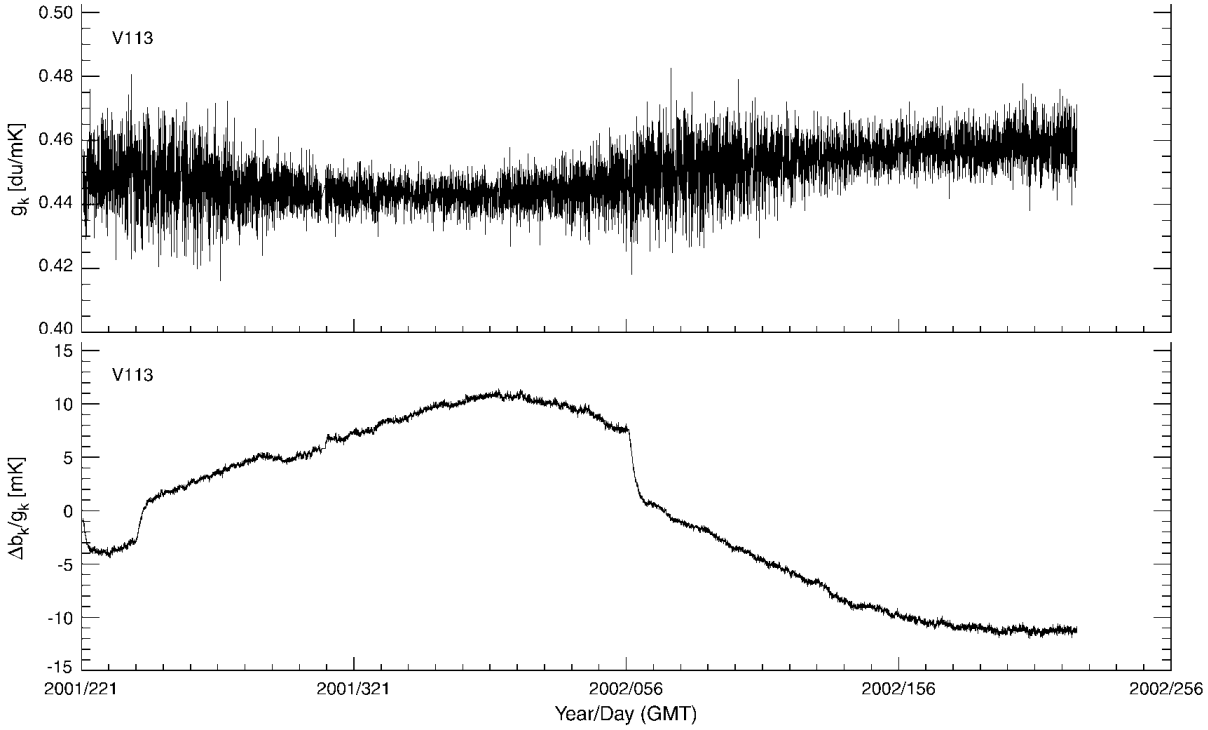

Figure 5: DV113 gain and baseline from [19, p.72].

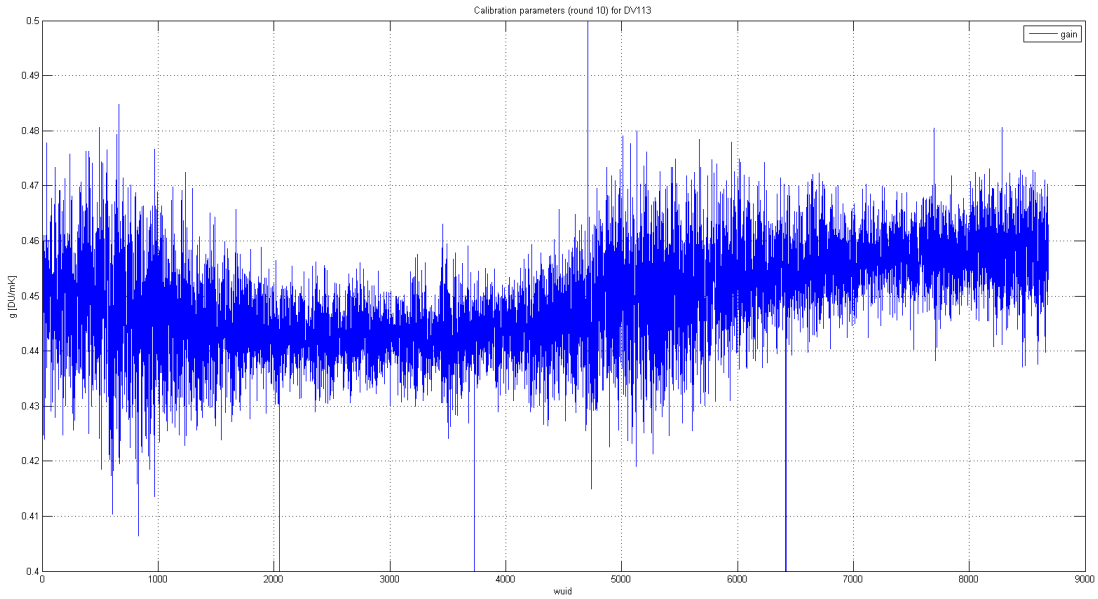

Figure 6: DV113 gain from iteration # 10.

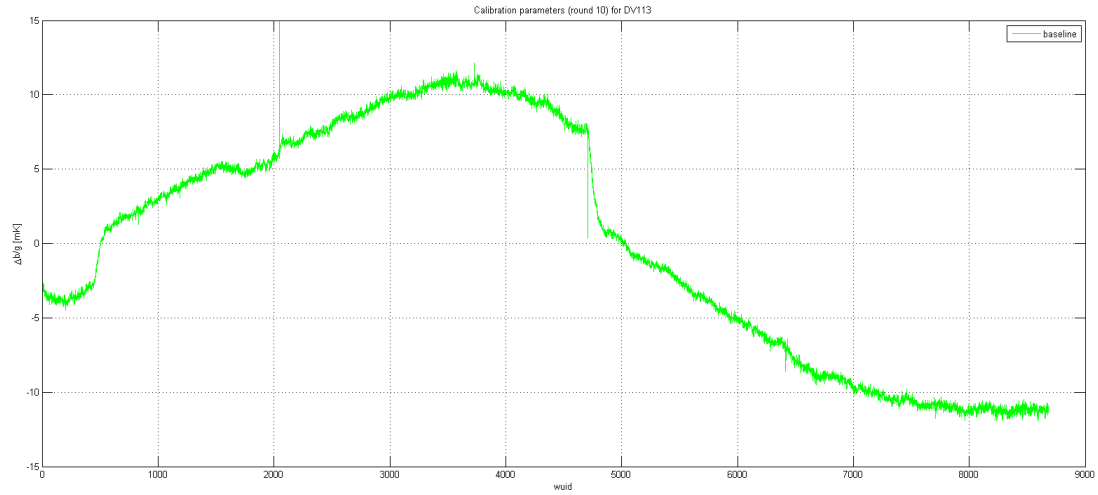

Figure 7: DV113 baseline variation around the yearly mean in units of mK from iteration # 10.

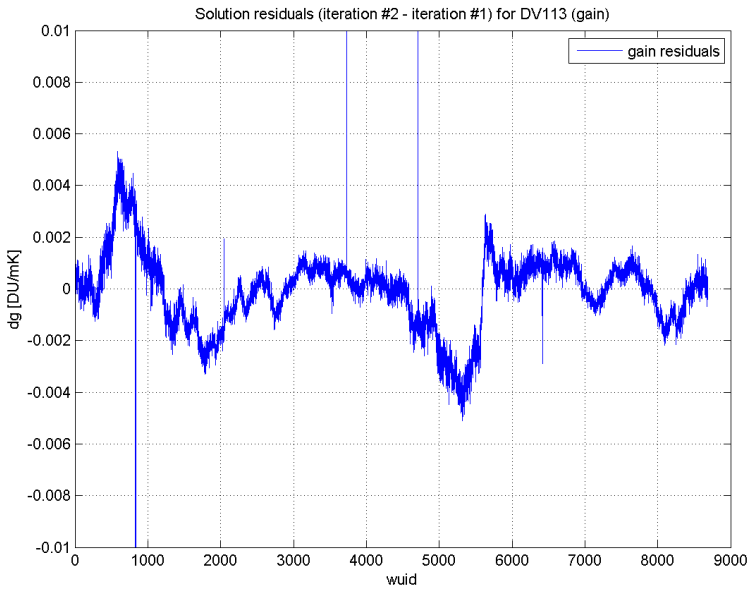

Figure 8: Change in DV113 gain between iteration # 1 and 2.

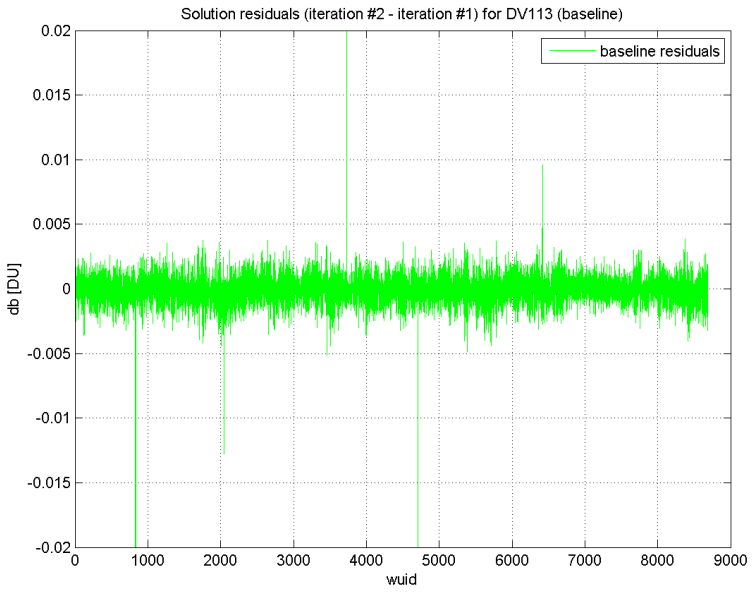

Figure 9: Change in DV113 baseline between iteration # 1 and 2.

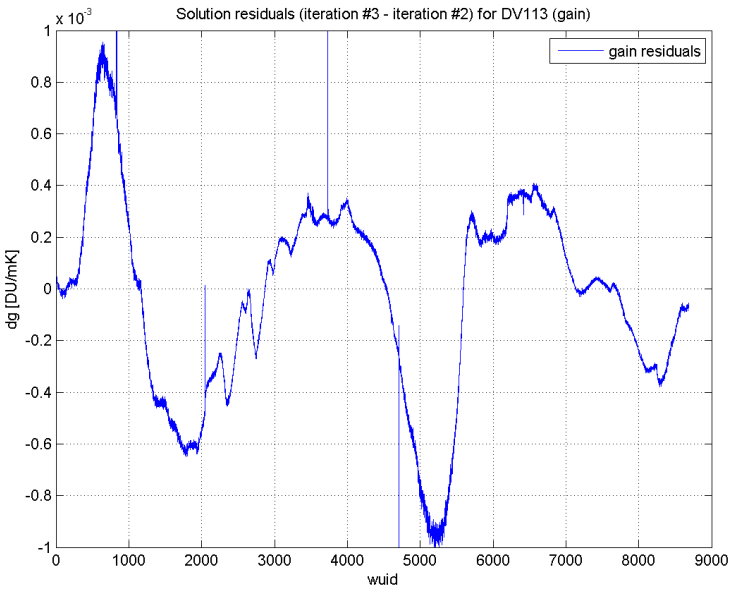

Figure 10: Change in DV113 gain between iteration # 2 and 3.

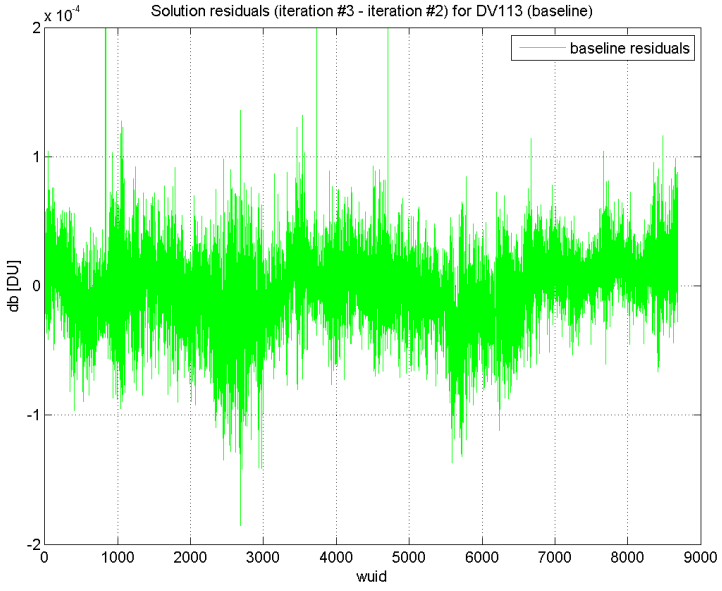

Figure 11: Change in DV113 baseline between iteration # 2 and 3.

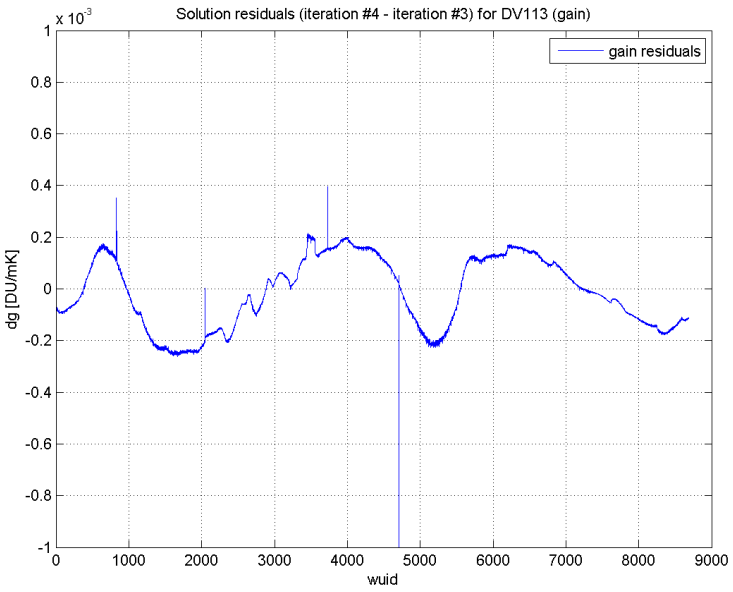

Figure 12: Change in DV113 gain between iteration # 3 and 4.

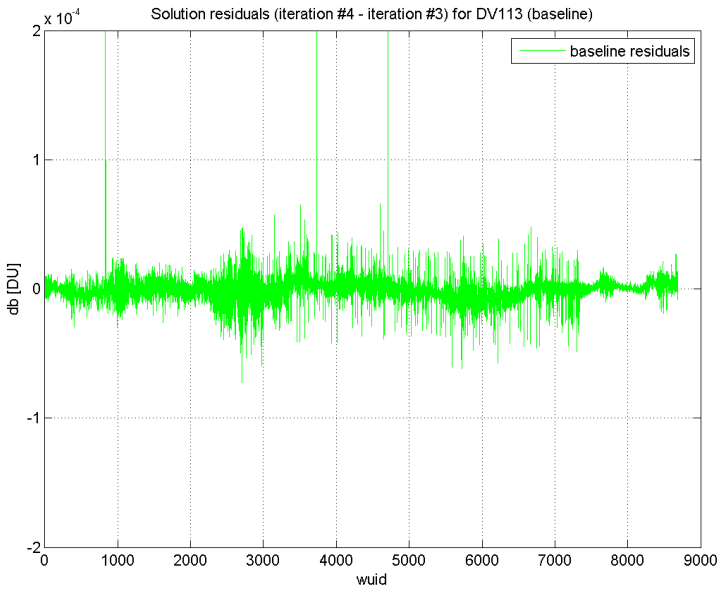

Figure 13: Change in DV113 baseline between iteration # 3 and 4.

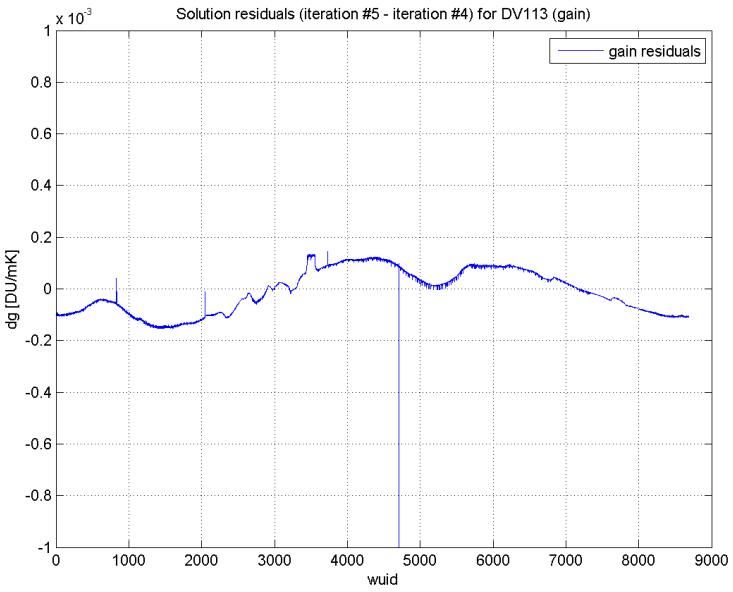

Figure 14: Change in DV113 gain between iteration # 4 and 5.

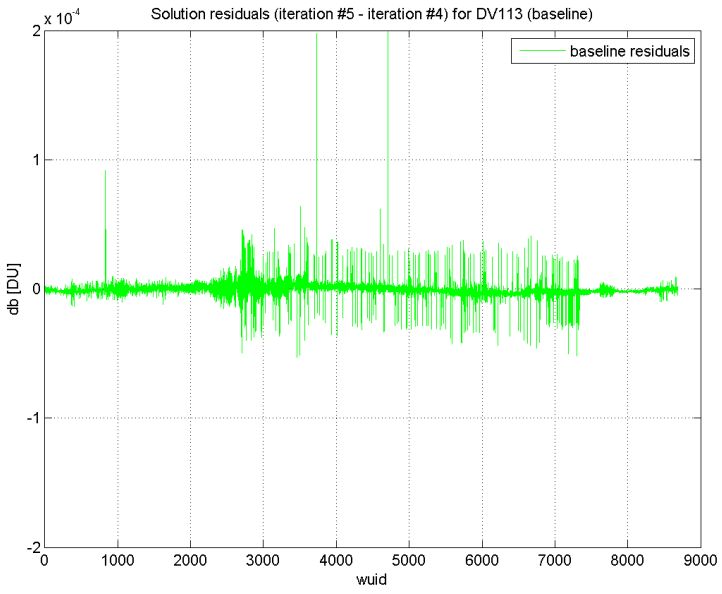

Figure 15: Change in DV113 baseline between iteration # 4 and 5.

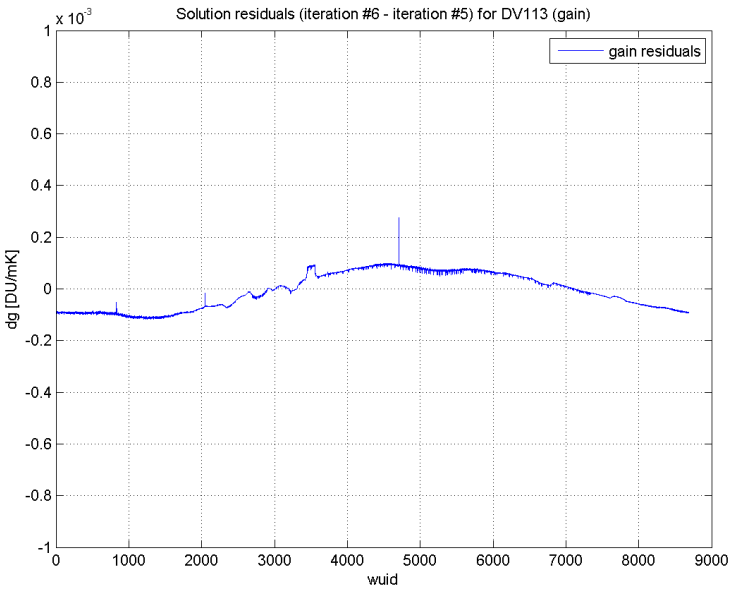

Figure 16: Change in DV113 gain between iteration # 5 and 6.

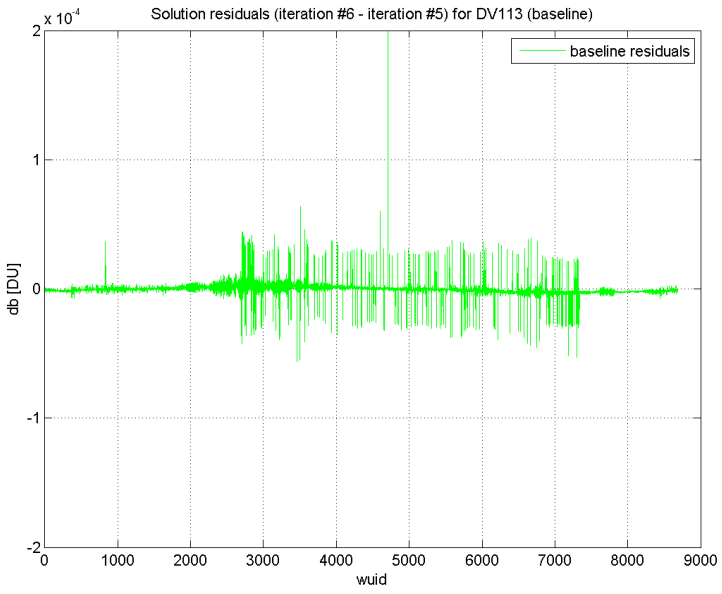

Figure 17: Change in DV113 baseline between iteration # 5 and 6.

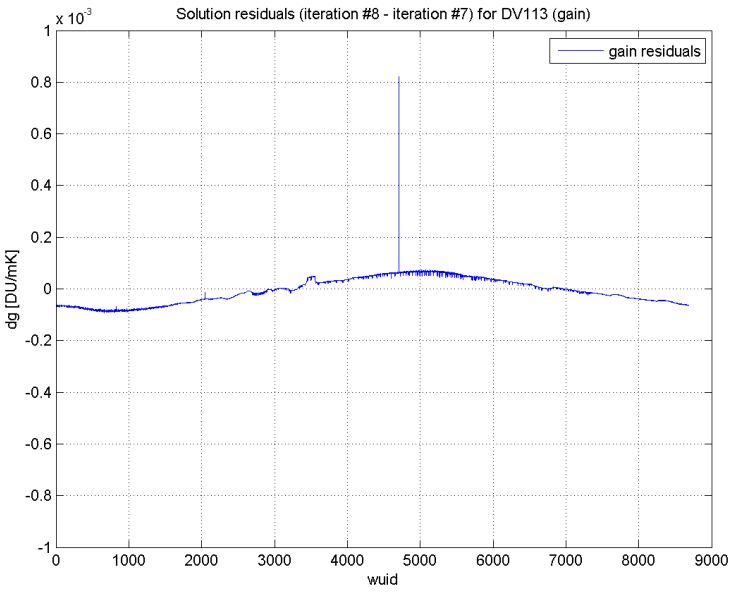

Figure 18: Change in DV113 gain between iteration # 7 and 8.

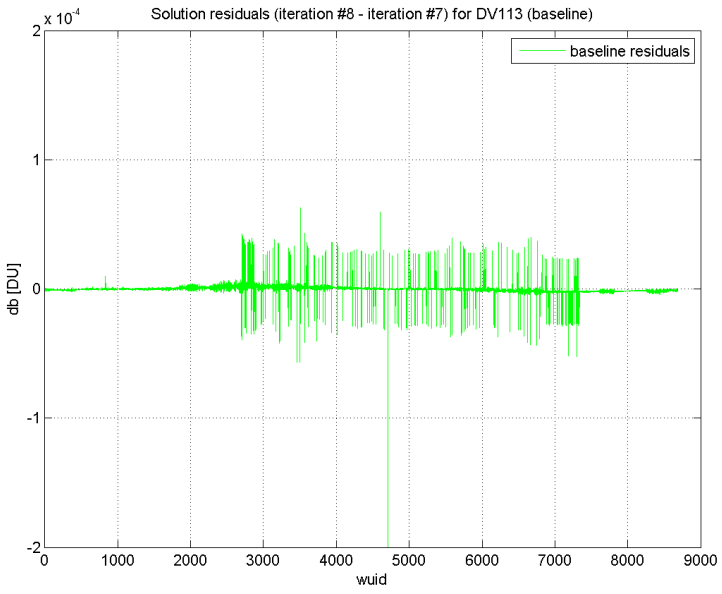

Figure 19: Change in DV113 baseline between iteration # 7 and 8.

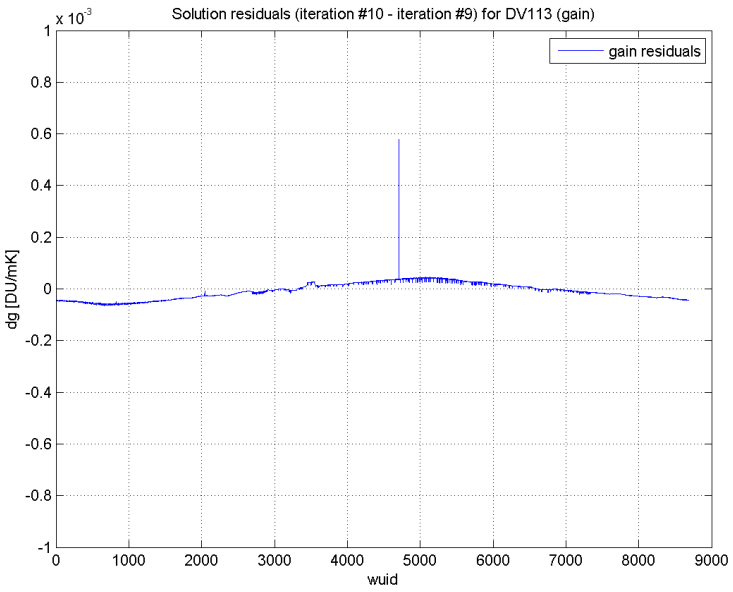

Figure 20: Change in DV113 gain between iteration # 9 and 10.

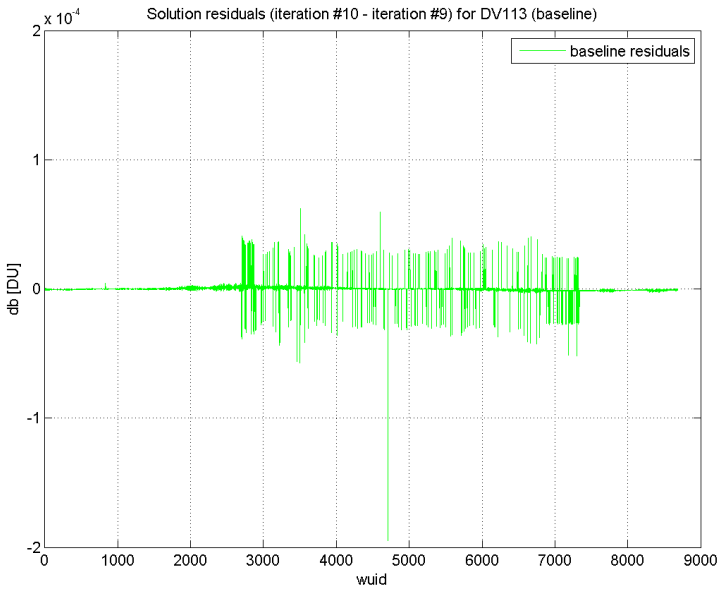

Figure 21: Change in DV113 baseline between iteration # 9 and 10.

Another source of information on the calibration convergence is the iterative raw TOD reduction and reduction maps discussed below. As described in the section on Data Calibration the estimate of CMB fluctuations and other deviations from the dipole is removed from the raw TOD at the end of each iterative run. The reduced raw data then enters the next iteration. The following five plots show statistics of the fluctuation estimates removed in ten consecutive reduction runs on the V1 detector assembly. These statistics include median, standard deviation and median of absolute values of fluctuation estimates in photon counts.

The conclusion is the same for all four V1 detectors. The calibration improvement is most marked during the first two runs. The magnitude of change in the raw data then converges around the fourth iteration and stays nearly constant thereafter.

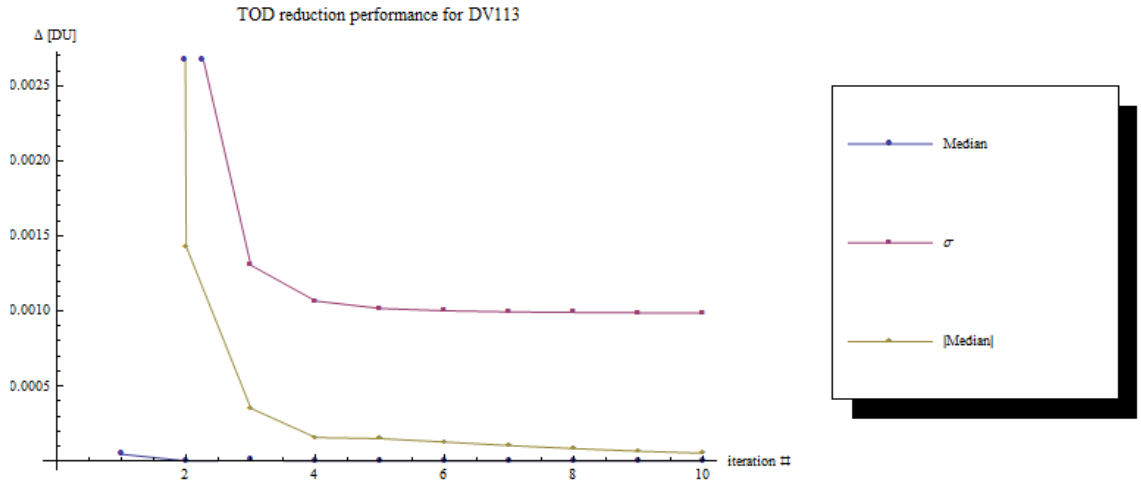

Figure 22: Fluctuation estimates in counts removed from V113 raw data during the iterative calibration procedure.

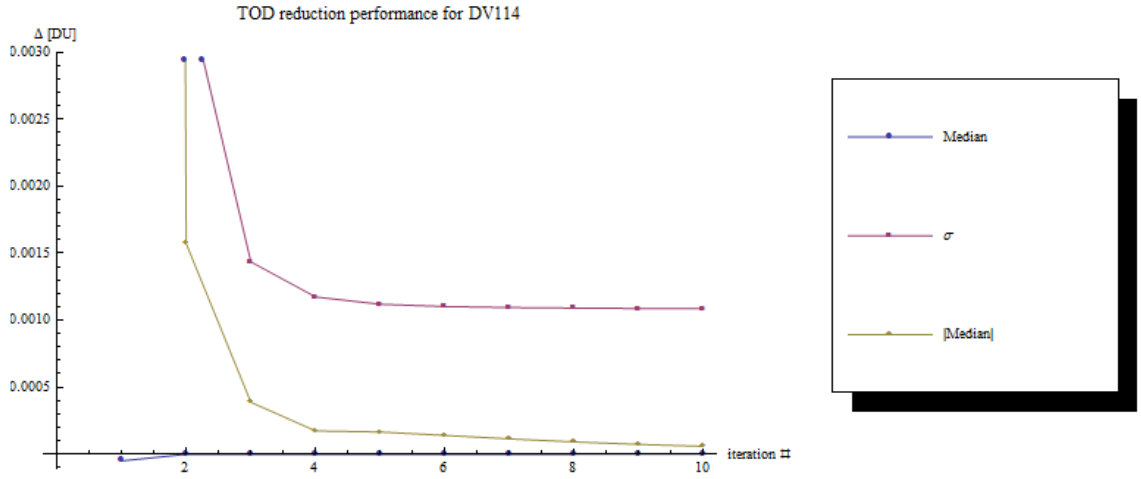

Figure 23: Fluctuation estimates in counts removed from V114 raw data during the iterative calibration procedure.

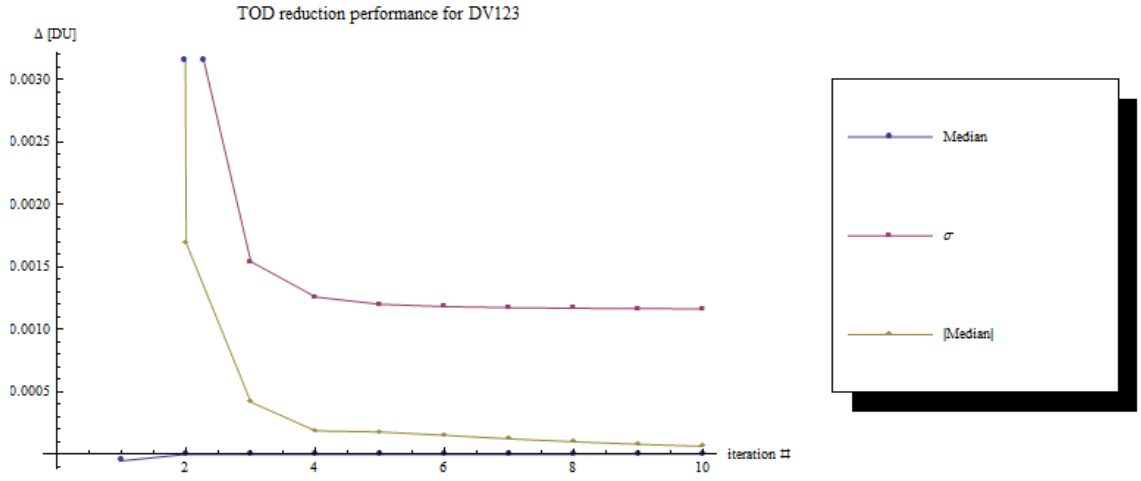

Figure 24: Fluctuation estimates in counts removed from V123 raw data during the iterative calibration procedure.

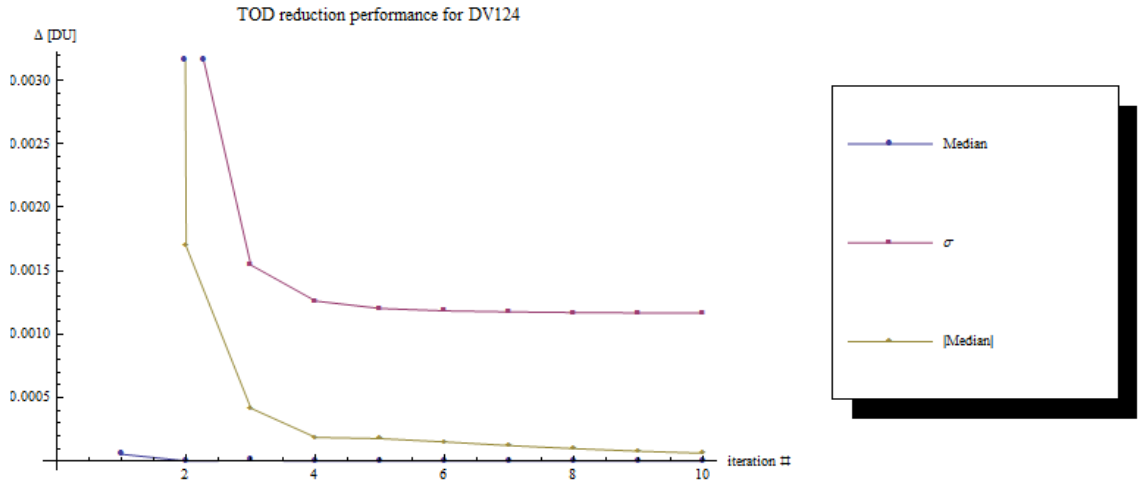

Figure 25: Fluctuation estimates in counts removed from V124 raw data during the iterative calibration procedure.

The following figures show differences between consecutive V1 final maps. The last significant change (relative to the temperature scale ± 0.025mK adopted in this work) is between the third and fourth iteration. The change between the subsequent iterative runs is visible only with reduced temperature scale.

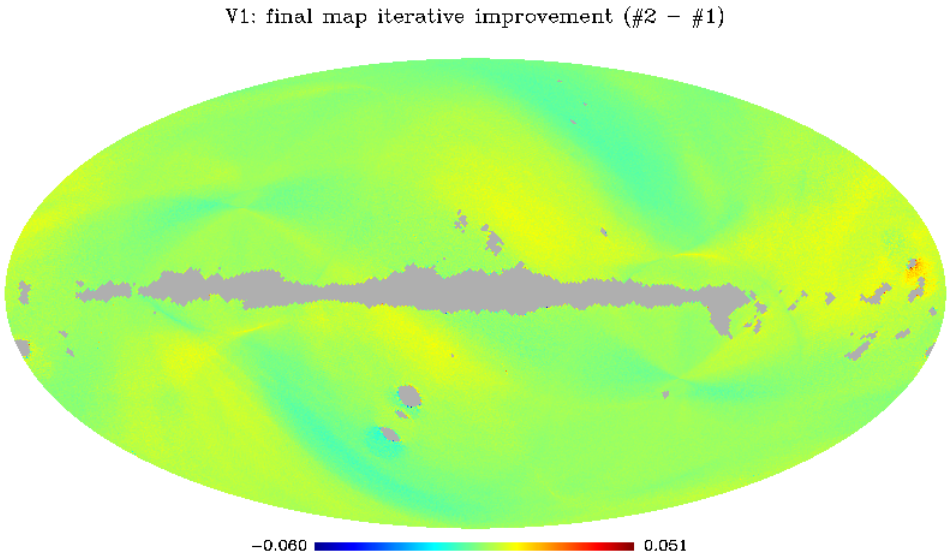

Figure 26: Change in V1 final map between iteration # 1 and 2 in units of mK ($N_{side} = 512$).

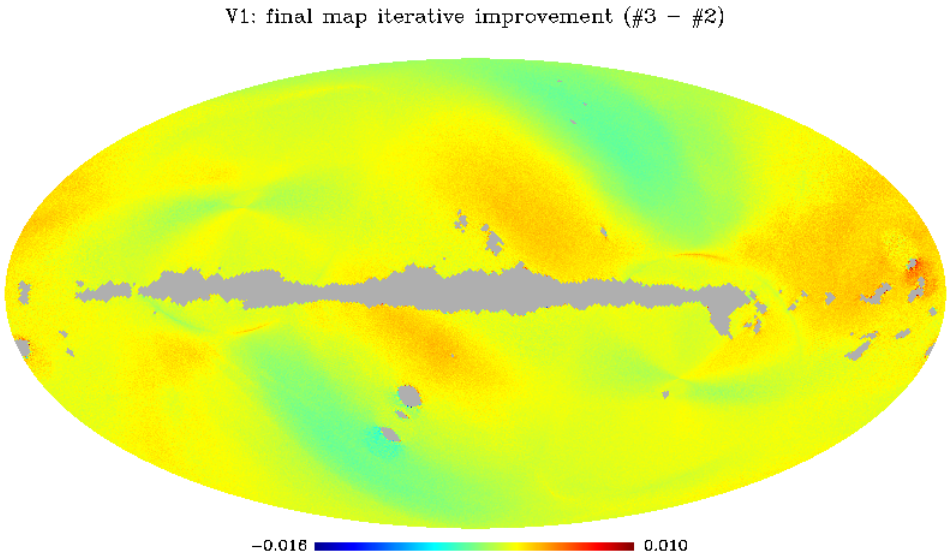

Figure 27: Change in V1 final map between iteration # 2 and 3 in units of mK ($N_{side} = 512$).

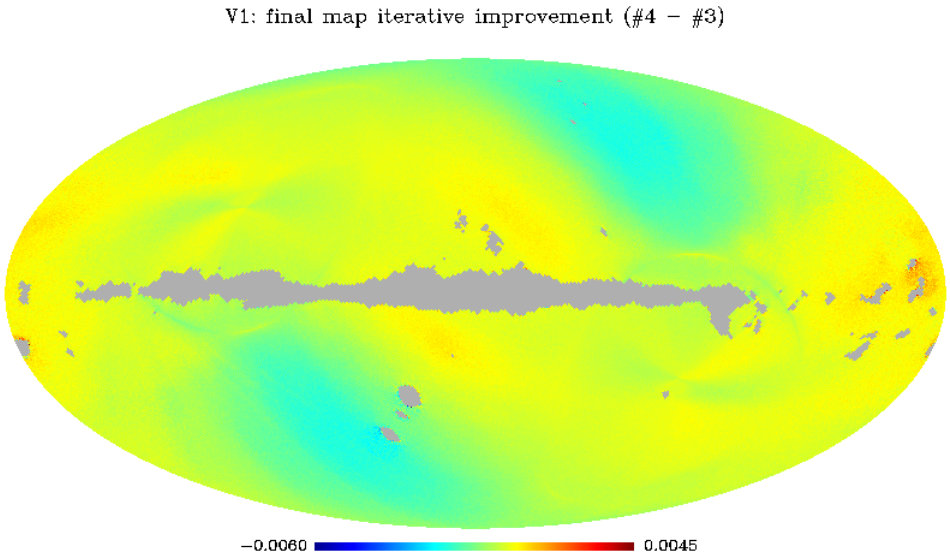

Figure 28: Change in V1 final map between iteration # 3 and 4 in units of mK ($N_{side} = 512$).

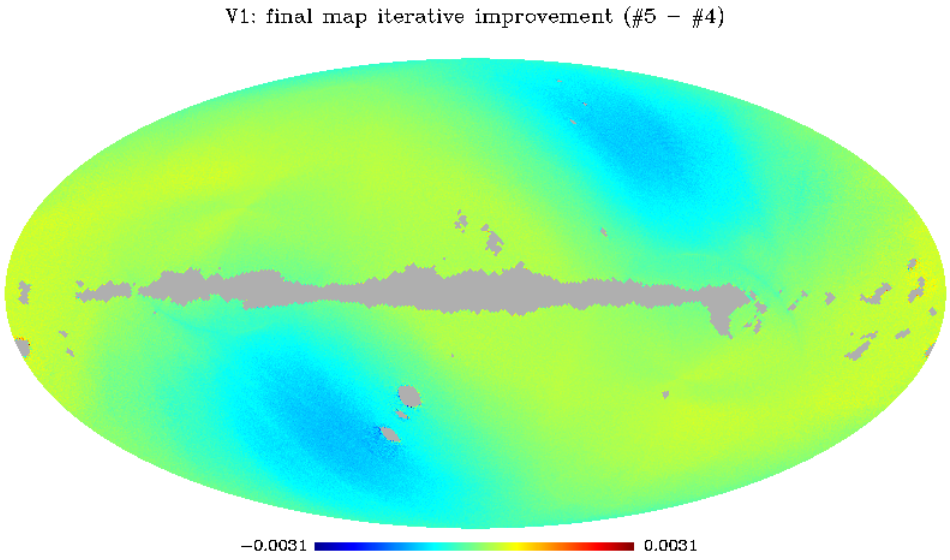

Figure 29: Change in V1 final map between iteration # 4 and 5 in units of mK ($N_{side} = 512$).

The following maps are iterative anisotropy (reduction) maps subtracted from raw data in the raw data reduction step of the calibration pipeline. As can be seen from a quick look at the figures there is progressively less structure with every iteration. Most of the fluctuation background is removed in the first run. Changing calibration parameters induce some visible structure into the maps but as the calibration solutions converge this induced structure diminishes with every iteration. This is in agreement with previous plots (8 - 17) that show decreasing change in the calibration parameters with every iteration.

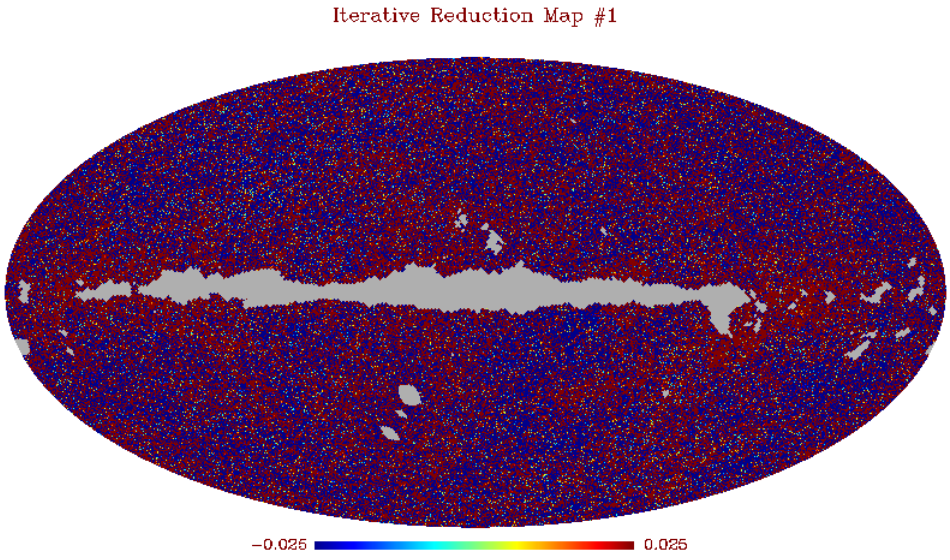

Figure 30: V1 reduction map from iteration # 1 in units of mK ($N_{side} = 512$).

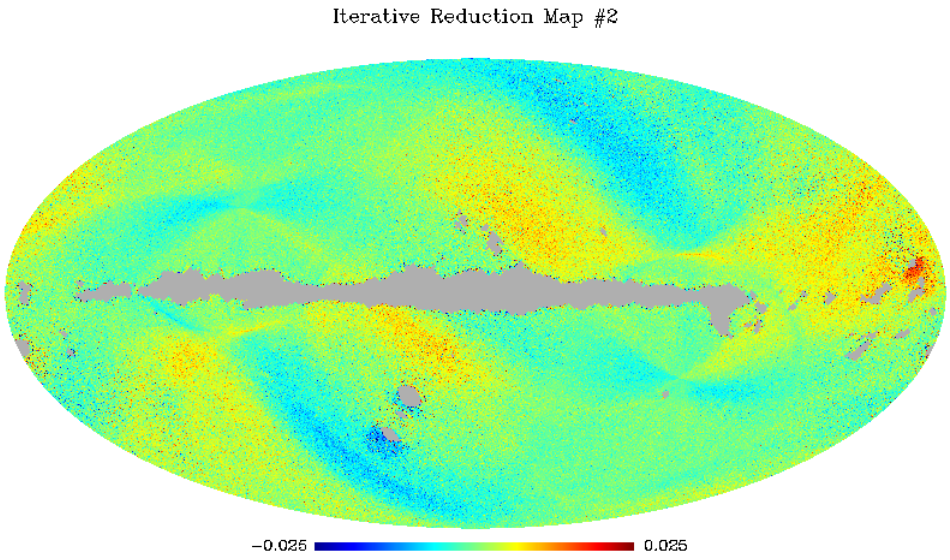

Figure 31: V1 reduction map from iteration # 2 in units of mK ($N_{side} = 512$).

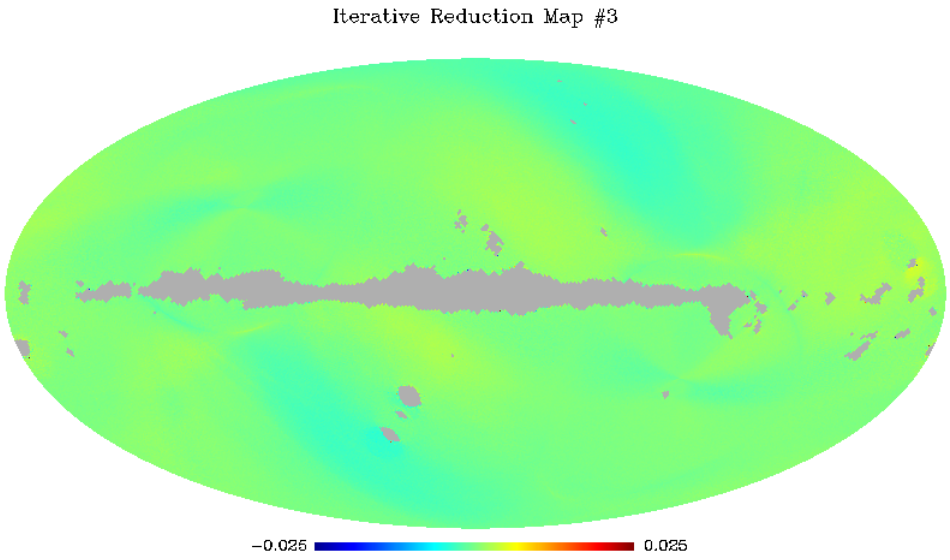

Figure 32: V1 reduction map from iteration # 3 in units of mK ($N_{side} = 512$).

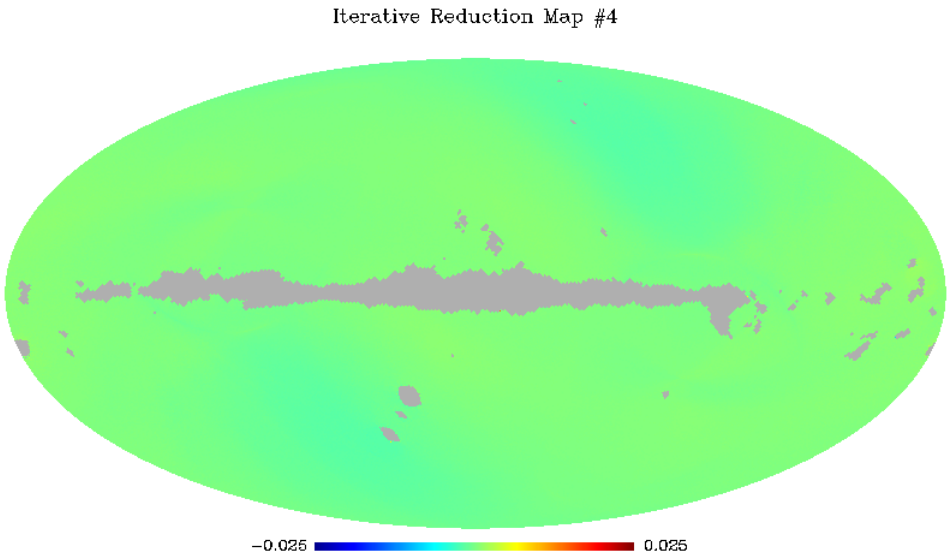

Figure 33: V1 reduction map from iteration # 4 in units of mK ($N_{side} = 512$).

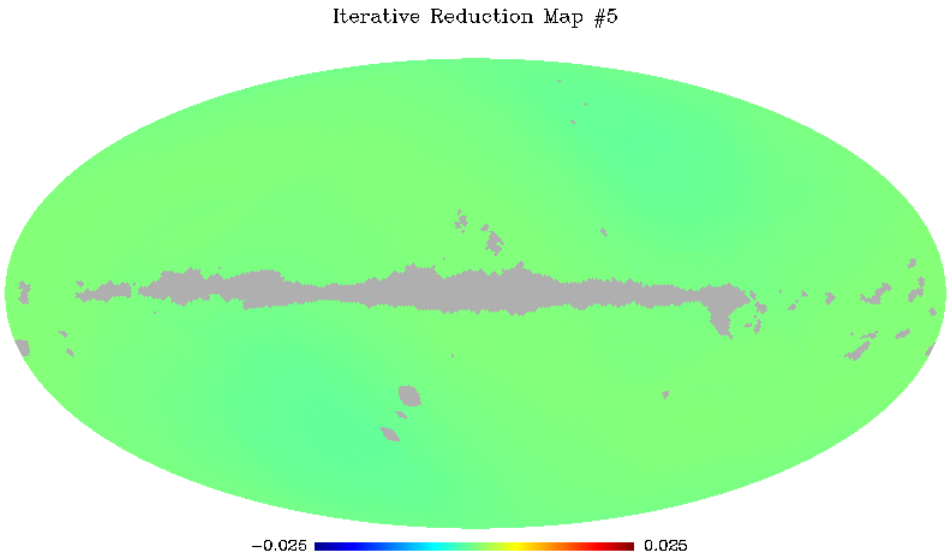

Figure 34: V1 reduction map from iteration # 5 in units of mK ($N_{side} = 512$).

The analysis above suggests that the change in the raw data due to TOD reduction is most significant during the first four iterations (figures 22 - 25). This conclusion is supported by the iterative reduction maps (figures 30 - 34), which are the sources of fluctuation estimates used in TOD reduction. The first four maps exhibit most marked relative pattern changes.

Since the raw data reduction in turn affects the calibration solutions computed in the following calibration run and the last marked reduction of the raw TOD is between iterations # 3 and 4 one would expect the corresponding calibration improvement between solutions from iterations # 4 and 5. The magnitude of the subsequent calibration improvements should be nearly constant. This claim is supported by DV113 solution residuals (figures 8 - 21).

By the same reasoning, the most significant improvement of the final maps should also occur in the first five iterations (figures 26 - 29). This is not to say that more iterations are not necessary. The calibration solutions and final maps keep improving past the fifth iteration. The magnitudes of further improvements are just relatively smaller and fairly constant (see figure 80 - Q1 iteration # 10 and 15 final map difference).

This and time constraints are essentially the reasons why we adopt ten-iteration calibration for our final products.

Table (4) compares officially published calibration statistics [19, Table 3] with our results for selected detectors. Note that only the gain yearly means were officially published.

detector	our gain	official gain	our baseline
DQ113	1.013100 ± 0.001307	1.015	$25621.959652 \pm 0.061394$
DQ114	-0.948072 ± 0.001084	-0.948	$25499.139122 \pm 0.063206$
DQ123	0.473398 ± 0.000446	0.475	$25500.045558 \pm 0.007559$
DQ124	-0.518809 ± 0.001297	-0.518	$25668.160299 \pm 0.009191$
DV113	0.449434 ± 0.000348	0.449	$19048.472815 \pm 0.037725$
DV114	-0.493716 ± 0.000161	-0.494	$19127.964297 \pm 0.032015$
DV123	-0.531618 ± 0.000229	-0.532	$19379.676324 \pm 0.011731$
DV124	0.532343 ± 0.000429	0.532	$19080.255483 \pm 0.015171$
DW113	0.309810 ± 0.000593	0.311	$12427.173020 \pm 0.017741$
DW114	-0.331145 ± 0.000268	-0.332	$13570.255796 \pm 0.038710$
DW123	0.261376 ± 0.000188	0.262	$13029.567858 \pm 0.193104$
DW124	-0.238436 ± 0.000164	-0.239	$12954.386459 \pm 0.227638$

Table 4: Yearly gain and baseline means.

Finally, we compare the final (after ten iterations) calibrated TOD to the officially released first-year calibrated data. In order to reduce the size of the official calibrated TOD only the average over the two channels is included for each radiometer. The data is therefore presented as two polarization vectors. In case of the first-year release, with which we compare our results, the polarization data was not available and all radiometer and polarization channels were averaged together.

This fact significantly limits our ability to reliably compare the results of our calibration to the official ones, as we can compare only the averages over all detector channels potentially resulting in misleading conclusions. We nevertheless decided to perform this comparison hoping that any significant deviations of our calibration from the official one would show up.

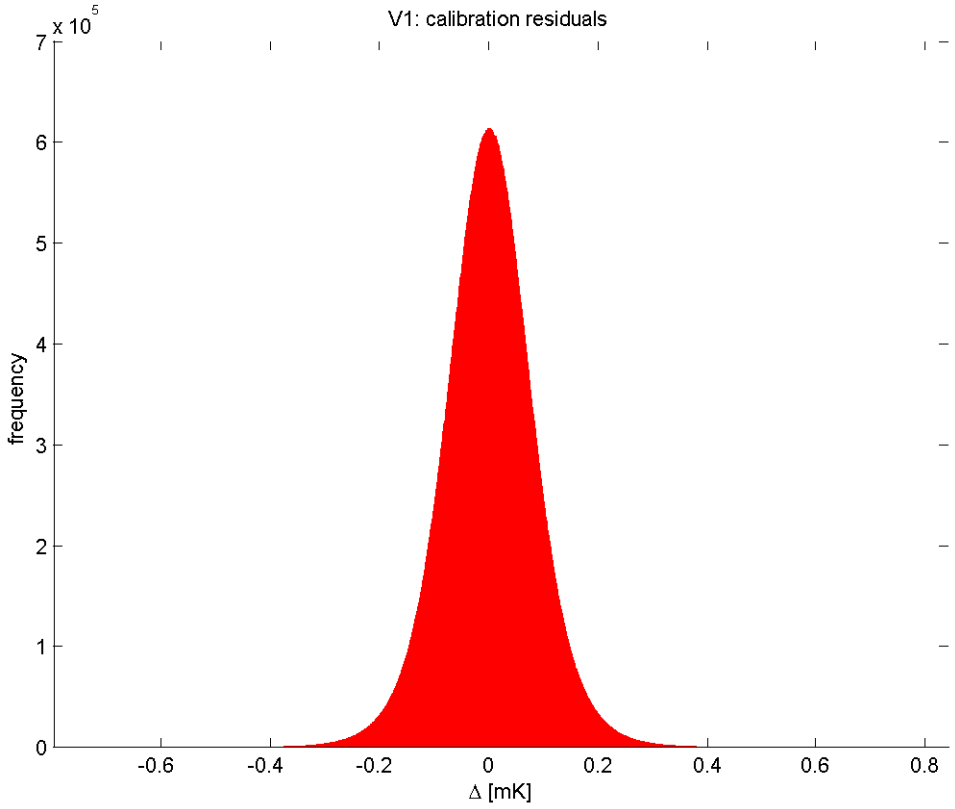

Figure 35: The residuals between our and official first-year official calibration (Freedman-Diaconis bins). $\tilde{\mu} = 0.000014$mK; MAD $= 0.052814$mK;

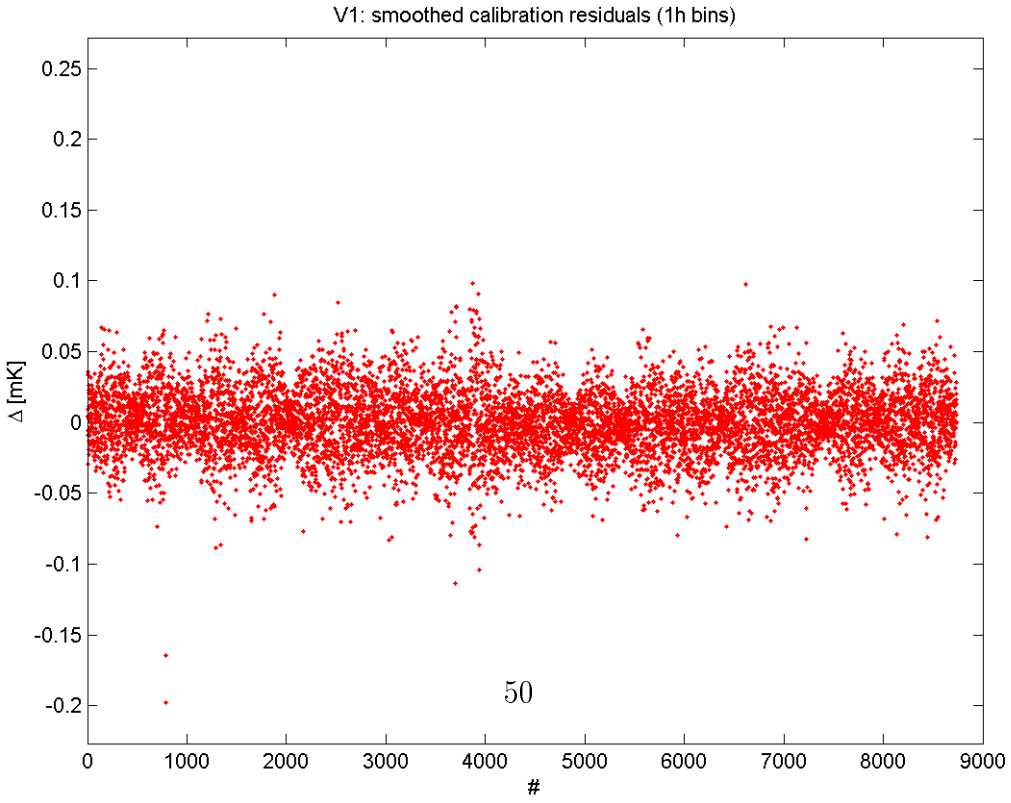

Figure 36: smoothed scatter plot of the calibration residuals (1 hour bins). $\tilde{\mu} = 0.000124$mK; MAD $= 0.014078$mK;

Because there are a few severe outliers in the data we prefer robust statistical measures such as median and median absolute deviation (MAD) to more common mean and standard deviation.

Although, we note the apparent periodic changes of the variance observed in the smoothed scatter plot, the residuals are random, narrowly centered around zero, not showing any overall trend. In addition to the qualitative analysis performed we take this as yet another indication supporting the confidence in the correctness of our reproduction of the official calibration procedure.

Based on the visual inspection of the plots discussed above we did not notice any significant discrepancies from the official calibration. We therefore feel confident to start using our calibration software for our subsequent work. But note that our current confidence is largely based on visual inspection of the above plots and although we did not find any significant discrepancies between our and official results the two parameter sets are not exactly equal as can be seen from the yearly gain means that in some cases show significant discrepancies from the official results. We discuss the effects of our calibration solutions on the final maps in section “Final Maps".

Before proceeding with timing-offset tests we would like to demonstrate the sensitivity of the solutions on a couple of changes in the calibration pipeline. Figures (37) and (38) show the effect of masking on the gain and baseline solutions from the first iterative calibration run (before fluctuation removal). The solutions were generated without masking. The figures are to be compared with preceding plots (6) and (7) which were using a processing mask available on the WMAP website [1].

[1] http://lambda.gsfc.nasa.gov/product/map/current/

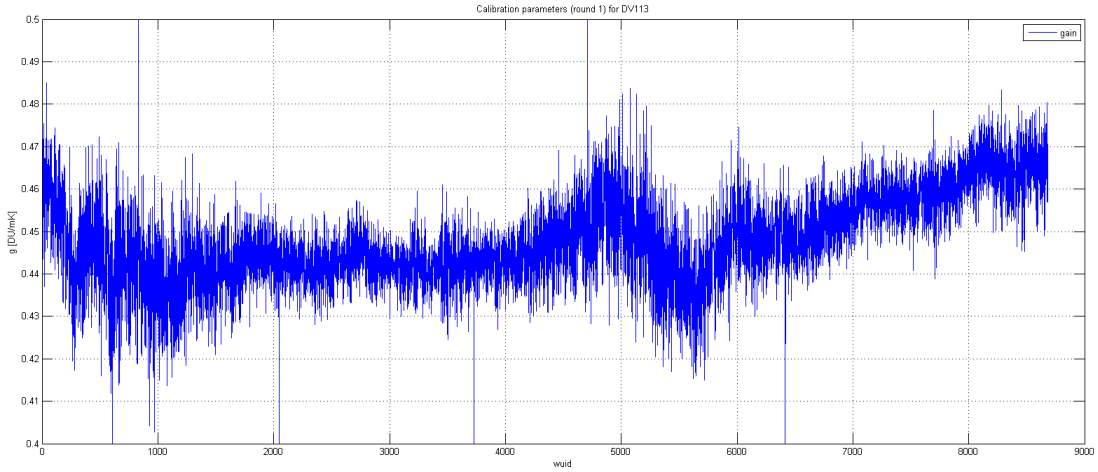

Figure 37: DV113 gain from iteration # 1 without masking.

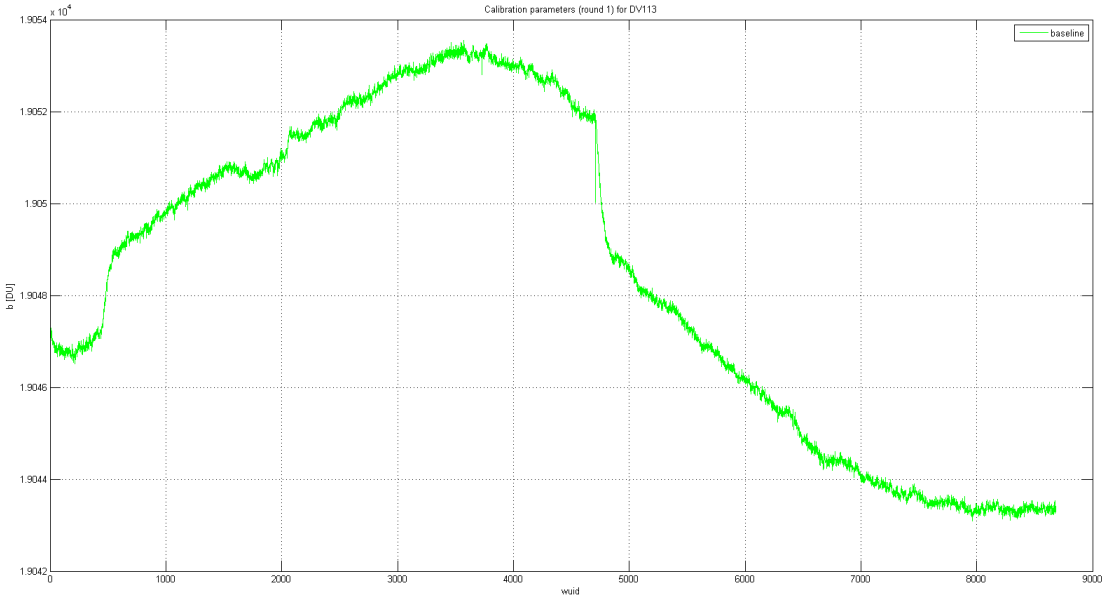

Figure 38: DV113 baseline from iteration # 1 without masking.

Although, we originally wanted to take a simple approach of not considering the satellite's own velocity around the Sun, we were finally forced to include all velocity components. Figures (39), (40) and (41) demonstrate the effect of not including the satellite's intrinsic velocity in the calibration stage (map-making still includes the velocity). Plots (39) and (40) show a systematic effect on the gain and baseline after five iterative runs. Figure (41) demonstrates the effect on the reduction map. These figures are to be compared to figures (6), (7) and (34).

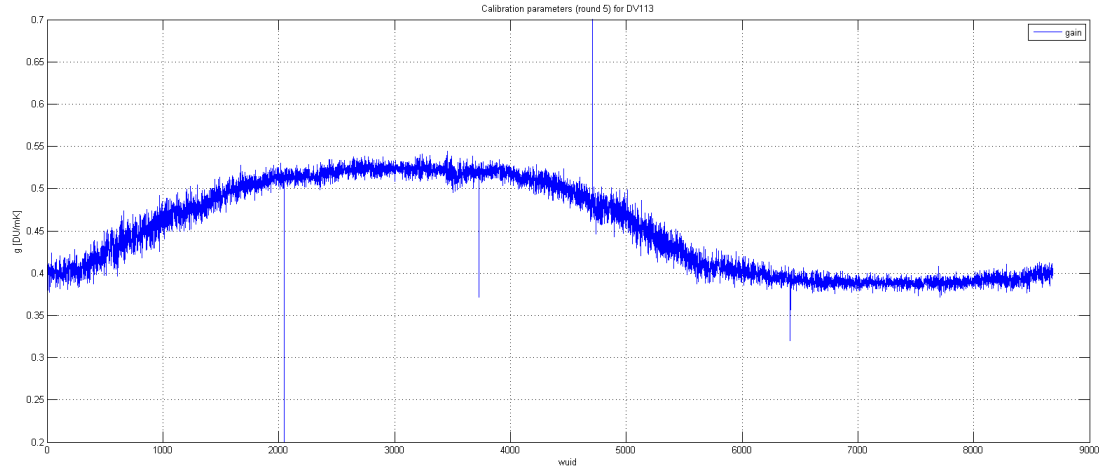

Figure 39: DV113 gain from iteration # 5 with only the galactic motion included.

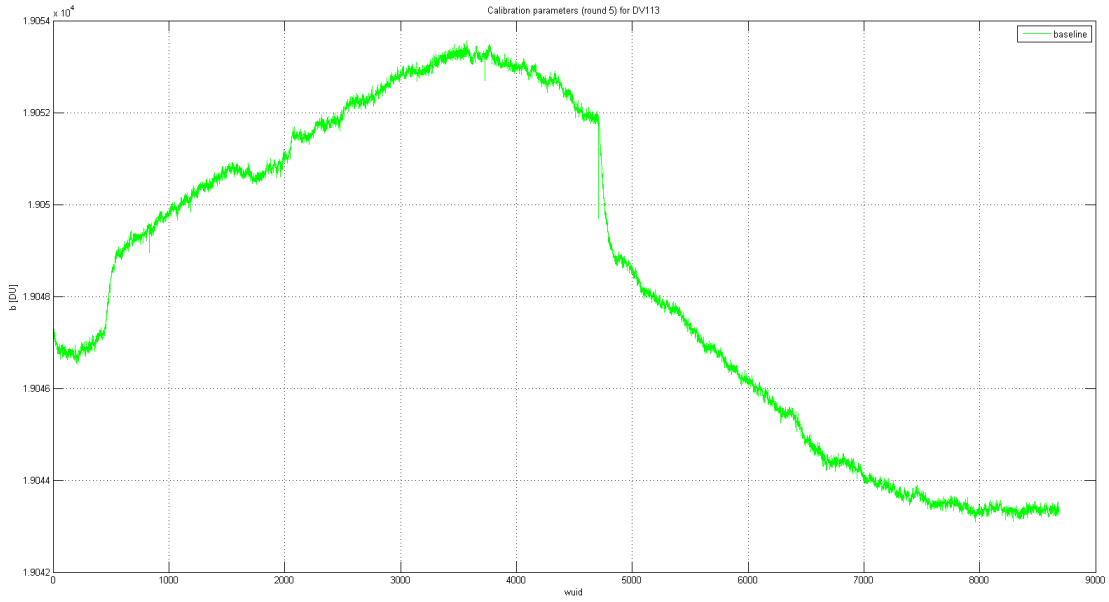

Figure 40: DV113 baseline from iteration # 5 with only the galactic motion included.

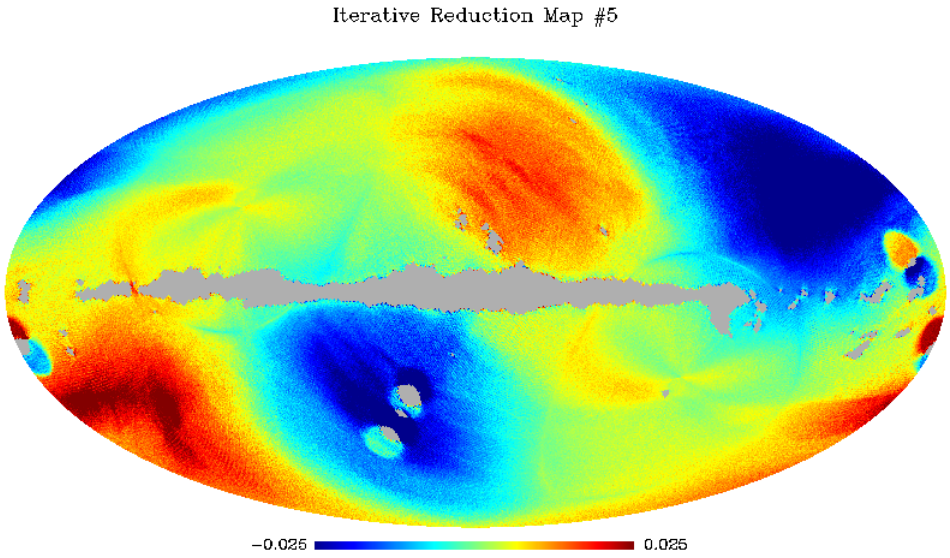

Figure 41: The effect of not including the satellite's intrinsic motion into dipole computations in the calibration stage. V1 reduction map from iteration # 5 in units of mK ($N_{side} = 512$).

8.2 Final Maps

Here we present final maps for three wavebands. Maps shown below are differences between maps generated from officially released WMAP1 calibrated data available on the WMAP website [1] and maps generated from data calibrated by our calibration software. We show two residual maps for each band. One comes from the first iteration (before any raw data reduction takes place). The second one is generated after ten calibration iterations. Both calibration and map-making stages of the processing pipeline use the same (WMAP) offset setting, evaluating pointing at the center of each observation.

We compare our results with the first WMAP release because our procedure most closely follows the first-year official pipeline. Our maps mostly agree with the official maps, however we note two problematic regions in the first and third quadrant. Although, they appear in all bands they are most prominent in the W1 band in which it is comparable in amplitude to the actual CMB fluctuation signal (0.05mK). Considering the Q1 band the magnitude of the problematic regions is comparable to magnitudes of the fluctuations seen in the differential map between the official WMAP3 map and a map produced by the map-making software from the officially released WMAP3 calibrated TOD shown in [1]. We also have to note that our pipeline does not include noise filtering performed on WMAP1 calibrated TOD. The fact that the same pattern is seen in all three bands (possibly with different magnitudes caused by different detector sensitivities) suggests that it originates from a systematic difference between our and the official pipelines. A few possible contributions to this effect include different masking (we apply the processing mask from WMAP3 release), different evaluation of quality

[1] http://lambda.gsfc.nasa.gov/product/map/current/

flags (we exclude all points flagged by documented flags), different dipole parameters (we use WMAP7 dipole) and dipole model (we use the relativistic version including the transmission imbalance coefficients). The official WMAP team also adopts an analytic gain model presented in [21] for the final calibration step which we do not use. The process of iterative calibration is lengthy (one calibration run often takes several hours), based on the observed convergence of calibration solutions and iterative reduction maps (see “Iterative Calibration") we opt for ten iterations. However, more iterations may, at least in theory, have unforeseen effects on the final products of this complex procedure. It could be well caused by some other undocumented difference between the processing pipelines.

The patterns just discussed are the residuals between maps generated from the officially published TOD and TOD calibrated using our software package. Nevertheless, we are ultimately interested in the residual maps produced by subtracting two final maps consistently generated from TOD calibrated by our calibration software using various calibration timing offset modes. Since the patterns discussed above do not appear to depend on the calibration offset mode they should subtract out in the residual maps making it possible to safely use those maps to assess the impacts of various offset modes on the final maps. We therefore proceed with our analysis.

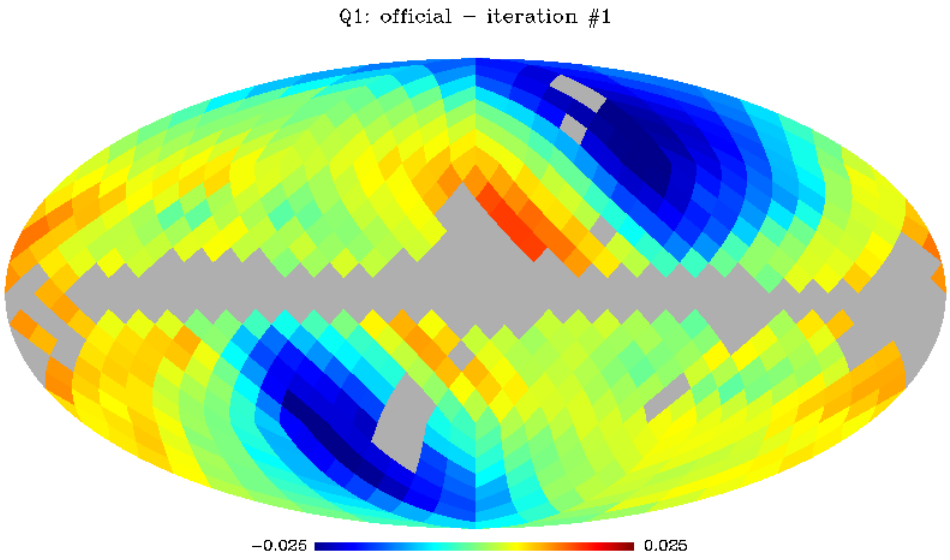

Figure 42: Q1 residual map from iteration # 1 in units of mK ($N_{side} = 8$).

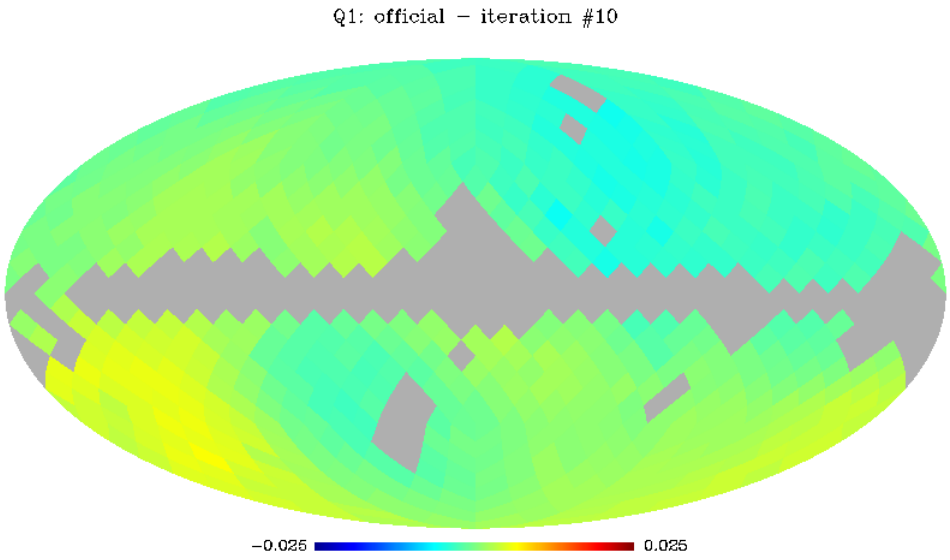

Figure 43: Q1 residual map from iteration # 10 in units of mK ($N_{side} = 8$).

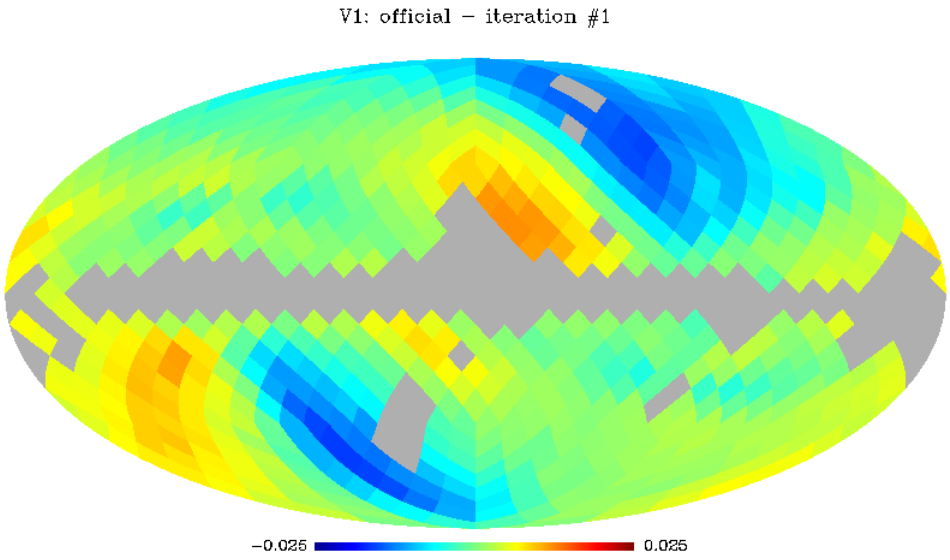

Figure 44: V1 residual map from iteration # 1 in units of mK ($N_{side} = 8$).

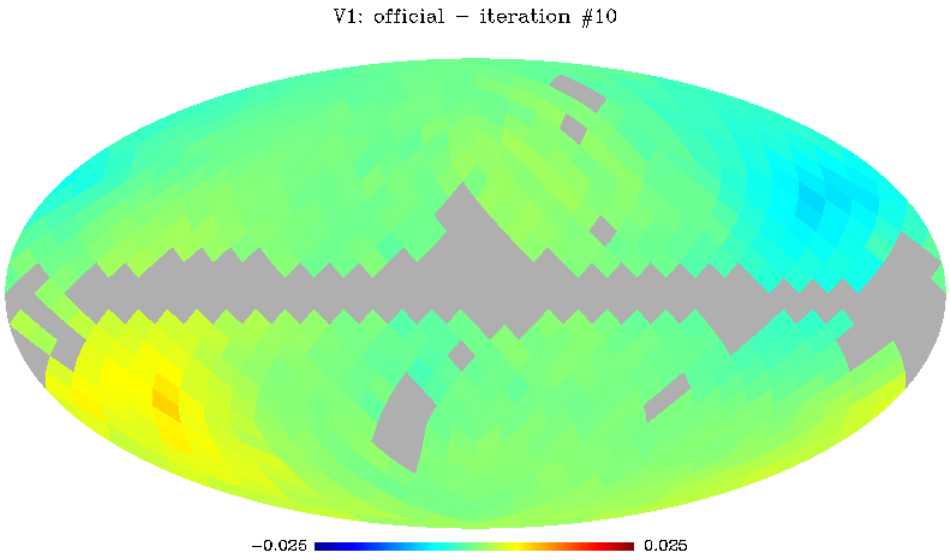

Figure 45: V1 residual map from iteration # 10 in units of mK ($N_{side} = 8$).

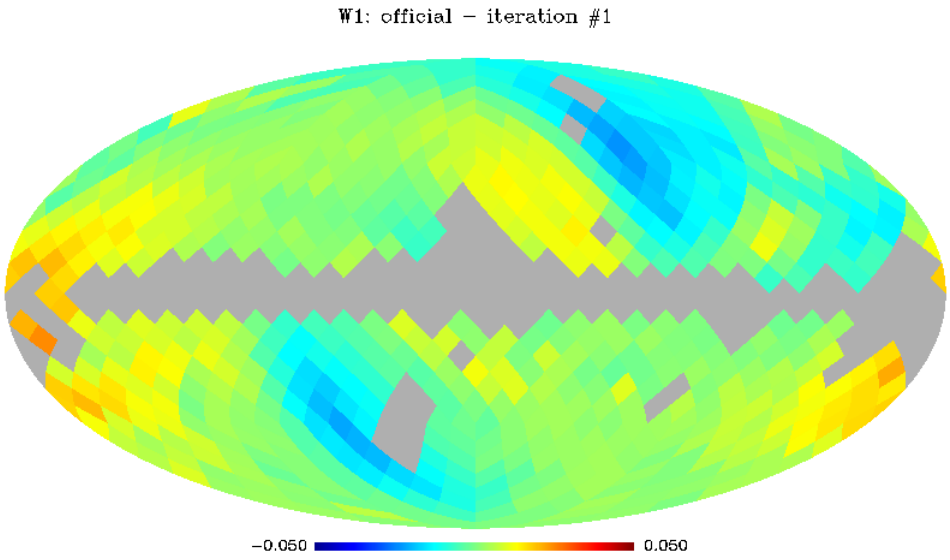

Figure 46: W1 residual map from iteration # 1 in units of mK ($N_{side} = 8$).

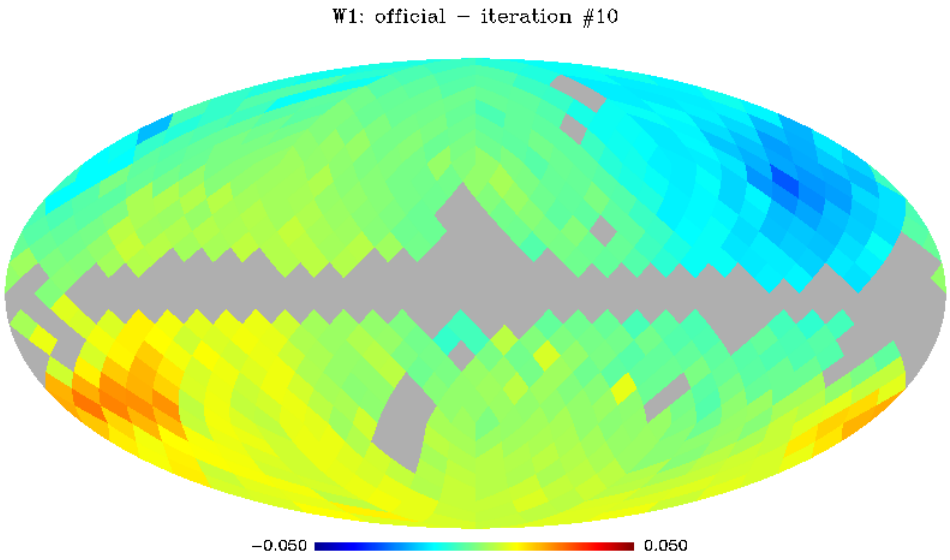

Figure 47: W1 residual map from iteration # 10 in units of mK ($N_{side} = 8$).

8.3 Induced Quadrupole

Our ultimate goal was to find out how significant is the effect of the timing offset on the calibration solutions and final maps. We therefore produced calibration solutions introducing various timing offsets into the calibration and observed the effects on the final maps.

Before proceeding one point has to be clarified. In the following discussion we refer to the “map-making stage" and “calibration stage". By “map-making stage" we mean the final map production from already calibrated TOD. The “calibration stage" refers to computation of calibration solutions. The calibration stage itself also includes some map-making (raw data reduction using intermediate maps). The same offset is always used in both evaluating the dipole in the fitting stage and in generating the reduction maps in the map-making stage of the iterative calibration. When we say that different offsets were used in “map-making" and “calibration" we are not referring to the map-making in the calibration stage which always follows the calibration stage offset, but to the final map production.

Our offset calculation (also referred to as “zero offset" mode) evaluated the pointing at the beginning rather at the center of each observation (WMAP official mode). The offsets used were half of the integration time of each detector (51.2ms for Q, 38.4ms for V and 25.6ms for W).

Table (5) presents yearly means of calibration parameters in the zero offset mode for selected detectors. This table is to be compared to Table (4) which presents yearly means in the WMAP offset mode.

detector	our gain	our baseline
DQ113	1.013453 ± 0.000786	$25621.961787 \pm 0.061348$
DQ114	-0.947368 ± 0.000577	$25499.141399 \pm 0.063022$
DQ123	0.473500 ± 0.000346	$25500.045941 \pm 0.007490$
DQ124	-0.518136 ± 0.000697	$25668.162896 \pm 0.008021$
DV113	0.449487 ± 0.000356	$19048.472787 \pm 0.037725$
DV114	-0.493780 ± 0.000152	$19127.964292 \pm 0.032015$
DV123	-0.531670 ± 0.000257	$19379.676321 \pm 0.011732$
DV124	0.532456 ± 0.000475	$19080.255419 \pm 0.015171$
DW113	0.309517 ± 0.000537	$12427.172958 \pm 0.017740$
DW114	-0.330607 ± 0.000186	$13570.255611 \pm 0.038709$
DW123	0.261007 ± 0.000150	$13029.567980 \pm 0.193103$
DW124	-0.238122 ± 0.000164	$12954.386455 \pm 0.227638$

Table 5: Yearly gain and baseline means in zero offset mode.

We now present the difference between WMAP offset and our (zero) offset calibration after ten iterations for Q1, V1 and W1 bands (figures 46 - 69). We present our results for all detectors and channels as they all enter the map-making procedure and individual detectors exhibit different performance (even within a single assembly) [21]. As can be seen from the following plots the calibration solutions exhibit only mild variations in some detectors (gain parameter for DQ113, DQ114). These discrepancies quantify the effects of various calibration offsets on the calibration solutions. They are not related to the systematic patterns discussed in the previous section because both solution sets were generated using our calibration software. Any systematics not dependent on the offset setting should therefore subtract out. We try to quantify the effect of these variations on the final maps in the

subsequent discussion.

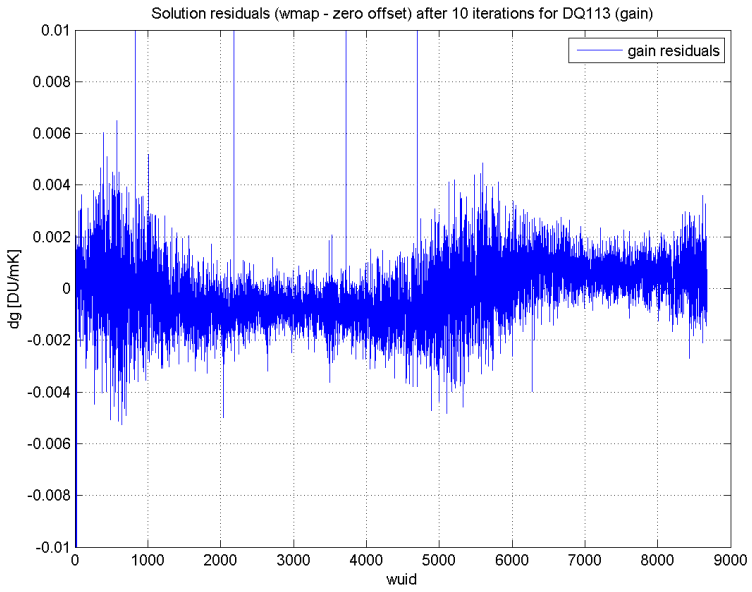

Figure 48: DQ113 gain timing-offset residuals from iteration # 10.

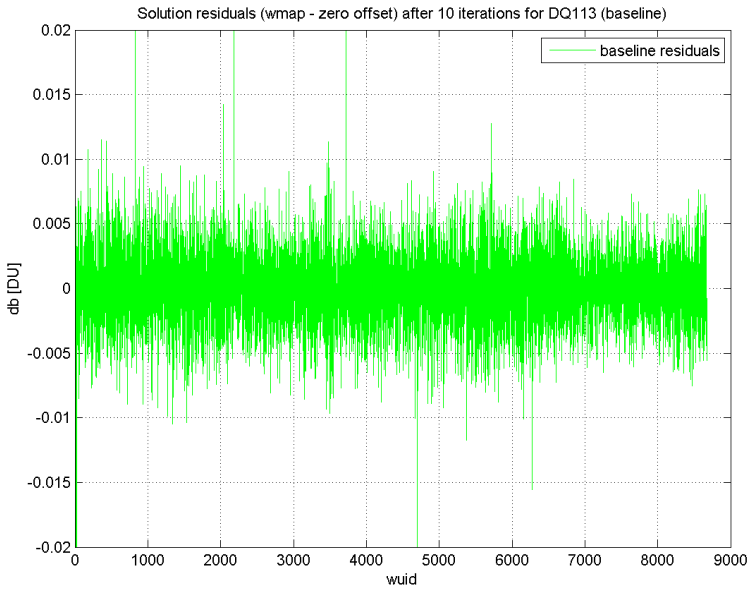

Figure 49: DQ113 baseline timing-offset residuals from iteration # 10.

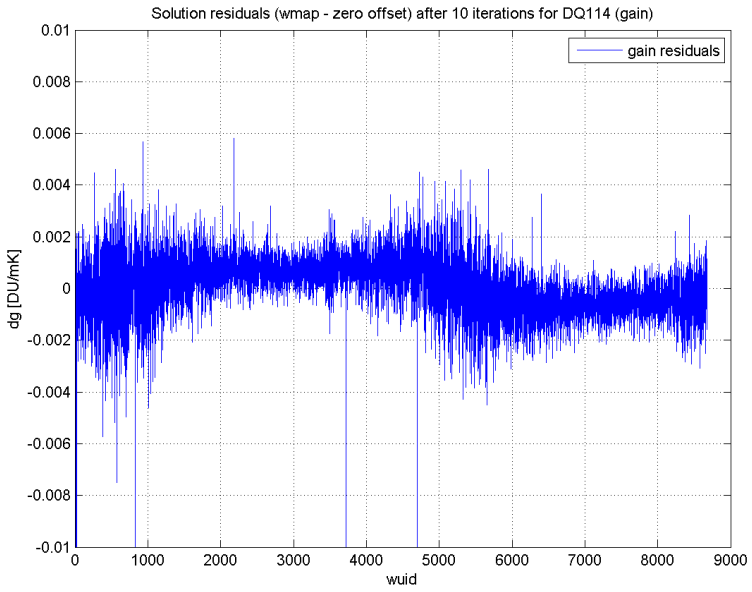

Figure 50: DQ114 gain timing-offset residuals from iteration # 10.

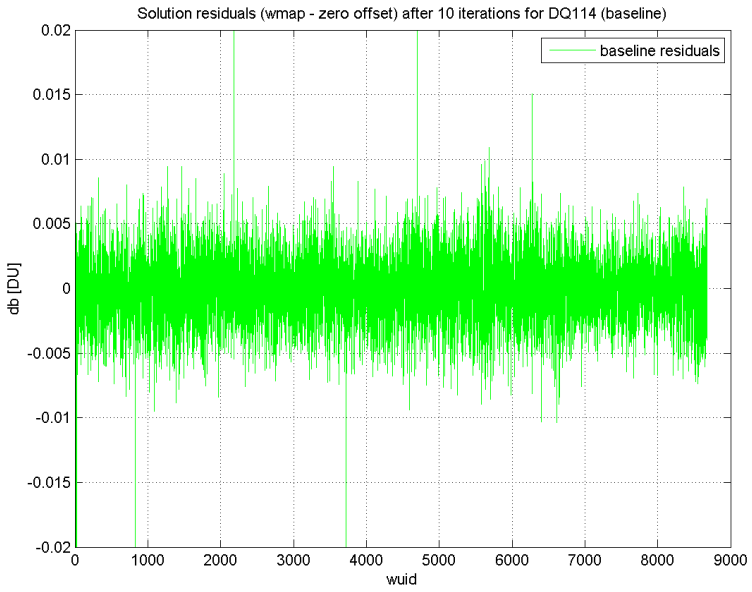

Figure 51: DQ114 baseline timing-offset residuals from iteration # 10.

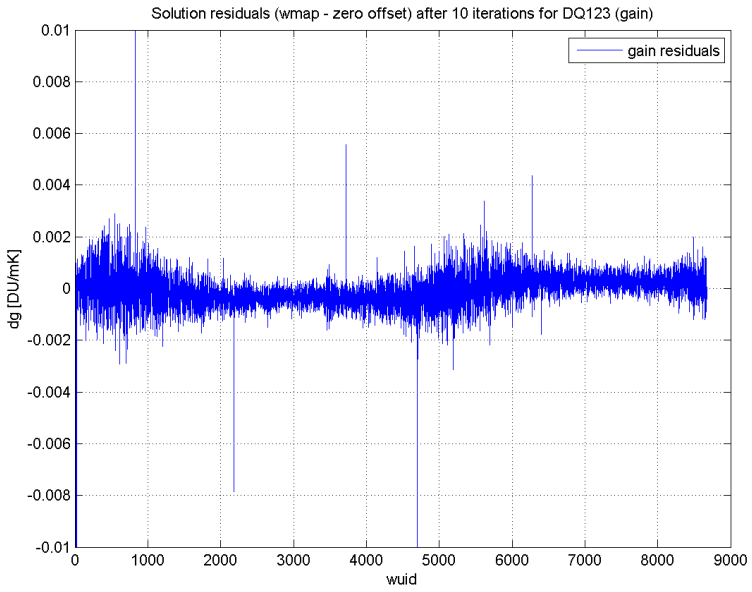

Figure 52: DQ123 gain timing-offset residuals from iteration # 10.

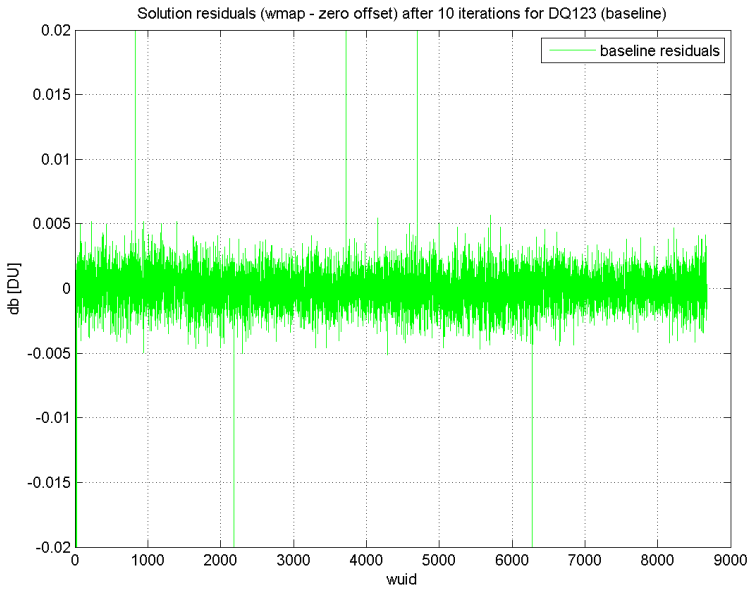

Figure 53: DQ123 baseline timing-offset residuals from iteration # 10.

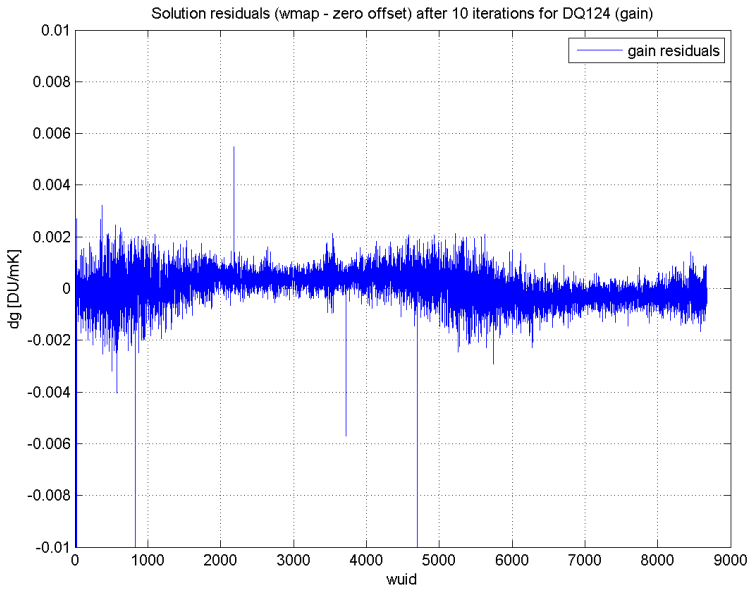

Figure 54: DQ124 gain timing-offset residuals from iteration # 10.

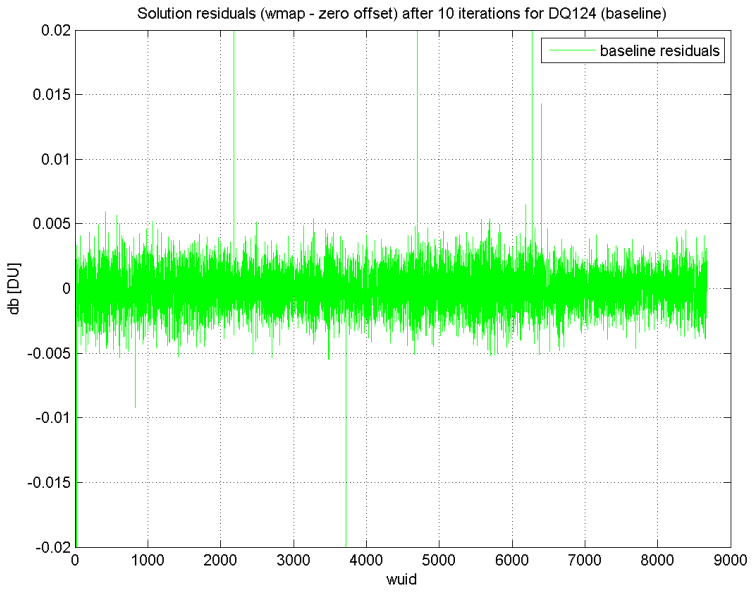

Figure 55: DQ124 baseline timing-offset residuals from iteration # 10.

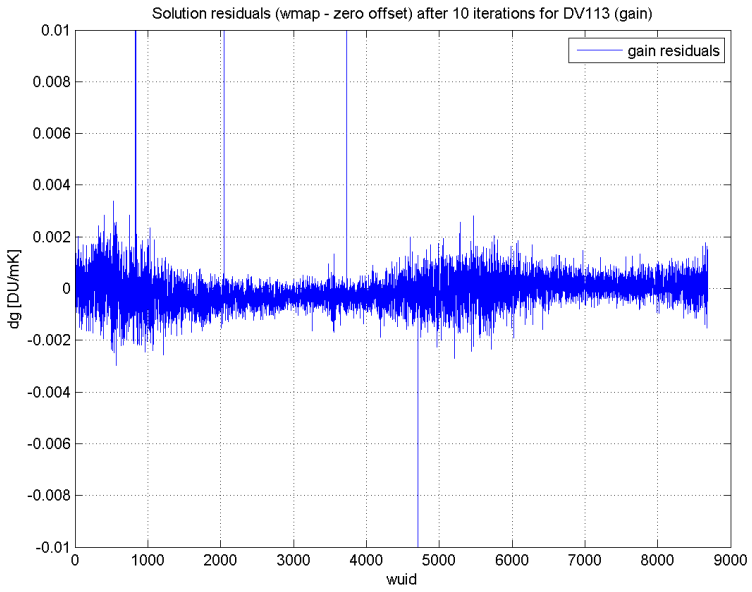

Figure 56: DV113 gain timing-offset residuals from iteration # 10.

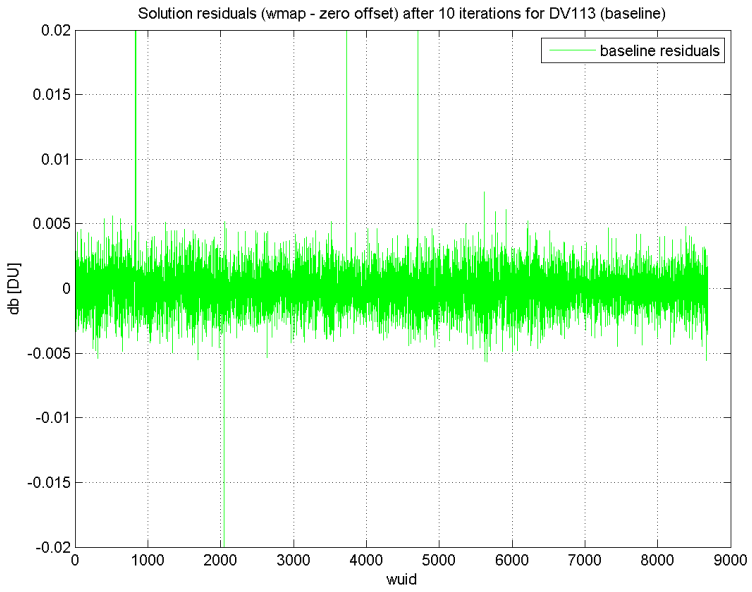

Figure 57: DV113 baseline timing-offset residuals from iteration # 10.

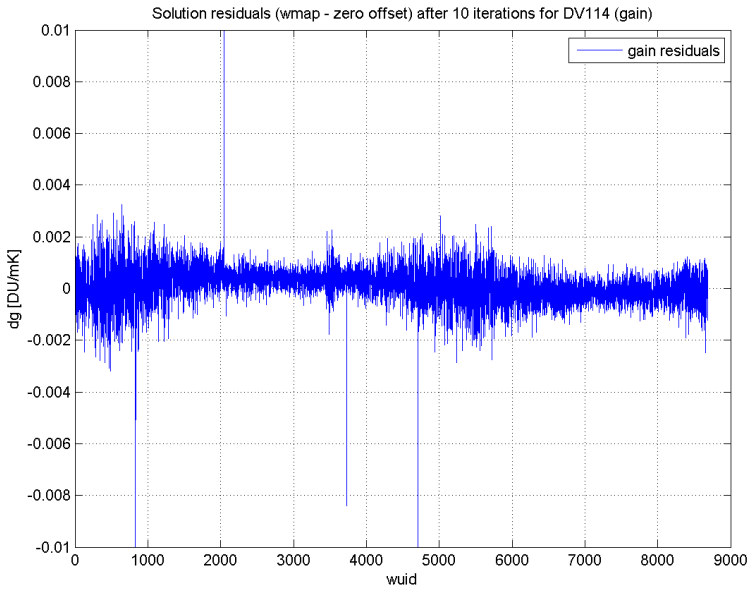

Figure 58: DV114 gain timing-offset residuals from iteration # 10.

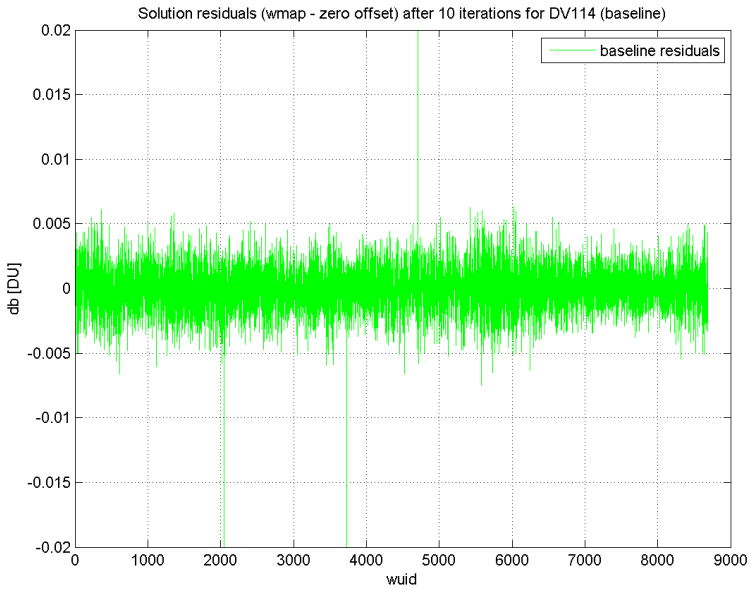

Figure 59: DV114 baseline timing-offset residuals from iteration # 10.

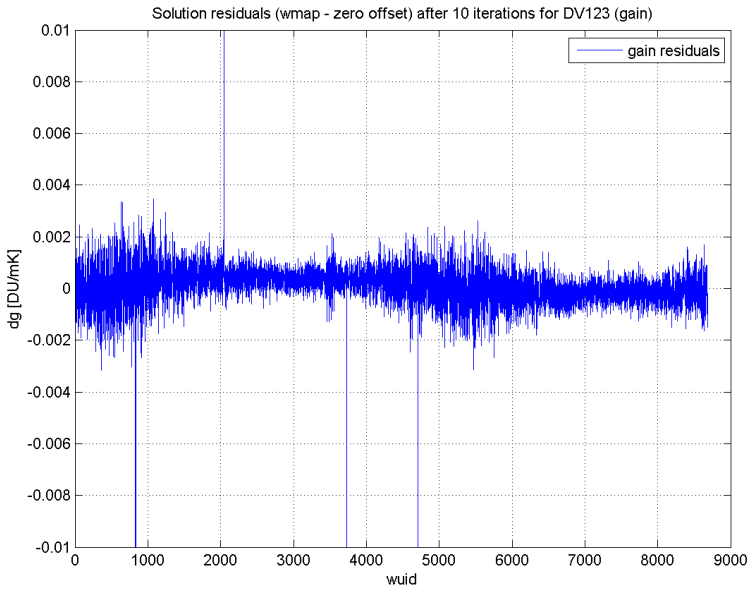

Figure 60: DV123 gain timing-offset residuals from iteration # 10.

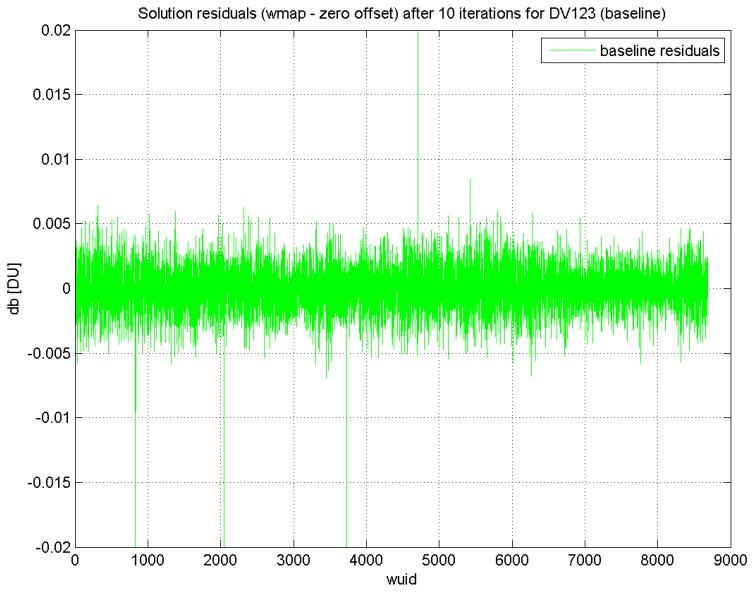

Figure 61: DV123 baseline timing-offset residuals from iteration # 10.

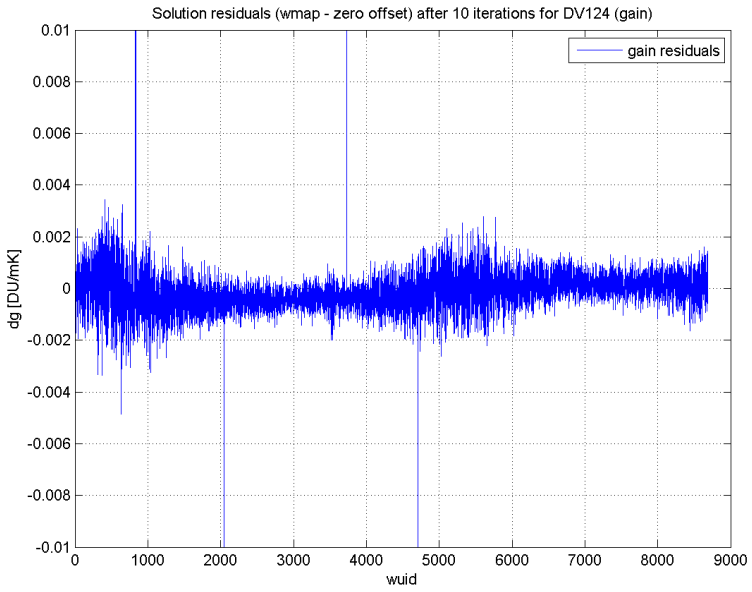

Figure 62: DV124 gain timing-offset residuals from iteration # 10.

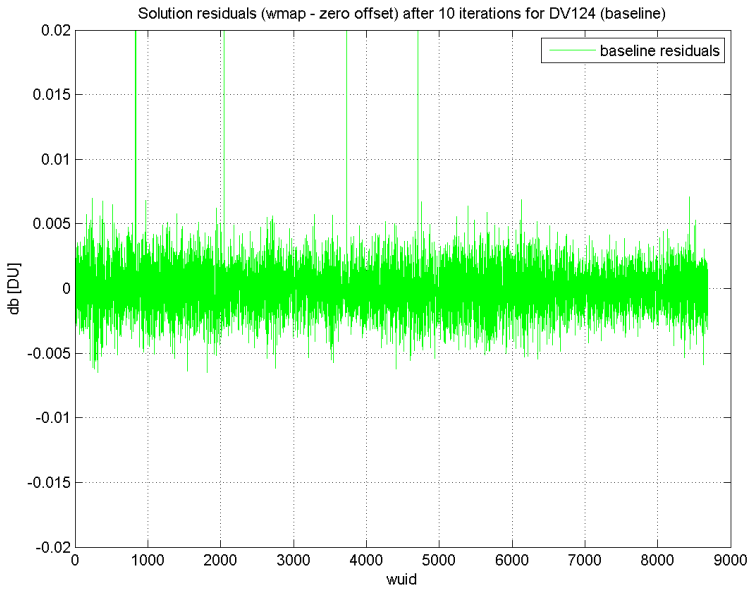

Figure 63: DV124 baseline timing-offset residuals from iteration # 10.

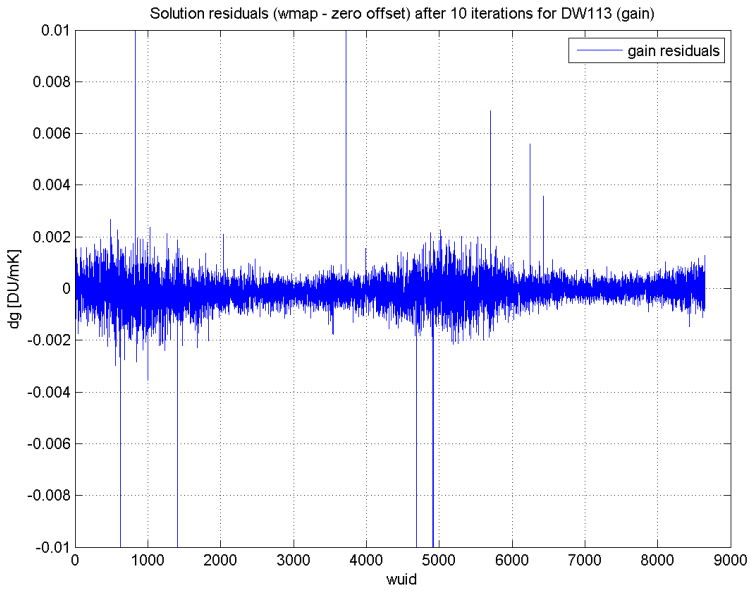

Figure 64: DW113 gain timing-offset residuals from iteration # 10.

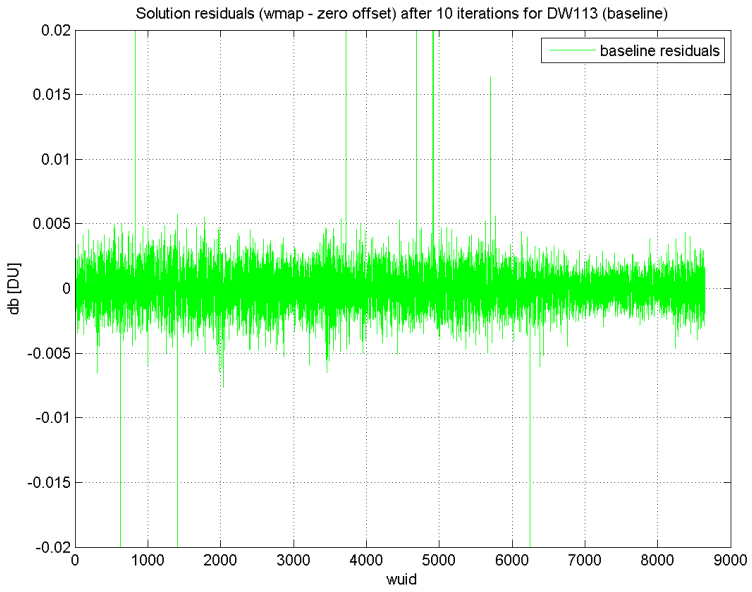

Figure 65: DW113 baseline timing-offset residuals from iteration # 10.

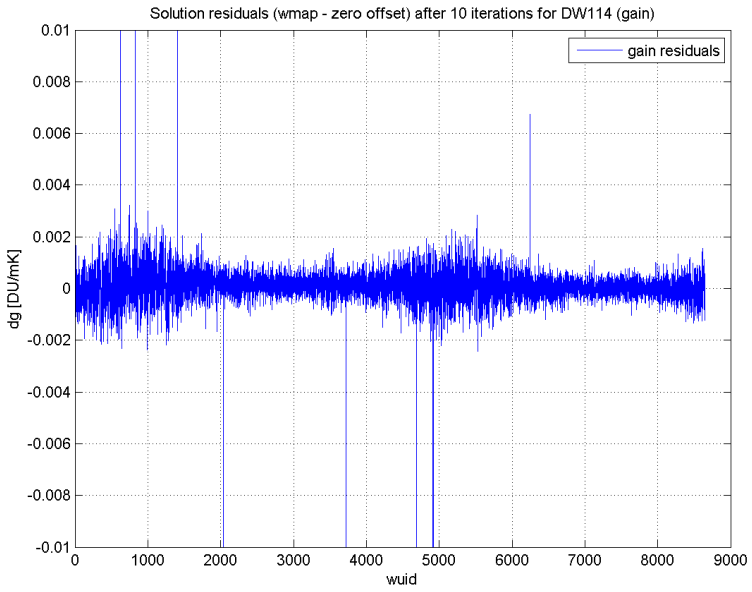

Figure 66: DW114 gain timing-offset residuals from iteration # 10.

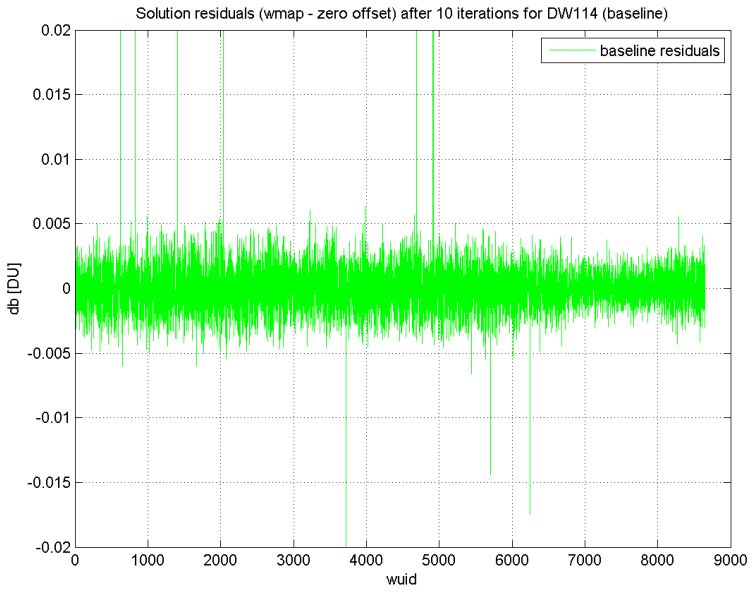

Figure 67: DW114 baseline timing-offset residuals from iteration # 10.

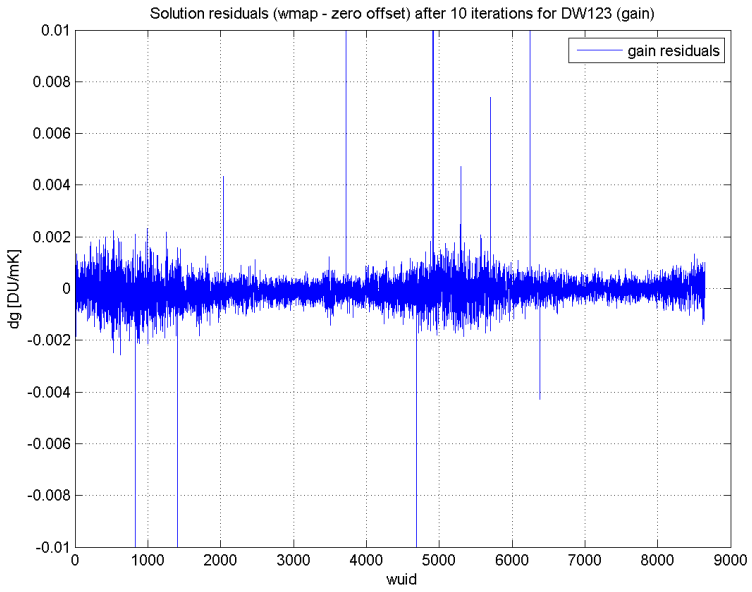

Figure 68: DW123 gain timing-offset residuals from iteration # 10.

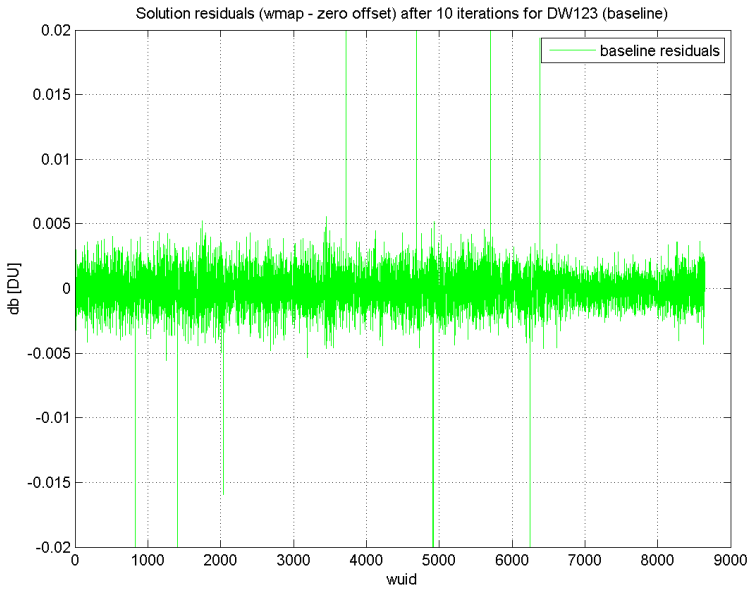

Figure 69: DW123 baseline timing-offset residuals from iteration # 10.

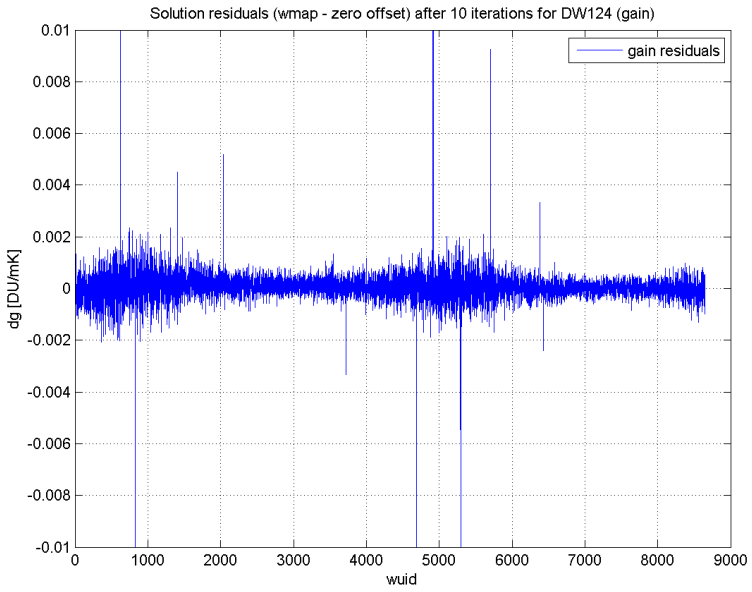

Figure 70: DW124 gain timing-offset residuals from iteration # 10.

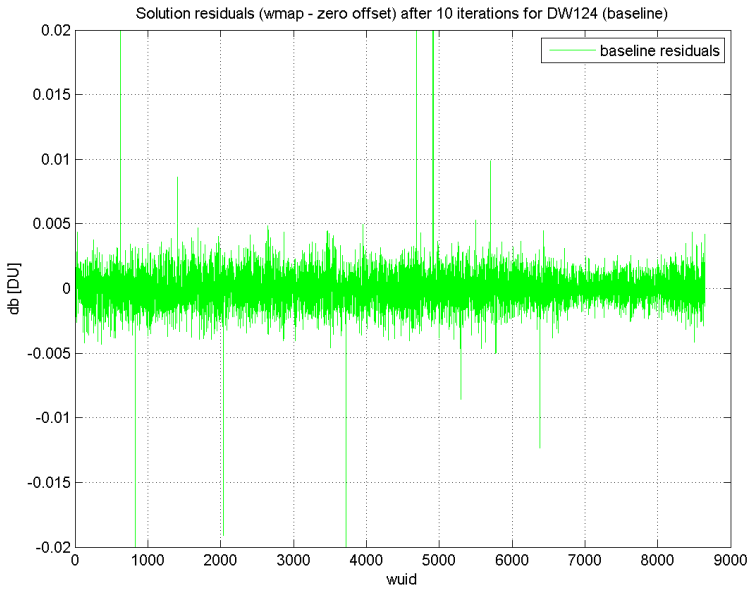

Figure 71: DW124 baseline timing-offset residuals from iteration # 10.

Note that all maps discussed in the following section are differences of the final maps consistently generated using our software package and therefore do not exhibit the systematic patterns noted in the previous sections. Our goal was to estimate the effect of our calibration on the induced quadrupole. Our hypothesis is that since the calibration solutions obtained from the two calibration modes are effectively indistinguishable (figures 48 - 71) there should be no significant effect on the induced quadrupole patterns. We generated final maps with our offset using the calibration solutions above and subtracted them from the maps calibrated and generated in the WMAP mode (see section “Final Maps"). The following figures (72 - 77) show the residual maps. The induced quadrupole does not seem to be affected by the difference between calibrated TOD. Not even in case of W1 (figures 76 and 77) in which our offset setting (one half of the integration time of W detectors is exactly 25.6ms) in the calibration exactly canceled the suspected erroneous offset in the official WMAP calibration [1]. The results seem to suggest that the induced quadrupole originates almost entirely from the final map-making stage and is not affected by offsets in the calibration stage.

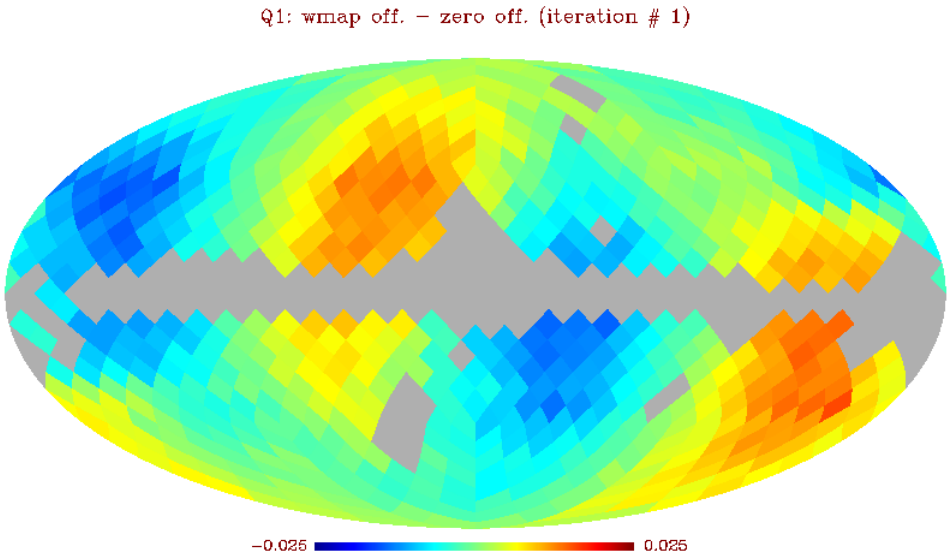

Figure 72: Q1 residual map (subtracted maps calibrated after iteration # 1) in units of mK ($N_{side} = 8$).

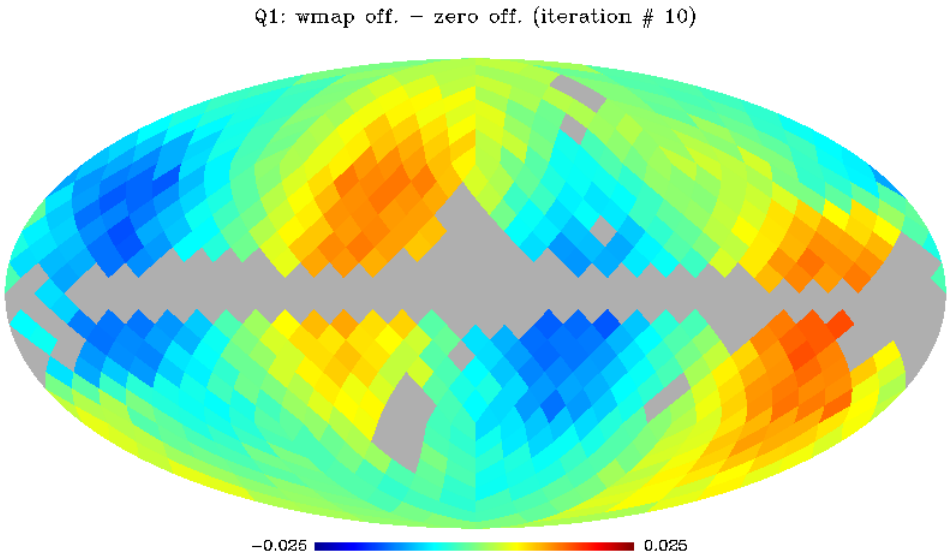

Figure 73: Q1 residual map (subtracted maps calibrated after iteration # 10) in units of mK ($N_{side} = 8$).

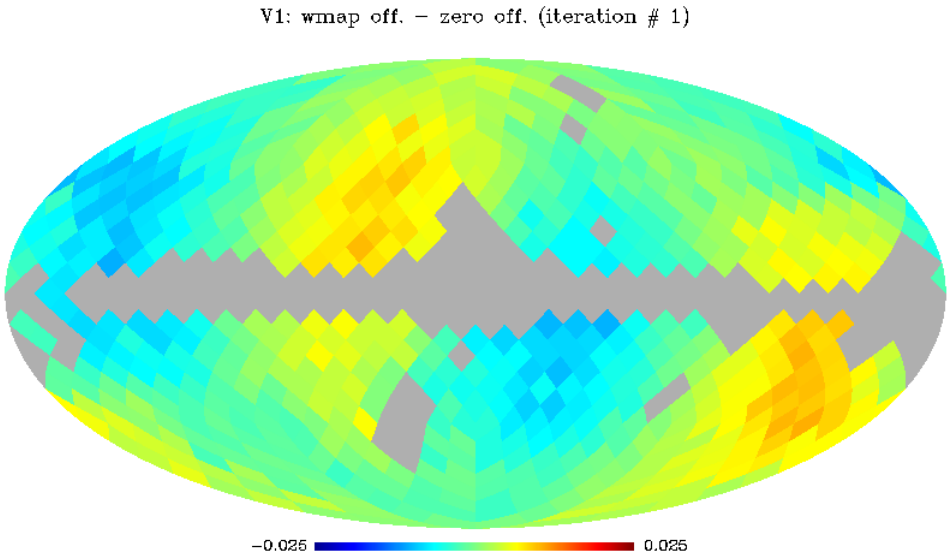

Figure 74: V1 residual map (subtracted maps calibrated after iteration # 1) in units of mK ($N_{side} = 8$).

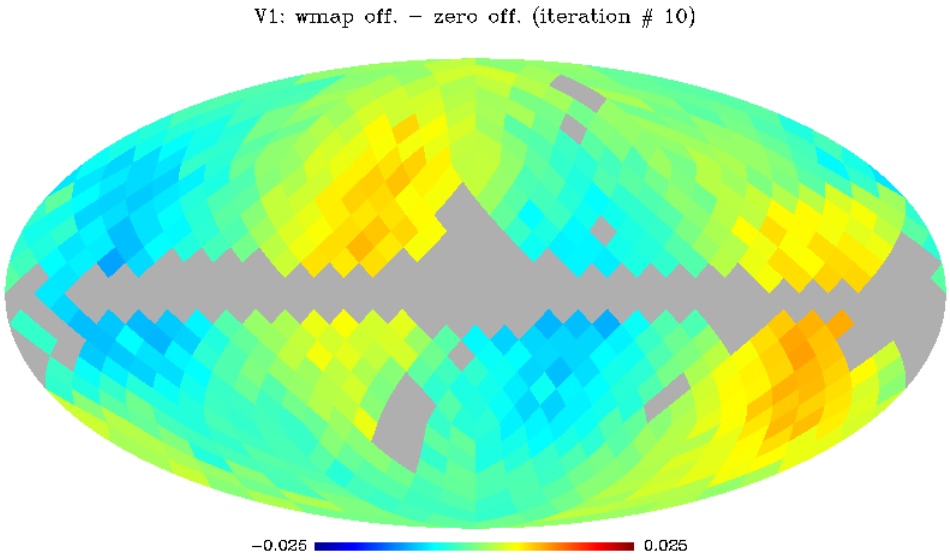

Figure 75: V1 residual map (subtracted maps calibrated after iteration # 10) in units of mK ($N_{side} = 8$).

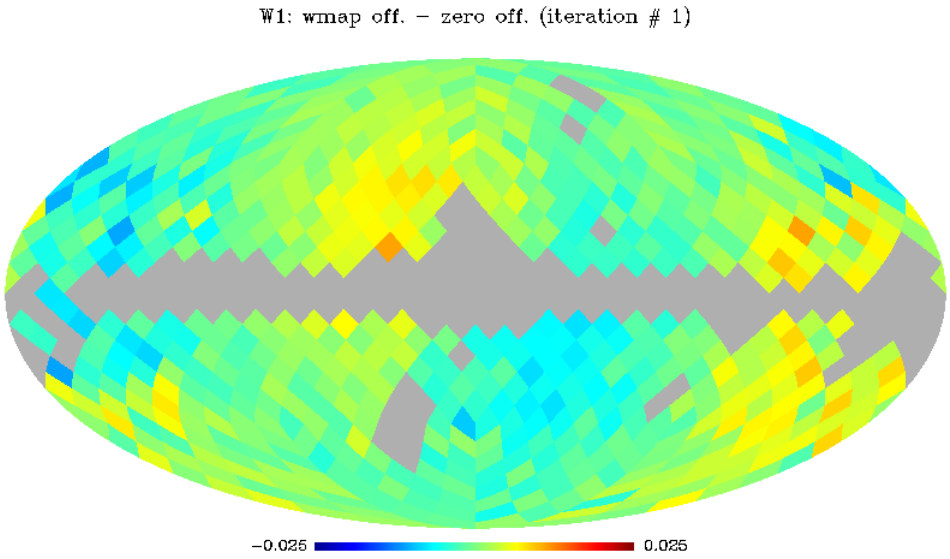

Figure 76: W1 residual map (subtracted maps calibrated after iteration # 1) in units of mK ($N_{side} = 8$).

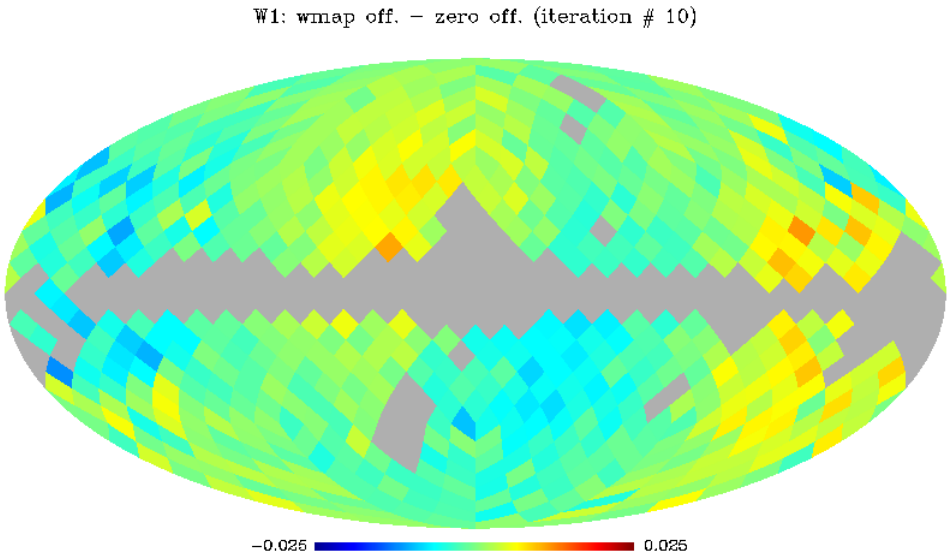

Figure 77: W1 residual map (subtracted maps calibrated after iteration # 10) in units of mK ($N_{side} = 8$).

Finally, we show the difference between maps generated from WMAP mode calibrated data and maps generated from calibrated TOD produced with our (zero) offset settings (figures 78 - 80). The subtracted maps were generated in the same (WMAP) mode. Any pattern in the residual maps must therefore originate solely from the calibration stage. As expected from solution residuals (figures 48 - 71) and induced dipole maps above the residual maps do not exhibit significant variation. Although not identically zero, this variation is not significant compared to the scale of the induced quadrupole. These maps should be compared to figures (73), (75) and (77) where we also introduced offsets into the final map-making stage.

The significance of this test is in that it quantifies the effect of a timing offset introduced solely into the calibration stage. As can be seen from the differential maps (figures 78 - 80) a timing offset in the calibration stage has little effect on the final calibrated TOD and resultant maps.

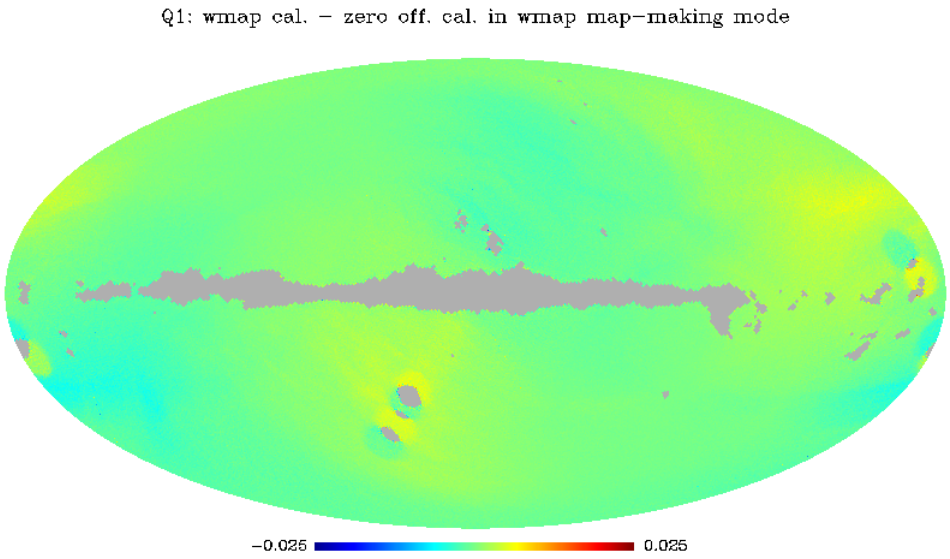

Figure 78: Q1 residual map (subtracted maps calibrated after iteration #10, $N_{side} = 512$) in units of mK.

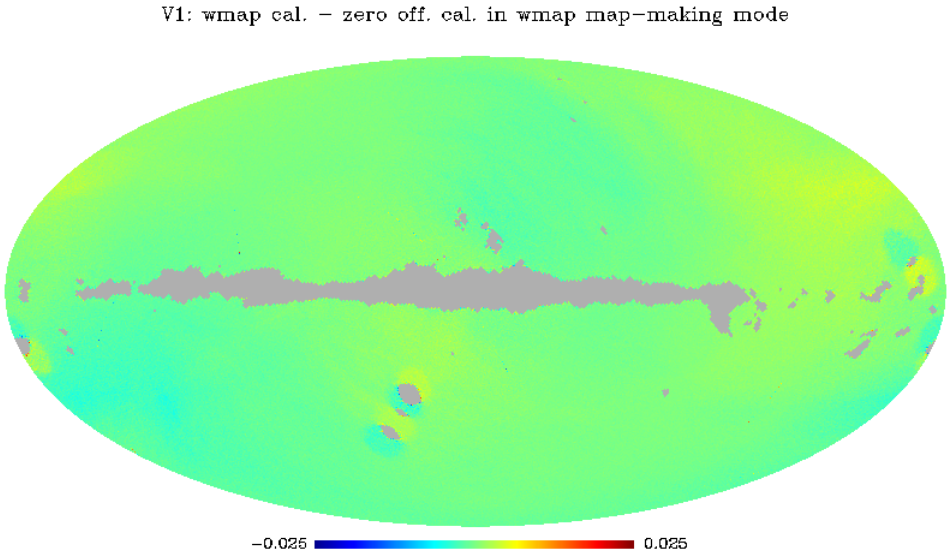

Figure 79: V1 residual map (subtracted maps calibrated after iteration #10, $N_{side} = 512$) in units of mK.

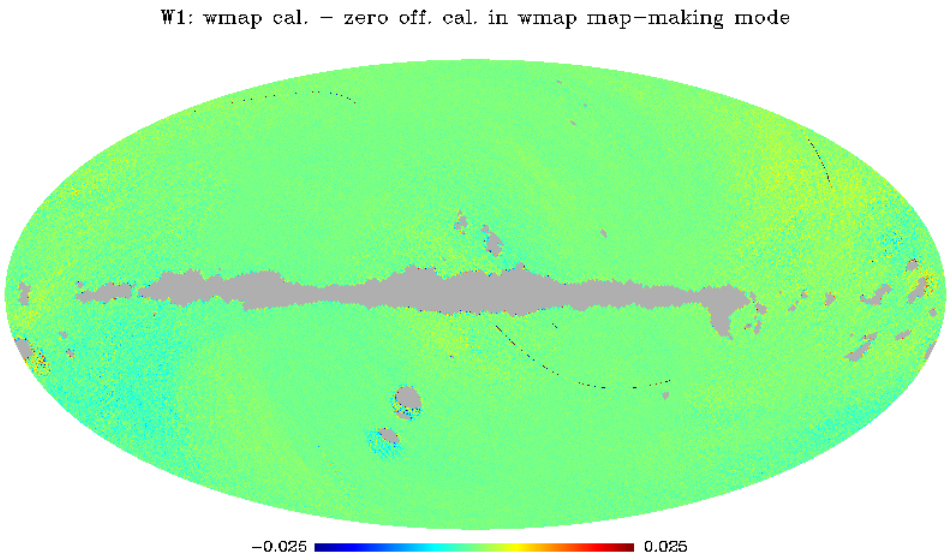

Figure 80: W1 residual map (subtracted maps calibrated after iteration #10, $N_{side} = 512$) in units of mK.

9 Summary

Wilkinson Microwave Anisotropy Probe accomplished many extremely important discoveries with profound impacts on our knowledge about the universe we live in at all levels. Its results are being used virtually every day not only in cosmology but also in more fundamental areas of physics such as high energy and quantum physics. The correctness and accuracy of its results were recently questioned form several directions (induced quadrupole [1], radio sources [24]). Any systematic error in the results could lead to reconsideration of our cosmological models as they are often validated based on the data acquired by WMAP.

In this work we focused on the induced quadrupole described in [1]. If real, the calibrated data and final maps released by WMAP group may be in question. Our main goal was to repeat the official calibration starting from raw data after removing the suspected offset and investigate impacts on the calibrated data and final maps. As the original calibration code was never released to public it was necessary to reproduce the whole processing pipeline based on published works. A great deal of work was done by the Chinese group mentioned above [13] in reproducing the map-making portion of the pipeline. We had to add the calibration part and put all the pieces together.

- We approximately reproduced the original calibration procedure and starting from the uncalibrated data produced our own set of calibration parameters. We then visually compared our calibration results plotted as a function of time to the same plots published by the original researches. We also compared mean values of the parameters over a period of a year to the officially published results. Based on this analysis we did not find any significant discrepancies between the officially

published calibration parameters and the results we obtained from our calibration pipeline.

- We have shown that the calibration parameters change with each iterative calibration step and converge to a particular value. The effects of solution convergence were observed in both the intermediate data and maps produced during the iterative calibration process and in the final maps. Both effects mentioned above are consistent with the behaviour expected from the official calibration procedure. Based on the analysis of the intermediate products we found that the relative calibration improvement is most significant during the first five iterations, we therefore opt for a ten-step iterative calibration, which is also consistent with the official procedure.

  We finally analyze the residuals between the final calibrated TOD and the official first-year release data. The residuals are random, narrowly centered around zero, not showing any overall trend. In addition to the qualitative analysis performed before we take this as yet another indication supporting the confidence in the correctness of our reproduction of the official calibration procedure.

- Using the solutions discussed we produced a set of calibrated TOD and final maps. Although, our maps mostly agree with the maps generated from the officially released WMAP1 TOD we note a couple of problematic regions which exhibit some degree of discrepancy even after ten iterations. This discrepancy is most prominent in W1 band in which it is comparable in amplitude to the actual CMB fluctuation signal (0.05 mK). We note several possible causes of this discrepancy, including the fact that more iterations may be required to achieve better results.

Nevertheless, we are ultimately interested in the residual maps produced by subtracting two final maps consistently generated from TOD calibrated by our calibration software using various calibration timing offset modes. Since the patterns discussed above do not appear to depend on the calibration offset mode they should subtract out in the residual maps making it possible to safely use those maps to assess the impacts of various offset modes on the final maps.

- We have applied half-integration-time timing offset to the calibration procedure and produced a new set of calibration parameters that we then compared to the calibration solutions discussed above. Here we occasionally found visible differences in the gain (if not the baseline) parameter. In order to investigate the effects of these parameter differences on the final maps and the induced quadrupole pattern discussed above we produced a set of residual maps by subtracting maps generated using the two parameter sets discussed above. We did not find any significant effects on the residual maps and the induced quadrupole patterns. The induced quadrupole pattern appeared only after subtracting two maps generated with a relative timing offset in the final map-making stage.

The timing offset in the calibration stage of the processing pipeline seems to have little effect on the final products. The induced quadrupole pattern in the residual maps was reproduced only after applying the offset into the final map-making stage.

Based on our results we can conclude that even if real the cited offset would not affect calibration solutions and therefore the final calibrated data to a significant degree (relative to the magnitude of the induced quadrupole pattern [1]).

Acknowledgements

I would like to acknowledge the support and help I received from my supervisor Tom Shanks, coworkers Utane Sawangwit, Joseph Whitbourn, the whole scientific team and technical staff at Durham University. I also thank Dr Hao Liu and Prof T.P. Li for making their map-making software, a substantial part of my calibration package, freely available.

10 Appendix

10.1 Software

Visit http://www.wmap-lx.net/ for details.

10.1.1 lx_wmap_tod_extract.pro

Extract required TOD (attitude, telemetry and scientific data) from given FITS archives to SQLite 3 databases, the format suitable for calibration.

10.1.2 Usage

pro lx_wmap_tod_extract, archiveDir, outputDbPrefix, mnemonics, coords, coordsHorn, Center = centerKey, auxDir, silent_mode = silent, fail_on_error = fail, exit_status = exitStatus

10.1.3 Parameters

- *archiveDir* Directory containing the source TOD FITS archives.
- *outputDbPrefix* Directory for output database files.
- *mnemonics* Comma separated mnemonics of detectors to extract.
- *coords* Coordinate system used for pointing (ECL, GAL, CEL).
- *coordsHorn* Horn for which to calculate the pointing (A, B, AB).
- *Center* If set, evaluate the pointing at the center of each observation. If not set use the beginning instead.
- *auxDir* Directory with shared library (lx_tod_to_sql).
- *silent_ mode* If set, print only critical messages.

- *fail_ on_ error* When an error occurs finish the current file and fail.
- *exit_ status* Status code. Non-zero on errors.

10.1.4 Examples

```
lx_wmap_tod_extract,"/home/user/uncalibrated-tod/","/home/user/
uncalibrated-tod-sql/","DQ113,DW123","GAL","AB",/Center,"/home/
user/auxiliary/"
```

Extract data from TOD FITS archives in "/home/user/uncalibrated-tod/" to SQLite databases in "/home/user/uncalibrated-tod-sql/". Scientific data extracted for detectors DQ113 and DW123. Pointings (both horns) extracted in galactic coordinates and evaluated at the center of each observation.

```
lx_wmap_tod_extract,"/home/user/uncalibrated-tod/","/home/user/
uncalibrated-tod-sql/",lx_wmap_da_to_mnemonics("V1"),"GAL","AB",
"/home/user/auxiliary/"
```

Extract scientific data from all V1 detectors (DV113, DV114, DV123, DV124). Evaluate pointings to the beginning of each observation.

10.1.5 lx_wmap_run_iterative_calibration.pro

Run the iterative calibration procedure for a given number of iterations.

10.1.6 Usage

pro lx_wmap_run_iterative_calibration, raw_fits_prefix, cal_fits_prefix, sol_prefix, calibration_dir, map_dir, aux_dir, mask, map_rounds, map_n_years, map_years, da, zero_offset=offset, iter_num, iter_start=iter_init

10.1.7 Parameters

- *raw_fits_prefix* Directory with raw TOD FITS archives.
- *cal_fits_prefix* Directory for calibrated FITS archives.
- *sol_prefix* Directory for calibration solutions (gain, baseline).
- *calibration_dir* Working directory for calibration (extracted raw data in SQL files).
- *map_dir* Working directory for mapmaking (output maps).
- *aux_dir* Auxiliary files (calibration application, masks, LOS tables, pre-compiled helper libraries).
- *mask* Mask file (name) used for masking in both calibration and map-making.
- *map_rounds* Number of map-making rounds (usually 80).
- *map_n_years* Number of years in the TOD set.
- *map_years* Years used in map-making.

- *da* Detector assembly (DA) to be calibrated.
- *zero_ offset* If set evaluate pointings at the beginning of each observation, use the center otherwise.
- *iter_ num* Number of iterations.
- *iter_ start* This can be used to restart iterations from a given index provided that "calibration_dir" still contains data from previous iterations.

10.1.8 Examples

```
lx_wmap_run_iterative_calibration,"/home/user/uncalibrated-tod/",
"/home/user/calibrated-tod/","/home/user/calibration-solutions/
","/home/user/uncalibrated-tod-sql/","/home/user/map-making/","/
home/user/auxiliary/","wmap_processing_r9_mask_3yr_v2.fits",80,
1,1,"Q1",5
```

Provided that there is one year of data in "/home/user/uncalibrated-tod/" use the whole year. The command above extracts the necessary information from the archives for calibration of "Q1" assembly into "/home/user/uncalibrated-tod-sql/". It also makes a copy of uncalibrated archives to "/home/user/calibrated-tod/" which will serve as calibrated archives for map-making. Calibration solutions for each iterative run go to "/home/user/calibration-solutions/" and maps to "/home/user/map-making/". Each map is iterated 80 times and the whole procedure is repeated in total 5 times.

NOTE #1: In case you already have extracted data. It is possible to copy the files manually into "/home/user/uncalibrated-tod-sql/" prior to calibration. This forces the routine to skip the extraction step.

NOTE #2: To save storage space, the routine does not store a copy of calibrated FITS files and raw SQL database files after each iteration. It rather overwrites any previous versions of the files. The number of calibration / raw data reduction runs already performed on any given assembly is stored in a calibration log file in the auxiliary directory. The log stores an IDL structure and can be loaded and edited in IDL. When re-running the procedure on an already processed assembly, make sure to first clear the associated log entry.

10.1.9 lx_wmap_print_iter_map.pro

Display an iterative map read from a given FITS file.

10.1.10 Usage

pro lx_wmap_print_iter_map, file, title, minT, maxT, smooth=smooth

10.1.11 Parameters

- *file* ath to map FITS file.
- *title* Window title.
- *minT* Min. temperature to display in mK.
- *maxT* Max. temperature to display in mK.
- *smooth* If set, smooth the map before displaying (reduce resolution to $N_{side} = 8$).

10.1.12 Examples

```
lx_wmap_print_iter_map,"/home/user/map-making/map01.fits","MyMap",
-0.025,0.025
```

Display a map from "/home/user/map-making/map01.fits" file with temperature scale from -0.025mK to 0.025mK.

10.1.13 lx_wmap_iterative_map_subtract.pro

Display a difference of two iterative maps given as FITS files.

10.1.14 Usage

pro lx_wmap_iterative_map_subtract, mapAPath, mapBPath, minT, maxT, smooth=smooth

10.1.15 Parameters

- *mapAPath* Path to map FITS file A.
- *mapBPath* Path to map FITS file B.
- *minT* Min. temperature to display in mK.
- *maxT* Max. temperature to display in mK.
- *smooth* If set, smooth the map before displaying (reduce resolution to $N_{side} = 8$).

10.1.16 Examples

```
lx_wmap_iterative_map_subtract,"/home/user/map-making/map01.fits",
"/home/user/map-making/map02.fits",-0.5,1.5,/smooth
```

Display a reduced resolution differential (A - B) map between “map01.fits" and “map02.fits" with temperature scale from -0.5mK to 1.5mK.

10.1.17 run_mapmaking.pro

Generate a sky map from calibrated TOD.

10.1.18 Usage

pro run_mapmaking, bandname, n_years, years, ximzero=ximzero, dipole_signal=dipole_signal, wmap_mode=wmap_mode, debug=debug, tod_dir, working_dir, wmapdir, maskfile, rounds, so_file

10.1.19 Parameters

- *bandname* The working band (DA).
- *n_years* Number of years in the TOD set.
- *years* Years used in map-making.
- *ximzero* If set, forces detector transmission imbalances to zero.
- *dipole_signal* Test the effect of offset setting upon the final map (compute differential dipole field).
- *wmap_mode* Use WMAP offset settings (center).
- *debug* Process only the first year data.
- *tod_dir* Directory with calibrated TOD FITS files.
- *working_dir* Working directory for mapmaking (output maps).
- *wmapdir* Auxiliary files (masks, LOS tables, pre-compiled helper libraries).
- *maskfile* Path to the mask file used for masking in both calibration and map-making.

- *rounds* Number of map-making rounds (usually 80).
- *so_file* Path to the FORTRAN helper function.

10.1.20 Examples

```
run_mapmaking,"W1",1,1,/wmap,"/home/user/calibrated-tod/","/home/
user/map-making/","/home/user/auxiliary/","/home/user/auxiliary/
wmap_processing_r9_mask_3yr_v2.fits",80,"/home/user/auxiliary/loop.
so"
```

Generate a first-year “W1" map in the WMAP offset mode from input TOD files in “/home/user/calibrated-tod/" using the processing mask. The output maps go to “/home/user/map-making/".

10.1.21 wmapLX

The calibration application accomplishes three main tasks. It fits a given calibration model (linear, dipole-based) on the raw temperature data and obtains calibration solutions (gain and baseline). It uses the solutions to calibrate the raw data and produces calibrated FITS archives suitable for map-making. Finally, given a sky map and calibration solutions it decalibrates the map and subtracts it from the raw data (data reduction).

10.1.22 Usage

wmapLX –set=<settings.ini> –action=model-fit-1 –raw_prefix=<raw SQL directory> –aux_prefix=<mask FITS file> –out_prefix=<directory for solution databases>

wmapLX –set=<settings.ini> –action=calibrate –raw_prefix=<raw SQL directory> –aux_prefix=<directory with solution databases> –out_prefix=<directory with FITS archives>

wmapLX –set=<settings.ini> –action=reduce –raw_prefix=<raw SQL directory> –aux_prefix=<map FITS file> –out_prefix=<directory with solution databases>

10.1.23 Parameters

- *set Path* to settings.ini. An auxiliary file containing advanced settings and presets.
- *action* Action to be performed.
- *raw_prefix* Directory with input (raw) SQL databases.
- *aux_prefix* Auxiliary data.

- *out_prefix* Output directory.
- *fail* If set, stop execution on recoverable errors.

10.1.24 Examples

```
wmapLX--set="/home/user/auxiliary/settings.ini"--action=model-fit-1--raw_
prefix="/home/user/uncalibrated-tod-sql/"--aux_prefix="/home/user/
auxiliary/wmap_processing_r9_mask_3yr_v2.fits"--out_prefix="/home/
user/calibration-solutions/"
```

Fit a dipole-based linear model on the raw data in "/home/user/uncalibrated-tod-sql/" and store the solutions in "/home/user/calibration-solutions/". Use "–residuals" switch to emit fit residuals.

```
wmapLX--set="/home/user/auxiliary/settings.ini"--action=calibrate--raw_
prefix="/home/user/uncalibrated-tod-sql/"--aux_prefix="/home/user/
calibration-solutions/"--out_prefix="/home/user/calibrated-tod/
```

Calibrate the raw data in "/home/user/uncalibrated-tod-sql/" using solutions from "/home/user/calibration-solutions/" and store the calibrated data in FITS archives prepared in "/home/user/calibrated-tod/".

```
wmapLX--set="/home/user/auxiliary/settings.ini"--action=reduce--raw_
prefix="/home/user/uncalibrated-tod-sql/"--aux_prefix="/home/user/
map-making/map01.fits"--out_prefix="/home/user/calibration-solutions/
"
```

Decalibrate a given map in "/home/user/map-making/map01.fits" using calibration solutions from "/home/user/calibration-solutions/" and subtract it from the raw data (reduce raw data) in "/home/user/uncalibrated-tod-sql/".

10.1.25 settings.ini

settings.ini is an auxiliary file which contains advanced presets for the calibration application.

10.1.26 Parameters

- *database_ext* Extension of database files.
- *fits_ext* Extension of FITS files.
- *period_length* Length of a calibration period (Julian Date) [default: 0.04167 = 1h].
- *query_select_tod_time* Load timestamps for a given DA from a TOD database.
- *query_select_tod_temp* Load temperature data for a given detector from a TOD database.
- *query_select_pointing* Load pointing data from a TOD database.
- *query_insert_tmp_mask* Create a temporary table for rowids masked out from the current DA. This table is then used to filter TOD in model fitting.
- *query_select_tod_mod* Load TOD for model fitting (pointing + temperature) from a TOD database.
- *query_select_attitude* Load attitude data (velocities) from a TOD database.
- *query_select_sol_cal* Load calibration solutions (gain + baseline) from a solution database.

- *query_insert_sol_cal_1* Save calibration solutions (linear).
- *query_insert_sol_cal_2* Save calibration solutions (non-linear).
- *query_insert_residuals* Save calibration residuals.
- *query_update_tod_temp* Reduce raw TOD.
- *query_select_det_tbls* Retrieve names of detector tables from a TOD database.

10.1.27 Examples

query_select_tod_mod = CREATE TEMPORARY TABLE IF NOT EXISTS _DA_cache AS SELECT rowid, frmInd, thetaA, phiA, thetaB, phiB FROM _TOD._DA WHERE ((sciInd NOT IN (SELECT rowid FROM _TOD.TELEMETRY WHERE (((genflags <> 0) AND (genflags <> 192)) OR (_DA <> 0)))) AND rowid NOT IN (SELECT id FROM _DA_mask) AND ((ABS(thetaA) > 15.0) AND (ABS(thetaB) > 15.0))));SELECT frmInd, thetaA, phiA, thetaB, phiB, dtemp FROM _TOD._DET INNER JOIN _DA_cache ON _TOD._DET.rowid = _DA_cache.rowid WHERE ((_DA_cache.rowid >= _BEG) AND (_DA_cache.rowid <= _END));

Select data for model fitting. Note the use of a temporary in-memory table to speed up repetitive JOIN operations. The blue term demonstrates how to selectively allow certain quality flags to enter the fit. The green part is responsible for masking. The red term shows how to exclude additional pointings from the fit.

query_select_det_tbls = SELECT name FROM _TOD.sqlite_master WHERE ((type = 'table') AND ((name <> 'LOG') AND (name <> 'ATTITUDE') AND (name <> 'TELEMETRY') AND (name <> 'K1') AND

(name <> ‘KA1’) AND (name <> ‘Q1’) AND (name <> ‘Q2’) AND (name <> ‘V1’) AND (name <> ‘V2’) AND (name <> ‘W1’) AND (name <> ‘W2’) AND (name <> ‘W3’) AND (name <> ‘W4’) AND (name LIKE ‘%Q1%’)));

Select detectors (tables) to process. The blue term demonstrates how to limit the processed tables to one particular assembly.

10.2 Additions to the First Release

We have obtained several new results since the first draft of this thesis. Because they are all closely related to the work published in this paper and may help to answer some of the reader's questions we present them in this short appendix as preliminary results.

- The authors of the map-making package used by our calibration software in the meantime released a new version. [1] In order to quantify the effects of this new map-making package we performed analysis somewhat similar to what we did on page 80 of the thesis. We used the new map-making package in the iterative calibration to generate calibrated TOD, but then generated the final maps with the old map-making software. This allowed us to estimate the impact of the changes in the latest version of the map-making package by comparing the maps to our original results. We conclude that the impact on the calibrated TOD is in case of the Q1 band very much negligible (Figure 81).

[1] http://arxiv.org/abs/1203.5720

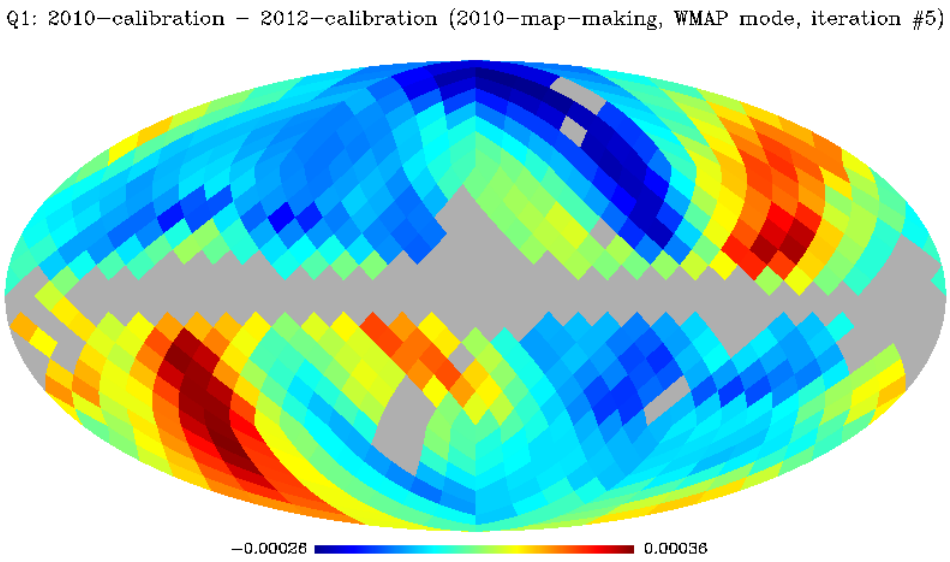

Figure 81: Q1 residual map after five iterations in units of mK ($N_{side} = 8$).

- In the discussion of our results we proposed that running the iterative calibration for more than ten iterations may, at least in theory, significantly improve the final products. In order to get a better feel for the impact of additional iterations we run our original iterative calibration on the Q1 band for five more iterations. In the agreement with the convergence tests (page 31 - 37) the additional iterations applied on this band did not lead to any significant changes of the final calibration solutions and maps (Figure 82).

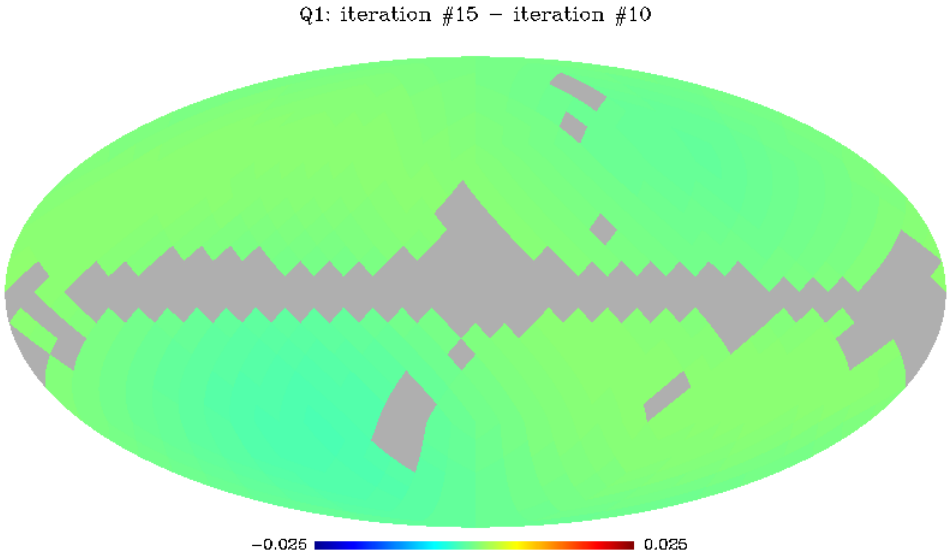

Figure 82: Q1 iteration #10 and #15 final map difference in units of mK ($N_{side} = 8$).

- So far, we have been consistent in applying the same timing offset in dipole-evaluation (fitting) and raw-tod reduction parts of the iterative pipeline (page 61). This time we assumed that there was an inconsistency and the fitting code was using timing different from the map-making code. The following figures (83 - 86) show the results after five iterations. There are two versions *V1* and *V2* referring to relative “fitting vs. map-making" offsets. In *V1* the fitting was following the WMAP timing while the row-tod reduction was using the Chinese (zero-offset) setting. *V2* had the two offsets swapped – dipole evaluation was using the zero-offset timing and raw-reduction was following the original WMAP setting. *NORMAL CAL.* refers to the usual consistent calibration in which both offsets are the same. The map-making mode mentioned in the brackets is the mode in which the final map was generated (*NORMAL CAL.* mode). We did this for all four combinations. The impact on the calibrated TOD is small, comparable to the effect of the timing offset presented on page 80.

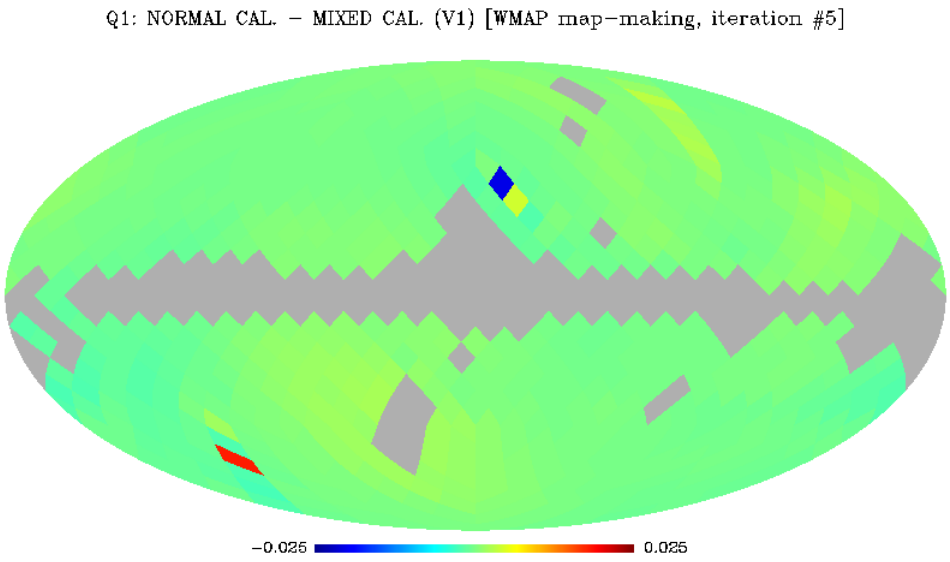

Figure 83: Q1 residual map after three iterations in units of mK ($N_{side} = 8$).

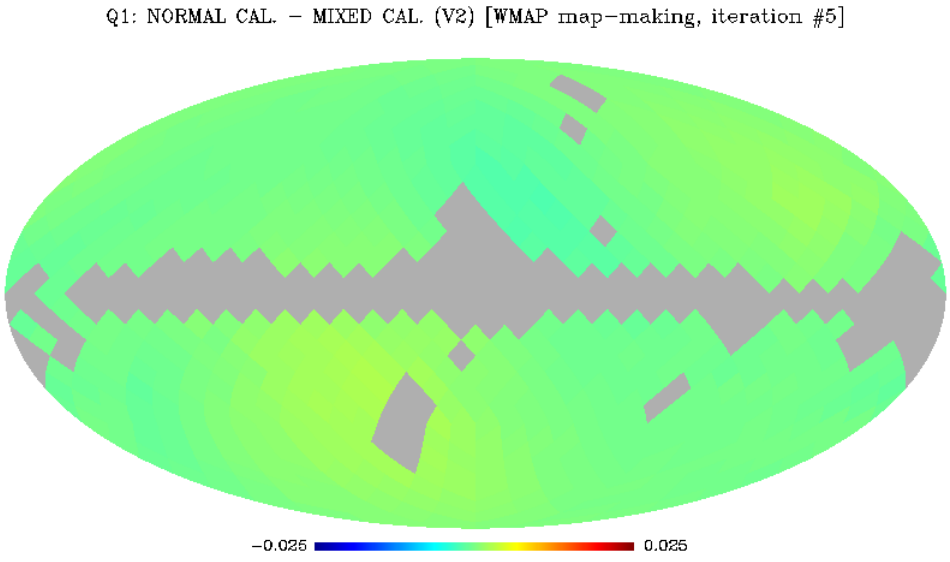

Figure 84: Q1 residual map after three iterations in units of mK ($N_{side} = 8$).

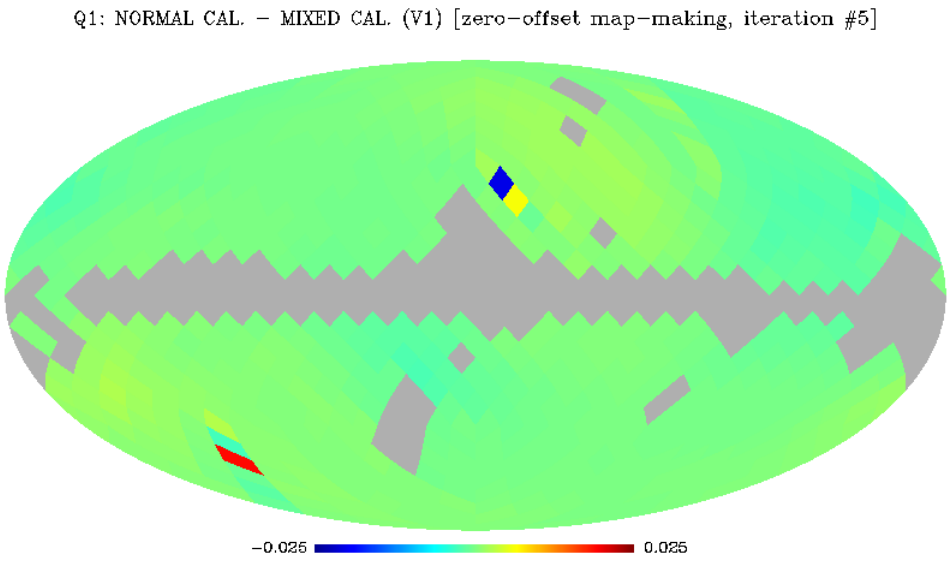

Figure 85: Q1 residual map after three iterations in units of mK ($N_{side} = 8$).

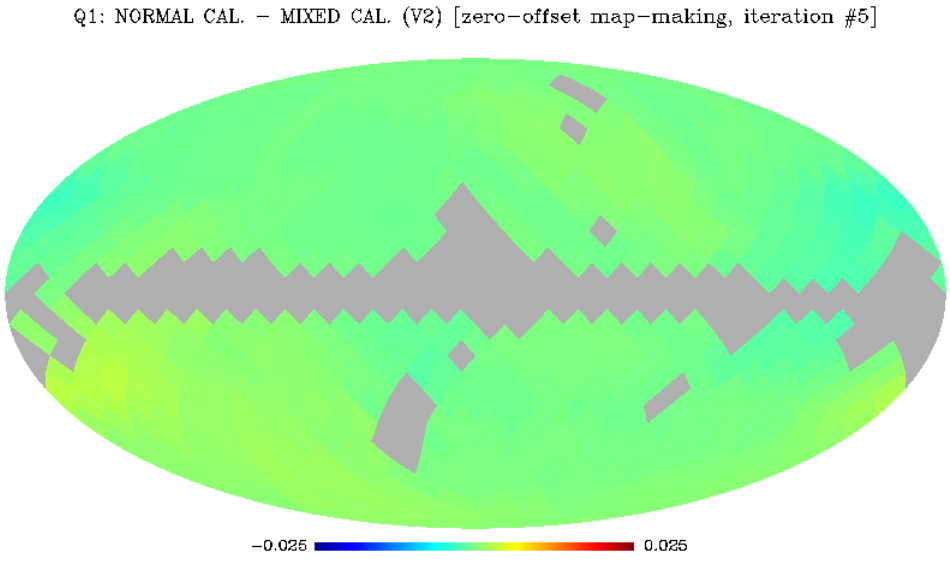

Figure 86: Q1 residual map after three iterations in units of mK ($N_{side} = 8$).

References

[1] Hao Liu, Shao-Lin Xiong, Ti-Pei Li, The origin of the WMAP quadrupole, arXiv:1003.1073v2 2, 23, 24, 25, 56, 76, 83, 85

[2] W. S. Adams, Some Results with the COUDÉ Spectrograph of the Mount Wilson Observatory, ApJ (1941) 93, 11 3

[3] A. McKellar, Interstellar Molecular Lines, Pub. Dominion Ap. Obs. (1941) 7, 251 3

[4] R. A. Alpher, H. A. Bethe, G. Gamow, The Origin of Chemical Elements, Physical Review 73 (1948), 803 3, 4

[5] Dicke, R. H., Peebles, P. J. E., Roll, P. G., Wilkinson, D. T., Cosmic Black-Body Radiation, ApJ (1965) 142, 414 3

[6] A. A. Penzias, R. W. Wilson, A Measurement Of Excess Antenna Temperature At 4080 Mc/s, ApJ Letters 142 (1965), 419 3

[7] B. W. Carroll, D. A. Ostlie, An Introduction to Modern Astrophysics 2^{nd} Edition 7, 8, 9

[8] X. Dupac, J. Tauber, Astronomy and Astrophysics (2005), v.430, p.363-371 10

[9] The WMAP Science Working Group, Wilkinson Microwave Anisotropy Probe (WMAP) Three–Year Explanatory Supplement (2007) 14

[10] The WMAP Science Working Group, Wilkinson Microwave Anisotropy Probe (WMAP) Seven–Year Explanatory Supplement (2010) 10, 12, 21

[11] B. Gold, Seven-Year Wilkinson Microwave Anisotropy Probe (WMAP) Observations: Galactic Foreground Emission, ApJ Supplement (2011), 192, 15 14

[12] S. Weinberg, Cosmology, Oxford University Press (2008) 15

[13] Hao Liu, Ti-Pei Li, Improved CMB Map from WMAP Data, arXiv:0907.2731v3 19, 20, 22, 83

[14] Hao Liu, Shao-Lin Xiong, Ti-Pei Li, Diagnosing Timing Error in WMAP Data, MNRAS (2011) 413, 1 20, 24, 25

[15] B. F. Roukema, On the suspected timing-offset-induced calibration error in the Wilkinson microwave anisotropy probe time-ordered data, arXiv:1007.5307v2 25

[16] B. F. Roukema, On the suspected timing error in WMAP map-making, Astronomy & Astrophysics (2010) 518, id.A34 26

[17] A. Moss, D. Scott, K. Sigurdson, Induced CMB quadrupole from pointing offsets, JCAP (2011) 001 25, 26

[18] W. H. Press, S. A. Teukolsky, W. T. Vetterling, B. P. Flannery, Numerical Recipes 3^{rd} Edition, http://www.nr.com 21

[19] G. Hinshaw, First Year Wilkinson Microwave Anisotropy Probe (WMAP) Observations: Data Processing Methods and Systematic Error Limits, ApJ Supplement (2003) 148, 63 18, 22, 26, 29, 47

[20] G. Hinshaw, Five-Year Wilkinson Microwave Anisotropy Probe (WMAP) Observations: Data Processing, Sky Maps, and Basic Results, ApJ Supplement (2009) 180, 225 19

[21] N. Jarosik, First Year Wilkinson Microwave Anisotropy Probe (WMAP) Observations: On-Orbit Radiometer Characterization, ApJ Supplement (2003) 148, 29 19, 57, 62

[22] N. Jarosik, Three-Year Wilkinson Microwave Anisotropy Probe (WMAP) Observations: Beam Profiles, Data Processing, Radiometer Characterization and Systematic Error Limits, ApJ Supplement (2007) 170, 263 19

[23] N. Jarosik, Seven-Year Wilkinson Microwave Anisotropy Probe (WMAP) Observations: Sky Maps, Systematic Errors, and Basic Results, ApJ Supplement (2011) 192, 14 19

[24] U. Sawangwit, T. Shanks, Beam profile sensitivity of the WMAP CMB power spectrum, MNARS (2010) 407, 1 26, 83

[25] K. Schultz, K. M. Huffenberger, Stacking Catalog Sources in WMAP Data, Bulletin of the American Astronomical Society (2011), 43 26